

THE ONSET CIRCUIT OF THE VENTRAL
NUCLEUS OF THE LATERAL LEMNISCUS
A MODELLING APPROACH

MICHAEL J. REBHAN



FACULTY OF BIOLOGY
LUDWIG-MAXIMILIANS-UNIVERSITY MUNICH

MUNICH 2020

THE ONSET CIRCUIT OF THE VENTRAL
NUCLEUS OF THE LATERAL LEMNISCUS
A MODELLING APPROACH

MICHAEL J. REBHAN

Dissertation at the Faculty of Biology
Ludwig–Maximilians–University
Munich

submitted by
Michael J. Rebhan
under the supervision of
Prof. Dr. Christian Leibold

Munich, 2020

First reviewer: Prof. Dr. Christian Leibold

Second reviewer: PD Dr. Conny Kopp-Scheinpflug

Date of submission: 22.10.2020

Date of oral exam: 22.01.2021

ERKLÄRUNG

Ich versichere hiermit an Eidesstatt, dass meine Dissertation selbständig und ohne unerlaubte Hilfsmittel angefertigt worden ist. Die vorliegende Dissertation wurde weder ganz, noch teilweise bei einer anderen Prüfungskommission vorgelegt. Ich habe noch zu keinem früheren Zeitpunkt versucht, eine Dissertation einzureichen oder an einer Doktorprüfung teilzunehmen.

München, den 01.02.2021

Michael J. Rebhan

*“You will hold this book in your hands, and learn all the things that I learned, right along with me: There is no immortality that is not built on friendship and work done with care. All the secrets in the world worth knowing are hiding in plain sight. It takes forty-one seconds to climb a ladder three stories tall. It’s not easy to imagine the year 3012, but that doesn’t mean you shouldn’t try. [...] The mountains are a message from Aldrag the Wyrn-Father. Your life must be an open city, with all sorts of ways to wander in.
After that, the book will fade, the way all books fade in your mind.”*

- Robin Sloan, Mr. Penumbra’s 24-Hour Bookstore

Contents

1	Introduction	1
1.1	Physiological foundations	1
1.1.1	Neuronal signals elicited by sound	1
1.1.2	The main auditory pathway	4
1.2	Onset sub-network	8
1.2.1	Octopus cells	8
1.2.2	Synapse crossing the hemispheres	11
1.2.3	Onset cells in the VNLL	17
1.3	Speech perception	21
2	Methods	25
2.1	Auditory periphery model	25
2.2	Synaptic models	26
2.3	Leaky-integrate-and-fire model	27
2.4	Information Theory	28
3	Results	31
3.1	Octopus Cells	31
3.1.1	Model	31
3.1.2	Mathematical analysis	35
3.1.3	Simulations	37
3.1.4	Modulation transfer functions	37
3.1.5	Complex Stimuli	39
3.1.6	Discussion	39
3.1.7	Additional Notes	43
3.2	Synaptic connection	45

3.2.1	Currents	45
3.2.2	Synaptic effects	46
3.3	VNLL onset cells	48
3.3.1	Test stimuli	49
3.3.2	Complex stimuli	57
4	Discussion	67
4.1	Mechanistic aspects	68
4.2	Functional aspects	72
	Bibliography	77

The auditory system is required to extract every single piece of acoustic information from only two strongly correlated, one-dimensional and time-dependent signals. To perform the extraordinary amount of computations necessary for the analysis of sound, the mammalian auditory pathway in the central nervous system has to be sophisticated and complex. The main focus of this study is a sub-network in the ventral stream of the auditory pathway that has most often been implicated in the detection of sound onsets. The octopus cells of the posteroventral cochlear nucleus (PVCN), as well as a cell population in the ventral nucleus of the lateral lemniscus (VNLL) have been reported to fire precise onset spikes and follow amplitude modulations faithfully. This study proposes a phenomenological, computationally efficient numerical model for a population of octopus cells. The model is constrained by the well-studied responses of octopus cells to pure tones as well as amplitude-modulated noise and implements their basic physiological operation of differentiation, to achieve strong and selective responses to naturalistic stimuli. Human speech is used as a test bed, as it needs to encompass a wide variety of acoustic effects - including sharp transients and strong modulation - to constitute an efficient tool for communication. A collaborating study has shown that the calyx-like synapse employs different types of currents as well as short term depression and facilitation. α -amino-3-hydroxy-5-methyl-4-isoxazolepropionic acid (AMPA) receptors mediate fast and powerful currents while the additional currents mediated by N-methyl-D-aspartate acid (NMDA) receptors are much weaker and slower. The present study investigates the interplay and consequences of these different properties. The firing behaviour of the onset cells in the VNLL for pure tone and modulated stimuli can be faithfully emulated by integrating over a pair of octopus cells in a simple leaky-integrate-and-fire model. As proposed by experiments, the effects of combining octopus cells with different centre frequencies is investigated as well. For pure tones the additional currents improve reliability without impairing the temporal precision of the elicited onset spikes. The phase locking to modulations severely decreased and are well below observed values if NMDA currents are not taken into account. Short term depression and facilitation are well balanced against each other. In all cases the inclusion of the additional currents increases the number of viable combinations of octopus cell centre frequencies. The population responses to speech stimuli show short, precise and selective islands of activity at the onsets of certain phonemes. Hereby, the observed effects, short term depression, facilitation as well as NMDA mediated currents complement each other, creating a balance between precision and reliability. In order to get an idea of the functionality of the observed circuit, model responses to naturalistic stimuli were analysed

from an information theoretical point of view. The information transmission rate is maximal in frequency bands around 1 Hz, corresponding to the mean temporal distance between islands of firing. A second peak between 10^2 Hz and 10^3 Hz might reflect formant like structure. While decreasing the firing rate by over 50%, the additional synaptic effects only reduce the information transmission rate by roughly 10%, making the system much more energy efficient. Similar to the analyses done on the test stimulation, the investigation into rate information revealed a larger area of viable combinations of octopus cells. Moreover, it has been shown, that the loss in information transmission caused by decreased firing is mostly restricted to rate information with only little loss in temporal information. Hence, the system is tuned to saliently and precisely mark the onset of broadband structures with strong formant-like and high frequency components.

Die Herausforderung des auditorischen Systems ist es, aus nur zwei stark korrelierten, eindimensionalen und zeitabhängigen Signalen alle akustischen Informationen zu extrahieren. Um diese außerordentliche Menge an Berechnungen zu bewältigen hat sich in Säugetieren ein komplexes Netz aus spezialisierten Nervenbahnen entwickelt. Diese Studie beschäftigt sich mit einem Teilnetzwerk, das hauptsächlich mit der Erkennung von Anlauten in Schallstimuli assoziiert wird. Es umfasst die Oktopuszellen im posteroventralen Nucleus cochleares (PVCN) und eine Neuronenpopulation im ventralen Nucleus des Lemniscus lateralis (VNLL). Beide Zelltypen feuern präzise Aktionspotentiale zu Beginn eines Reintones und folgen der Phase von Amplitudenmodulationen. Für diese Studie wurde ein phänomenologisches, numerisch effizientes Modell entwickelt, um eine Population von Oktopuszellen zu simulieren. Es emuliert die bekannten Zellantworten auf Reintöne und amplitudenmoduliertes Rauschen gleichermaßen und beinhaltet die Ableitungseigenschaften der physiologischen Vorbilder. Außerdem zeigt das Modell eine starke Reaktion auf naturalistische Stimuli, welche hier am Beispiel menschlicher Sprache analysiert wurde. Um ein effizientes Mittel zur Kommunikation darzustellen, muss Sprache eine Vielzahl von auditiven Eigenschaften, insbesondere starke Transienten und Modulationen, aufweisen. Eine Partnerstudie hat gezeigt, dass die calxyartige Synapse nicht nur Kurz-Zeit-Depression sowie Fazilitation aufweist, sondern auch verschieden Ströme beinhaltet. Ströme, die von α -amino-3-hydroxy-5-methyl-4-isoxazolepropion Säure (AMPA) Rezeptoren vermittelt werden zeichnen sich durch eine hohe Amplitude und kurze Zeitskalen aus, während N-methyl-D-aspartat (NMDA) Ströme, vergleichsweise schwach und langsam sind. Die Wechselwirkungen und Konsequenzen dieser zusätzlichen Effekte auf die Zellantworten sind ein Schwerpunkt der vorliegenden Arbeit. Die Verhalten der Zellen des VNLL bei Stimulation mit Reintönen und amplitudenmodulierten Stimuli kann zuverlässig simuliert werden, indem ein einfaches "leaky-integrate-and-fire" Modell über zwei eingehende Oktopuszellen integriert. Die Kombinationsmöglichkeiten verschiedener Oktopuszellen bezüglich ihrer Zentralfrequenzen wurde ebenfalls untersucht. Es kann gezeigt werden, dass die zusätzlichen NMDA Ströme die Zuverlässigkeit der Anlautantworten der VNLL Zellen verbessern ohne deren Präzession zu reduzieren. Bei amplitudenmodulierter Stimulation erweisen sie sich als notwendig, um die experimentell bestimmten Feuerraten zu ermöglichen. Bei beiden Stimulationstypen werden die Anzahl an Kombinationen von Oktopuszellen, die in dem erwarteten Verhalten resultieren, erhöht. Die Kurz-Zeit-Depression

und Fazilitation halten sich unter diesen Testbedingungen die Waage. Die Populationsantwort auf menschliche Sprache zeichnen sich durch kurze und selektive Feuerphasen an den Anlauten bestimmter Phoneme aus, wohingegen die Zelle auf den Rest des Stimulus nicht oder nur geringfügig reagiert. In diesem Falle ergänzen sich die spezifischen Eigenschaften der Synapse und stellen eine Balance zwischen Präzision und Zuverlässigkeit her. Eine informationstheoretische Untersuchung der Antworten auf naturalistische Stimuli zeigt, dass das Maximum der Informationstransmission in einem Frequenzband von etwa 1 Hz liegt, was dem zeitlichen Abstand der Feuerphasen entspricht. Ein zweiter Modus der Verteilung hat sein Maximum zwischen Bändern der Größenordnung 10^2 Hz und 10^3 Hz und könnte Residuen der Formantenstruktur repräsentieren. Obwohl die synaptischen Effekte die Feuerrate um über 50% senken, reduzieren sie die Informationstransmissionsrate lediglich um circa 10%. Das System wird also deutlich energieeffizienter. Eine Untersuchung der reinen Rateninformation zeigt, dass , vergleichbar mit den Teststimuli, eine größere Anzahl an Kombination verschiedener Oktopuszellen konsistente Antworten liefern. Darüber hinaus konnte gezeigt werden, dass sich der Informationsverlust, der durch die Verminderung der mittleren Feuerrate verursacht wird, hauptsächlich auf die Rateninformation beschränkt, während die zeitliche Information weitgehend erhalten bleibt. Das System scheint daher darauf ausgelegt zu sein, den Anlaut von breitbandigen Strukturen mit starken formantenartigen und hochfrequenten Komponenten zu markieren.

Chapter 1

Introduction

From the perspective of physics, sound is a time-dependent fluctuation in pressure. Since most physical processes cause the surrounding medium to vibrate, a great amount of information about the environment can be inferred by analysing the incoming sound. The challenges that analyses of auditory stimuli pose are remarkable. While other sensory systems have multiple different receptor cells available, sound signals are received by only a single type. Therefore, the auditory system is required to extract a multitude of information from only two highly correlated, one-dimensional, time-dependent signals. Following the principle of superposition, every sound adds its frequency and modulation patterns to a single auditory stimulus at each ear. Furthermore, since sound is fundamentally the vibration of a medium, it is impossible to consider sound independent of time. Moreover, sound is processed on multiple time scales in the auditory system. Extracting and processing the large amount of information encoded in such a low dimensional input requires great computational effort. To perform the extraordinary amount of computations necessary for the analysis of sound, the mammalian auditory pathways in the central nervous system have evolved to be sophisticated and complex. In order to illustrate the computational complexities and the challenges faced by this system, this chapter will give a brief overview of the auditory brainstem.

1.1 Physiological foundations

1.1.1 Neuronal signals elicited by sound

After being collected and mechanically amplified by the outer and middle ear the sound wave reaches the cochlea in the inner ear [58]. The cochlea is a fluid-filled spiral consisting of three

chambers, the *scalae*. Separating the *scala media* and the *scala tympani* is the basilar membrane, which plays a pivotal role in transducing the mechanical pressure into an electrochemical signal. The auditory nerve itself is seated in the centre of the spiral. Frequency separation in the cochlea is then achieved by the dependency of the local amplitude on the position on the basilar membrane. The maximum amplitude for high frequencies is located basally while lower frequencies are located more apically. Since the overall amplitude of the travelling waves is large and its peaks are sharply tuned, a high degree of frequency selectivity can be achieved [69]. Therefore, the mechanics of the travelling wave on the basilar membrane lead to a mapping of sound frequencies onto spatial positions.

The basilar membrane also houses the organ of Corti. Its inner and outer haircells are involved in an active and a passive process, which when combined enable the neuronal response to sound. Protruding from these haircells are tiny interconnected projections, called stereocilia. The inner haircells are the principal sensory cells and are responsible for passive transduction via deflection of local vibrations by the stereocilia. These deflections mechanically open ion channels located at the tip of the inner haircells [6]. The flux of ions then leads to a change in intracellular potential and an activation of the connected auditory nerve fibers (ANF) [59]. The active reverse transduction, the process responsible for additional amplification of the travelling wave, is mostly mediated by the outer haircells. The protein prestin allows the outer haircells to react to a change of transmembrane potential by contracting or expanding. [58]. This process feeds energy back into the travelling wave to lower the response thresholds, improve temporal and spectral precision and further increase the amplitude of components with lower frequencies.

The time scale of the electromechanical transduction is short enough to follow the local vibrations closely for lower frequencies. Therefore the neuronal signal is locked to the phase of the incoming sound waves. In cats, this phase-locking starts to degenerate around 1kHz and is completely destroyed for frequencies above 5kHz where the spiking occurs entirely independent of the phase of the stimulus [37]. Figure 1.1 shows the response of three simulated cat ANFs to pure tones with 40 dB sound pressure level (SPL) and a frequency of the ANFs' centre frequencies. The frequency of the stimulus can be inferred using different cues. Figure 1.1 shows the decay of the phase-locking with rising centre frequency as well as the travelling wave delay, i.e. high frequency sounds are registered earlier.

Since the dynamics of the basilar membrane lead to a mapping from frequency space onto spatial position, each ANF only carries signals from a well defined frequency range. Figure 1.2 shows the threshold tuning curves for the same simulated ANFs depicted in figure 1.1. For low to

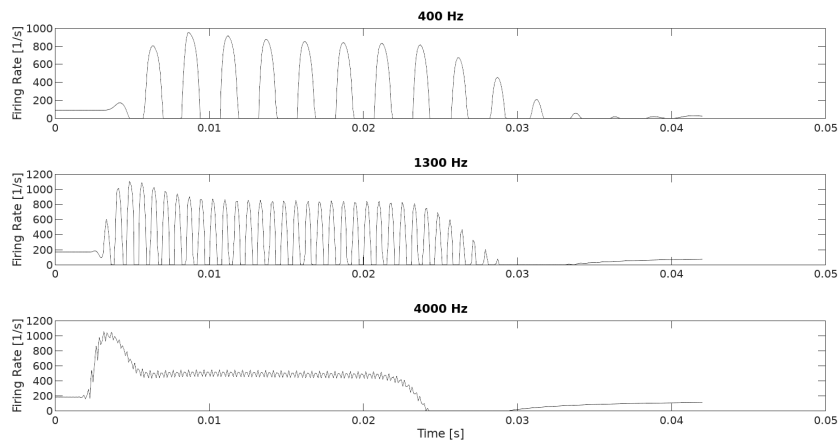


Figure 1.1: Firing patterns of different simulated ANFs as a response to pure tones with the cell's centre frequency, generated with the models proposed in [92, 28, 91].

medium intensities the responsive areas are well defined. However, stimuli with higher amplitudes evoke responses in off-frequency ANFs as well. Generally speaking, response thresholds of ANFs to stimuli with centre frequency are very low, lying between 0 and 15 SPL. Response thresholds further downstream in the auditory path in part are significantly higher. This frequency decomposition

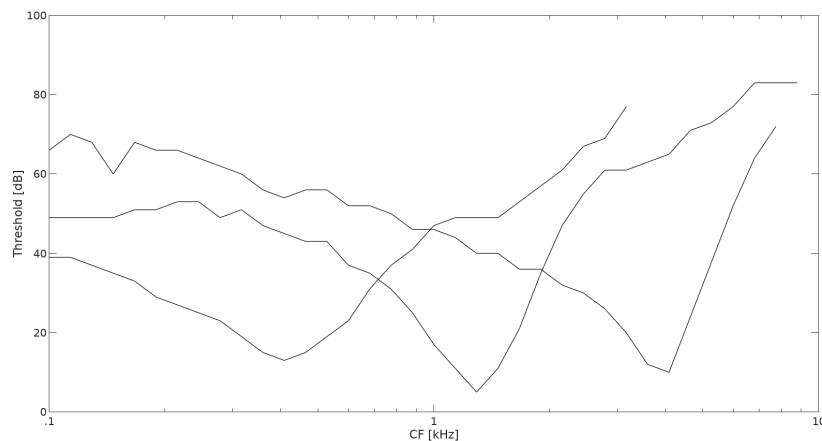


Figure 1.2: Threshold tuning curves of ANFs with different centre frequencies, generated with the models proposed in [92, 28, 91].

is crucial for the further analysis of the auditory signals. The ANFs are therefore in tonotopical order, an order that is preserved downstream on the auditory pathway. Apart from frequency ranges, ANFs differ in spontaneous firing rate and responsiveness as well [40]. ANFs with a high

spontaneous firing rate have a low response threshold and make up around 61% of all ANFs in cats. Around 16% of ANFs only respond to strong stimulation, as very low spontaneous firing rates correspond to low sensitivity. A third group (23%) lies in between [40]. This distribution accounts for the extraordinary dynamic range of the hearing in mammals.

1.1.2 The main auditory pathway

The population of ANFs carries a neuronal representation of the auditory signal in phase space. Figure 1.3 shows the main excitatory pathway from the ipsilateral ear to the inferior colliculus (IC). This overview, as presented in this study, will mostly follow the structure of [58]. The many bridges between hemispheres suggest that the contralateral counterparts of these pathways play a significant role as well, but these have been omitted from figure 1.3 for clarity. The pathways branch out and reintegrate with each node getting different inputs, performing different calculations and therefore extracting different information to be transmitted to the downstream nodes.

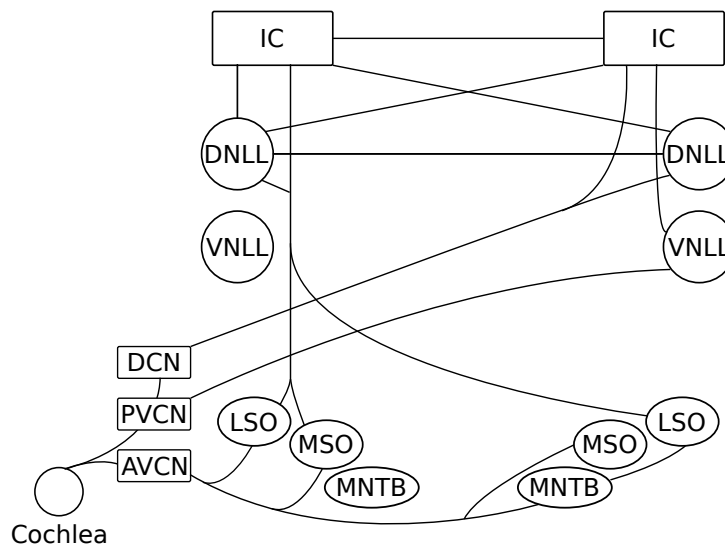


Figure 1.3: Main excitatory auditory pathway through the brainstem. Redrawn from [58].

Due to the complexity of sound stimuli and the subsequent requirement to maintain both precise timing information as well as the spectral pattern, the auditory pathways are split in two

major branches, the ventral and the dorsal paths [58]. The ANFs corresponding to the different pathways already branch off at their roots. The first brain areas innervated by the auditory nerve is the cochlear nucleus. The anteroventral cochlear nucleus (AVCN) is considered the first step on the ventral pathway while the posteroventral (PVCN) and the subsequent dorsal cochlear nucleus (DCN) contribute to the dorsal pathway [50].

In the ventral pathway, the AVCN transmits its signal to the superior olivary complex with high temporal precision [58], which is required for sound source localisation via comparison of the signals from the ipsi- and contralateral ear [26]. Within the AVCN exist two different populations of cells, globular and spherical bushy cells. The spherical bushy cell are innervated by a small number of ANFs. These inputs are transmitted by the endbulbs of Held, large synaptic terminals that transmit information very fast and with a high degree of reliability. The spherical bushy cell can thereby reproduce the firing of the input ANFs faithfully. For high-intensity stimuli, however, additional inhibition builds up. As a consequence, multiple simultaneous input spikes are necessary to elicit an action potential [38]. Therefore the spherical bushy cells provide accurate timing information about the ANFs signal, which is transmitted downstream to the ipsilateral medial and lateral superior olivary nuclei (MSO and LSO respectively) and the contralateral MSO [26]. The globular bushy cells receive up to 40 inputs from different ANFs and project mainly towards the contralateral medial nucleus of the trapezoid body (MNTB) via the calyxes of Held as well as to the ipsilateral MSO. The calyx of Held is arguably the most studied synapse in the mammalian brain and is well known for its size, precision and speed of information transmission. Via the MNTB, the globular bushy cells inhibit the contralateral LSO.

The superior olivary complex is mainly associated with sound localisation. Two different, binaural mechanisms are deployed for localising a sound source on the horizontal plain: comparisons of interaural level differences (ILD), which happen primarily in the LSO, and of interaural time differences (ITD), which are processed mainly in the MSO. The LSO receives excitatory input from the ipsilateral spherical bushy cells and inhibitory inputs from glycinergic MNTB cells, that in turn are innervated by contralateral globular bushy cells. This results in a subtractive dynamics directly comparing the magnitude of the inputs from both ears. MSO cells receive inhibitory and excitatory inputs from both hemispheres. The interplay of these inputs is complex and its details are still debated. However, typical MSO neurons respond strongest to specific positive (meaning contralateral leading) ITDs. Spatial information about the sound source can therefore be inferred from the activity pattern on a population level. The location information from the LSO and the MSO are consequently projected further downstream to the dorsal nucleus of the lateral lemniscus

(DNLL) and the IC directly.

The dorsal pathway is specialised on extracting, preserving and transmitting spectral as well as temporal information. It first passes through the PVCN [58], which contains the octopus cell area. Octopus Cells integrate over a large number of auditory nerve fibers with a wide range of centre frequencies [44, 22] which enables the detection of amplitude modulations in the auditory stimulus with a high degree of precision [24]. They project mostly onto the contralateral ventral nucleus of the lateral lemniscus (VNLL). As octopus cells are a major focal point of this study, they will be treated in greater detail in 3.1. The ventral cochlear nucleus also contains a multitude of other cell types such as multipolar cells or stellate cells that send collaterals throughout the cochlear nucleus. They also project onto the contralateral VNLL and IC as well as the ipsilateral LSO. They have in many cases found to be GABAergic. A population of t-stellate cells in particular is known to encode the frequency spectra of tones [86]. This spectral information is then transmitted to the DCN [54]. The ANFs passing through the PVCN terminate in the DCN as well [58]. Complex spectral analyses are performed therein by a multitude of different cell types. Apart from primary-like cells, it contains a large number of interneurons that provide strong inhibition all over the entire nucleus. Complex tuning curves combining different excitatory and inhibitory inputs are likely crucial to perform these spectral analyses. The DCN has also been implicated in the integration of multimodal information into the auditory pathways [55] and the reflexive response to acoustic stimuli [81]. As shown in figure 1.3 it feeds afferents into the DNLL. The DCN also has projections that pass by the lateral lemniscus all together, terminating directly in the IC.

The lateral lemniscus consists of two major nuclei, the DNLL and the VNLL [17]. The DNLL is associated with binaural integrating pathways [17], as its major input stems from the ventral path, namely the LSO and MSO [21, 36] and its contralateral counterpart [21]; the latter connection is known as commissure of Probst. It also receives collateral inputs from the cochlear nuclei [21]. Projections from the DNLL are towards the IC and across the commissure of Probst. Neurons within the DNLL are morphologically diverse [1]. However, this diversity seems uncorrelated to the firing behaviour of the cells [85] as 80% of the neurons are GABAergic [68]. Therefore the output of the DNLL is dominantly inhibitory. Consistent with its afferent inputs, the inhibition of the IC by the DNLL is consistent with binaural stimulation [16].

In contrast, the VNLL mainly responds to monaural stimulation [17] and can therefore be considered to be associated with the dorsal stream of the auditory pathways [58]. However, similar to the DNLL its major projection is towards the IC and is inhibitory in nature [36]. VNLL cells in part are GABAergic, as well as glycinergic [47]. It receives afferent inputs from the cochlear

nuclei and the MNTB [21, 36] most notably via a calyx-like synapse from the PVCN [20]. The cell populations are diverse and species dependant [14]. However, there is consistently a population of globular cells that elicit a precise onset response to monaural stimulations [11]. These are most likely the target of the afferents from the VNLL [2]. These onset cells and the targeting synapse are major parts of the sub-network and will be revisited below. Combined, the nuclei of the lateral lemniscus selectively inhibit the the IC for bin- and monaural stimulations [17].

The inferior colliculus (IC) is the first step of reintegration of the different information components [58]. Monaural pattern and timing information streams from the DCN and the VNLL as well as binaural location information streams from the superior olivary complex (LSO, MSO) and the DNLL all terminate there. The IC is sub-divided in three compartments [57]. The central nucleus (ICC) is surrounded by the dorsal and lateral cortices (ICD/ICL). The ICC exhibits a tonotopically organised laminar structure [56]. The laminae each receive heterogeneous inputs, each being innervated by afferents from multiple downstream nuclei. Along with the inputs, this creates domains within the laminae that are consistent with mon- as well as binaural stimulation, respectively. Consequently, the activity in each of these domains can be governed by temporal, spatial or spectral cues [42]. Additionally, there are a multitude of local collaterals that are inhibitory and excitatory in nature [80], which allows ICC neurons to have sophisticated response patterns. Furthermore the ICC is thought to respond in very specific ways to complex tones [31], as there has been evidence for Neurons responding to specific sound durations [12] or the direction of chirps[39]. All of this suggests that the ICC recombines spectral, temporal and spatial information, extracted by the downstream nuclei, in a meaningful and context-dependent manner. The cortices around the IC are less well understood but likely serve important and specialised functions. The ICD does not receive ascending auditory input but is instead stimulated by the ICC and descending nerve fibres from the auditory cortex [29]. Interestingly, the ICD receives visual input from the retina [30], which suggests a multimodal function. Since many neurons in the ICD exhibit stimulus-specific adaptation (strong responses to changes in auditory stimulation but adaptation to ongoing sounds) it has been implicated with the identification of novel sounds as well [43]. The ICL is also assumed to be involved in multimodal processes as it receives somatosensory inputs in additions to projections from the ICC and DCN [29]. Many neurons are excited by auditory and inhibited by somatosensory stimulation. This has given rise to the theory that one function of the ICL is to evoke reflexive responses to sounds [32].

The IC hands this reintegrated information over to the auditory cortex via the medial geniculate body, where further processing will occur. The computational effort to preprocess the acoustical

stimulus within the auditory brainstem before the IC can reintegrate it in a meaning full way is enormous. It is therefore necessary to examine each computational step, each involved nucleus and multiple sub-networks separately to get a proper understanding of the information processing that happens in the auditory system of the central nervous system.

1.2 Onset sub-network

The main focus of this study is a sub-network in the ventral stream of the auditory pathway that has most often been implicated in the detection of sound onsets. The octopus cells of the PVCN, as well as a cell population in the VNLL have been reported to fire precise onset spikes and follow amplitude modulations faithfully. Both areas are connected by a calyx-like synapse [19]. Therefore, it stands to reason to assume that the behaviour of the VNLL onset cells is inherited from precursors in the PVCN.

1.2.1 Octopus cells

The octopus cell of the PVCN stand out as they robustly, reliably and rapidly respond only to the onset of pure tones [22, 66, 20, 25], as shown in the peristimulus time histograms in figure 1.2.1. The peak firing rates of $10000 \frac{\text{spikes}}{\text{s}}$ at onset are extraordinarily high. Given that, due to the refractory period, only a single action potential is produced, this suggests a window of reliable firing far smaller than 1 ms.

Octopus cells are named for their multiple large dendrites that are usually oriented in one direction (see figure 1.5) [75]. These dendrites receive inputs from a multitude of ANFs with a broad range of characteristic frequencies [75, 67, 22], Therefore integration over this tonotopic arborisation of inputs seems crucial for the distinct firing pattern [35, 44, 53] and consequently for the processing of amplitude modulation information. This gives rise to the large receptive fields of the octopus cell that can be seen in the upper left panel of figure 1.2.1. The width of the tuning curves span hundreds of Hz at the low frequency and to multiple kHz at the high frequency range. Additionally, secondary, local minima of the thresholds off the centre frequencies are evident. It is noteworthy that response threshold of octopus cells tend to be significantly higher than those of the afferent ANFs. Furthermore, there appears to be a tendency for the response thresholds to increase with rising centre frequency of the octopus cell.

Contrary to pure tone responses, octopus cells persistently phase-lock to amplitude modulations

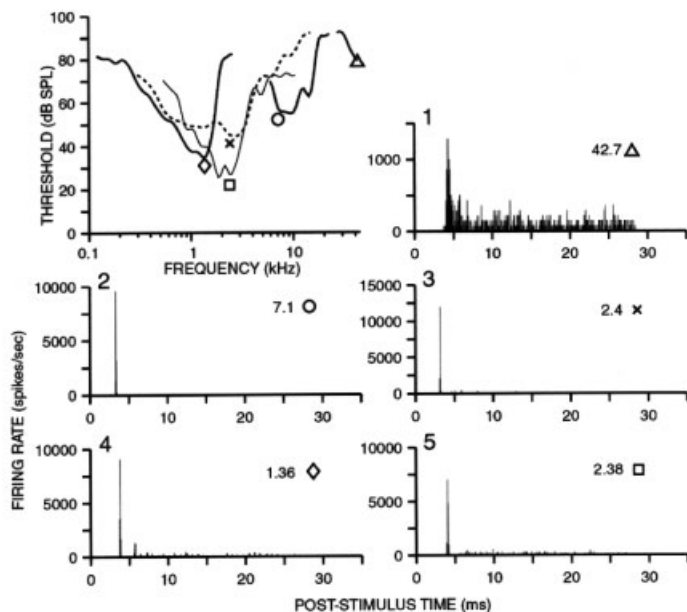


Figure 1.4: Octopus cell responses to pure tones. The top left panel shows the receptive field of neurons with different *cfs*. Additionally, the firing patterns of the indicated cells are shown in the other panels. The cell marked with a triangle is at the edge of the detection range and therefore not reliable. Taken from [75] (with permission).

(AM) in a specific AM frequency band [67, 52] as shown in figures 1.6, 1.7 and 1.8. Figure 1.6 shows the responses AM-stimuli using sinusoidals with the respective cell's best frequency as carrier on different SPLs (marked within the plots). The rate transfer functions in the top panels show the mean firing response to stimuli of different modulation frequencies. The temporal transfer functions give the synchronicity of the responses to stimulation with different modulation frequencies [63]. Figure 1.7 depict the temporal transfer functions as response to AM broadband noise [63] of different SPLs (40dB, 60dB, 80dB and 100dB symbolised in the plots by -4,6,8, and 0 respectively). The AM response of octopus cells is even more pronounced when stimulated with click trains 30 dB above threshold shown in figure 1.8, as clicks draw even stronger on onset response pattern of octopus cells [52]. AMs provide important information about natural sounds [61]. It is therefore believed that octopus cells encode these informations [63, 65]. This gave rise to the assumption that octopus cells contribute to the analysis of natural sounds such as human speech and other conspecific vocalisation [64, 52, 51].

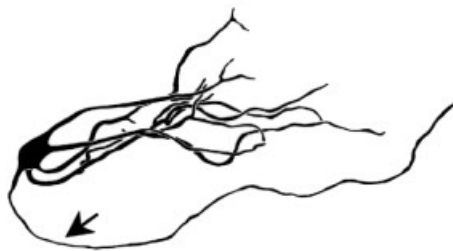


Figure 1.5: Camera lucida representation of an octopus cell. Taken from [75] (with permission).

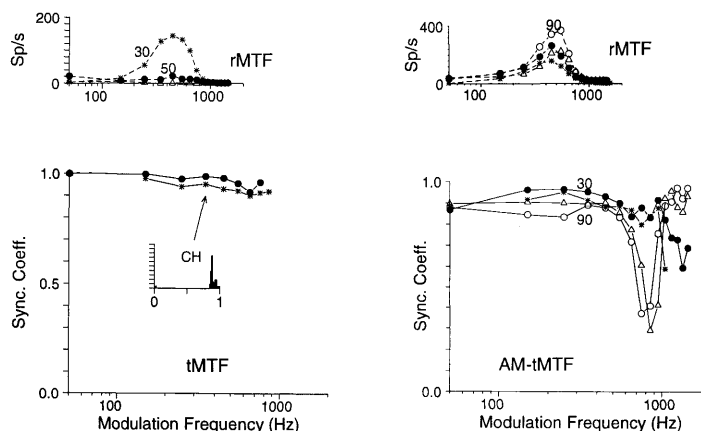


Figure 1.6: Rate and temporal modulation functions (upper and lower panels) of two onset (centre frequencies 6.7 kHz and 7 kHz, left and right panels) units in the PVCN. Taken from [63] (with permission).

As in other parts of the auditory brainstem, octopus cells show very fast response times. This is due to a high density of low-threshold potassium channels that lead to very low input resistances [52, 23] and a very fast membrane time constant [52, 23]. As a further consequence, octopus cells respond to the rate of depolarisation from the integrated inputs [18, 70]. This differentiation acts as an additional high pass filter and, most likely, contributes to the distinct pure tone and AM responses.

To study this interplay of effects, a novel phenomenological octopus cell model was conceived [61]. The proposed model was designed to only have a low-dimensional, strongly constrained parameter space. In order for the model to provide a practical tool for simulating octopus cells responses for long and complex stimuli, an additional focus was placed on its computational efficiency.

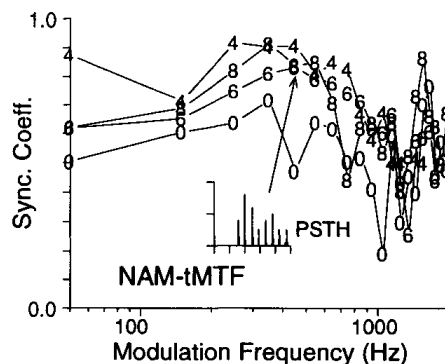


Figure 1.7: Temporal modulation function of an onset unit in the PVCN, stimulated by an amplitude modulated broadband noise. Taken from [63] (with permission).

Within the model paradigm, it becomes evident that the interplay between the differentiation properties and the afferent arborisation of inputs with a broad frequency spectrum indeed gives rise to the firing behaviour of octopus cells for pure tone as well as AM stimuli. The simulated spiking responses, even to complex stimuli, can with some confidence be used to model additional downstream nodes of the pathway.

1.2.2 Synapse crossing the hemispheres

The synaptic connection leading from the octopus cell area of the ipsilateral PVCN towards the contralateral VNLL has been found to be comparable to the Calyx of Held as well as the endbulbs and modified endbulbs of held [5, 2, 20, 75]. The Calyx of Held connects the globular bushy cells in the AVCN to the MNTB [20, 74, 33], the endbulbs and modified endbulbs transmit the signals from the ANFs towards the globular and spherical bushy cells in the AVCN [41, 78]. These synapses have been studied in great detail in the past and stand out by their extraordinary reliability and precision [82, 84]. This high temporal precision is necessary for these synapses in the cochlear nuclei. Since octopus cells are known for their high reliability and temporal precision, it is consistent that the synapse arising there is similar in nature. This large myelinated synapse has been found in cats [2, 75], rodents [5, 11, 20, 72], bats [14] and humans [2]. Since such a synapse arises projects from the octopus cells to the VNLL, where a similarly onset-sensitive cell population can be found, it seems logical to assume and test for an inherited behaviour of the latter.

Further properties of this synapse have recently been quantified in a collaboration with this study [19]. In particular, the investigations revealed a double exponential current shape as well as

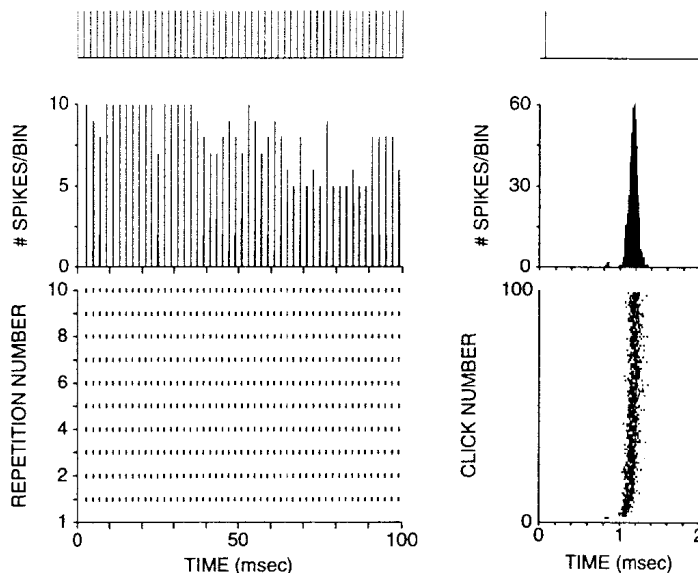


Figure 1.8: Octopus cell response to click stimulation with a click frequency of 500Hz. Depicted in the right panels are the timing of the stimulation (top), the post-stimulus time histograms (middle) and the dot raster diagram for 10 trials (bottom). The right panels show the collapsed result onto a 2ms period: the single click stimulus in this time window (top), the period histogram with a bin-width of $8\mu\text{s}$ (middle) and the ordered dot rasters (bottom). Taken from [52] (with permission, copyright 2000 National Academy of Science, U.S.A).

short-term depression and facilitation.

The short-term depression and the facilitation will here be treated together as both effects are a form of short-term synaptic plasticity and arise from the basic functionalities of the Synapses. Figure 1.9 illustrates the effect of this short-term neuronal plasticity on the synapse crossing the hemisphere between the octopus cells and the VNLL. The synapse was stimulated 20 times with different frequencies ranging from 1 Hz to 333 Hz (denoted by different symbols). The peak amplitudes of the elicited currents have been normalised relative to the first. For repeated stimulation the peak amplitude decreases for every pulse (with the exceptions below). The steady-state amplitude is frequency dependent and decreases with inter-pulse interval length. Facilitation is present as well: the amplitudes of second pulses for frequencies above 50 Hz are higher than the baseline. After that short-term depression is reflected by the decrease of the current amplitudes.

Synapses are the very structure that permit information transmission from one neuron to another. Figure 1.10 shows a rudimentary schematic representation of a synaptic junction. The two cells are separated by the synaptic cleft. Attached to the membrane wall on the presynaptic side

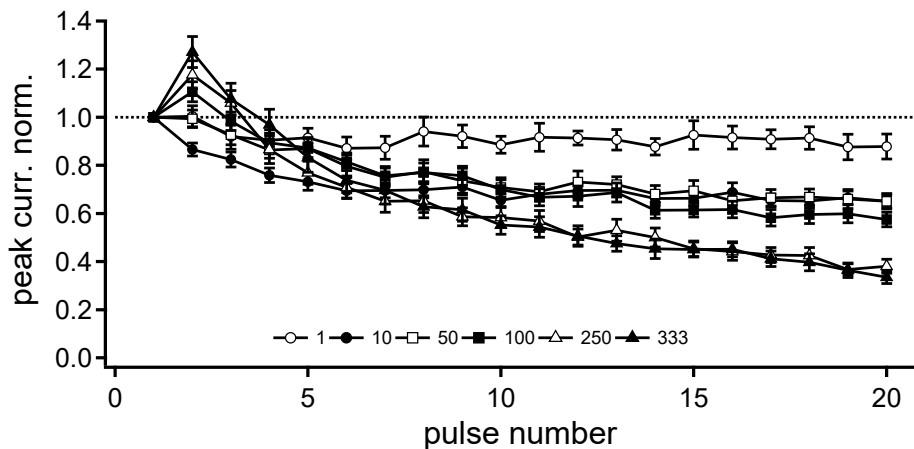


Figure 1.9: Effects of short-plasticity on the projection to the VNLL arising in the octopus cell area of the PVCN. From [19] (with permission).

are vesicles that hold the neurotransmitters. Upon stimulation the vesicles release the contained neurotransmitter into the synaptic cleft with a certain probability. These neurotransmitters diffuse through the synaptic cleft and then bind to the receptors on the postsynaptic side. This will then open ligand gated ion channels, allowing an inflow of ions into the postsynaptic neuron, therefore changing the postsynaptic potential. Finally the released neurotransmitters are purged from the synaptic cleft and the activated vesicles will recover over time, being supplied with new neurotransmitters from within the presynaptic cell. Depending on the receptors activated, the ion influx might carry a positive or negative charge. Positively charged ions, like Na^+ or Ca^{2+} cause depolarisation, exciting the target neuron. Conversely, negatively charged ions, such as Cl^- , hyperpolarise and therefore inhibit the postsynaptic neuron. A multitude of different neurotransmitters bind to different receptors on different types of neurons. Probably the most common ones are glutamate, implicated with excitation, as well as gamma-aminobutyric acid (GABA) and glycine, both of which transmit inhibitory signals.

The number of vesicles on the presynaptic membrane wall is limited and it takes time to recover. Repeated stimulation in rapid succession will deplete the reservoir as a larger portion of vesicles are activated. This causes the change in the postsynaptic potential to decrease after each activation. Since the pool of readily releasable vesicles will be recovered over time, this effect is known as short-term depression. Facilitation arises from the change of the release probability attributed to the vesicles in the synapse. If the probability of release is relatively high in the

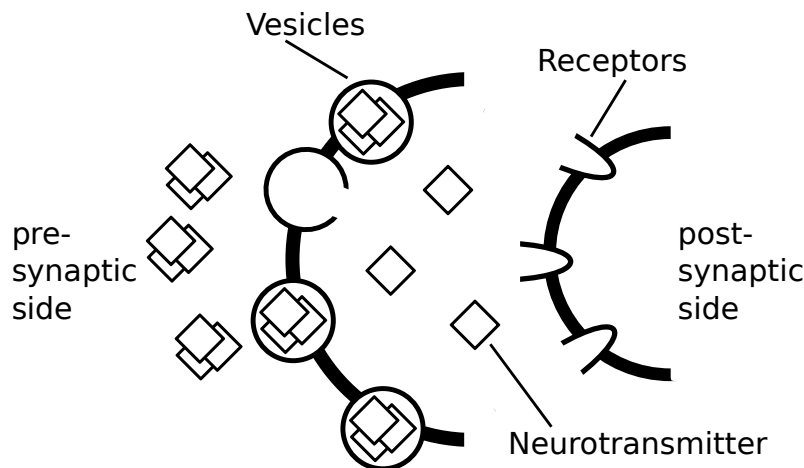


Figure 1.10: Schematic representation of a synapse to illustrate its basic function. See text for explanation.

steady-state, the change is negligible; an almost constant portion of the readily available vesicle will discharge upon activation. In synapses with low probabilities of release the change becomes significant. An accumulation of Ca^{2+} on the pre-synaptic side causes more vesicles to be released upon activation. If this probability increase is faster than the number of readily available vesicle decreases, an overcompensation occurs. When repeatedly activated in rapid succession, the change of postsynaptic potential will increase before it decreases due to short-term depression.

Glutamate is a neurotransmitter most often implicated with excitatory synapses. For the particular synapse investigated in this study the excitatory postsynaptic currents have been determined as shown in Figure 1.11 [19]. Depicted are the currents evoked after activation of this synapse with different holding potentials. The double exponential shape, consisting of a fast and a slow component, of the currents is most pronounced for positive holding potentials but is present at all potentials. Glutamate can activate multiple kinds of receptors types, among them α -amino-3-hydroxy-5-methyl-4-isoxazolepropionic acid (AMPA) and N-methyl-D-aspartate acid (NMDA) receptors [3, 85]. Figure 1.12 shows the currents in the presence of CPP in the top panel and additionally GYKI in the lower panel. Since CPP is antagonistic at NMDA receptors, it isolates AMPA currents. This deactivates the slow component, which, therefore, can be concluded to be mediated by said NMDA receptors. A similar argument can be made for the fast component stemming from AMPA receptor, due to GYKI being an antagonists to the latter. It has been shown that NMDA can increase sensory information transmission and firing rates in the target neurons [60, 73].

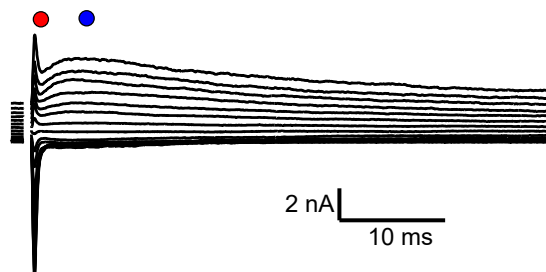


Figure 1.11: Glutamatergic postsynaptic currents at different holding potentials. Taken from [19] (with permission)

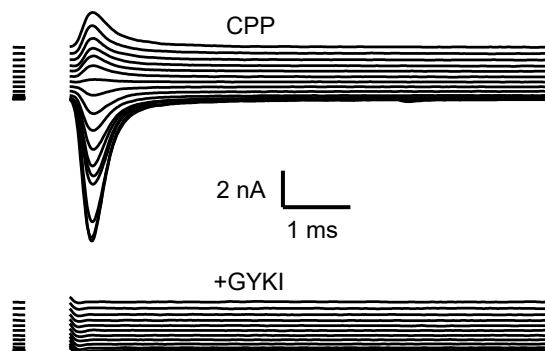


Figure 1.12: Currents for 1.11 with NMDA blocker (top panel) and additionally AMPA blocker (bottom panel) applied. Taken from [19] (with permission).

Figure 1.13 illustrates the amplitudes of the different components of the currents for varying holding potentials [19]. Apart from the fact that CPP blocks the NMDA current, one can see that its amplitudes converges to very small absolute values for negative holding potential. The behaviour of the AMPA component is linear in this voltage regime. The influence of CPP on the AMPA currents is comparably small.

Figure 1.14 compares the two components of the current in a physiologically realist voltage regime of -63 mV [19]. When comparing the AMPA current (top panel) to the NMDA current (bottom panel), it is important to note the vastly different scales. Since the amplitudes and the time scales differ by orders of magnitude investigating the interplay between the respective currents as well as between the currents and the effects of short-term plasticity, outlined above, will be a

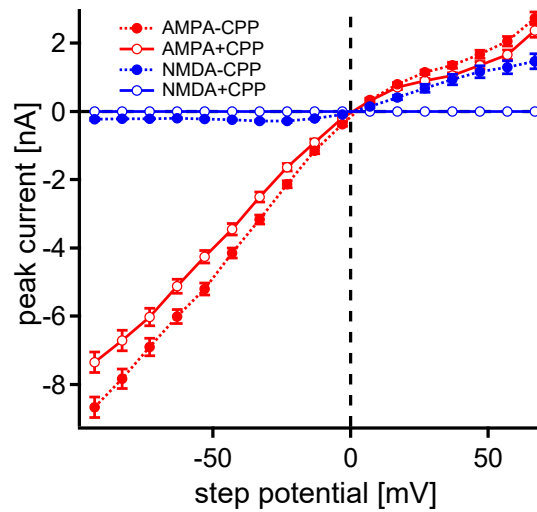


Figure 1.13: Amplitude of both current components with and without CPP for different holding potentials. Taken from [19] (with permission).

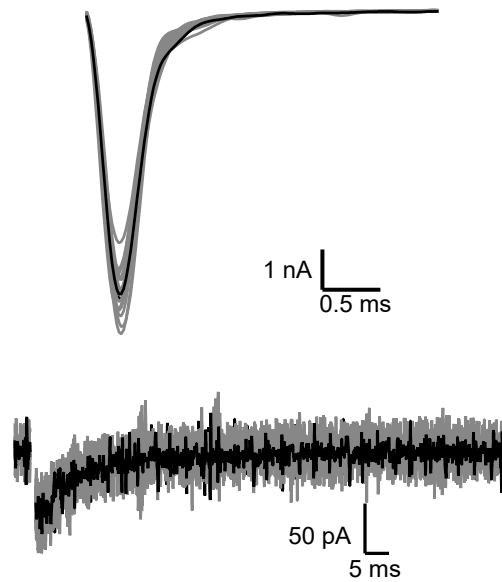


Figure 1.14: Components of the glutamatergic postsynaptic potential change. AMPA currents are shown on the top, NMDA currents on the bottom. Taken from [19] (with permission).

major focus of this study.

1.2.3 Onset cells in the VNLL

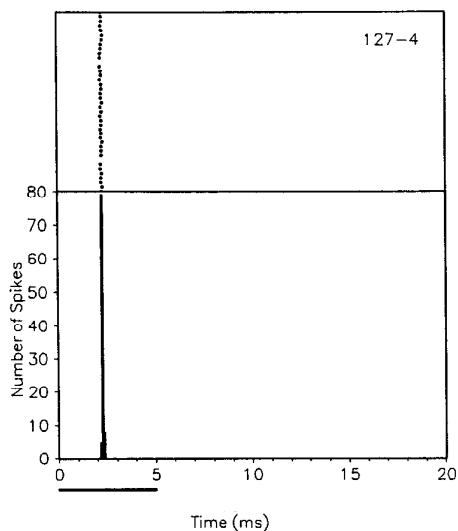


Figure 1.15: Constant-latency onset Neuron in the VNLLc. Shown are single trials above a PTSH of 100 trials as response to a 5 ms stimulation (black bar). Taken from [15] (with permission, copyright 1991 Society for Neuroscience).

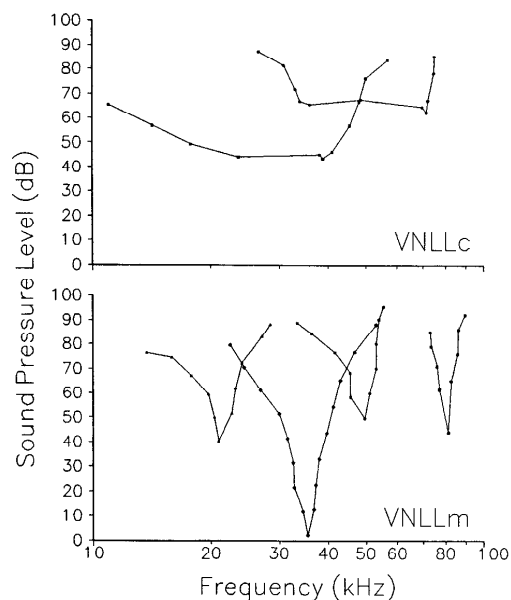


Figure 1.16: Receptive fields of VNLLc cells (top) compared to those of cells in another part of the VNLL. Taken from [15] (with permission, copyright 1991 Society for Neuroscience).

The VNLL contains an eclectic and species-dependent population of cells [48, 14, 62]. However, in echo-locating bats, a distinct columnar region has been found that is populated by onset firing neurons (there called VNLLc) [14, 15], as shown in figure 1.2.3. Globular cells in the VNLL have been implicated with this sharp onset firing behaviour [11]. While this columnar structure seems unique, a similar population of cells, concentrated in the ventral part of the nucleus, has been observed in rodents [49, 88, 72, 89], rabbits [4], cats [1] and humans [2]. Responses of these cells exhibit similarities to octopus cell' [67] and are targeted by the calyx-like synapses ascending from the octopus cell area of the PVCN [2, 72, 20, 14, 2, 75]. Similar to the endbulbs of held, the synaptic

terminals are wrapped around the somata of the cells [5]. In young Mongolian gerbils integration over a pair of such synaptic inputs is necessary for a reliably evoking of action potentials [5]. While this might not be true for older gerbils or other mammals, integration might still be useful as fail-safe mechanism or to broaden the receptive fields. Figure 1.16 shows that VNLLc cells respond to a far wider range of stimulus frequencies compared to cells in other parts of the VNLL.

It has also been shown that a single afferent action potential is not sufficient to reliably drive the VNLL cell, as illustrated in 1.17 [19]. NMDA currents mitigate this effect but are not sufficient to negate it. This hints towards an integration of inputs as well. The model network here proposed will therefore deploy two octopus cell inputs. VNLL cells in general receive additional inputs from the bushy cells of the cochlear nuclei [20], the MNTB [21, 36] as well as internal collaterals [49]. These inputs are, in part, inhibitory.

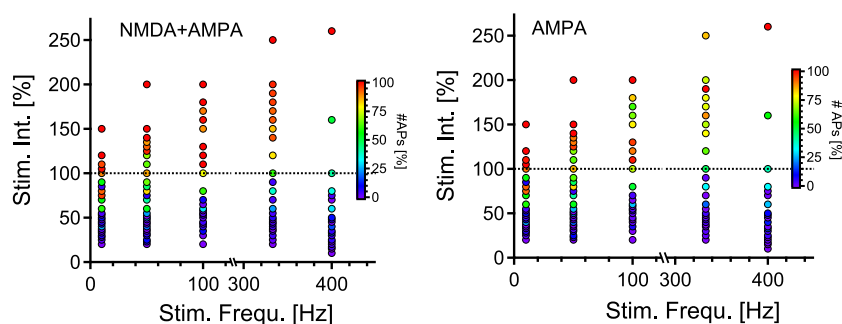


Figure 1.17: Reliability of VNLL cells for different input intensities and stimulus frequencies. In the left panel NMDA currents are taken into account while it is absent in the right panel. Taken from [19] (with permission).

The globular neurons in the ventral part of the VNLL tend to elicit a single onset spike, as shown for cats in the right panels of figure 1.18, upon stimulation with a pure tone with the cell's centre frequency at 20 - 30dB above threshold [62]. While both cells (upper and lower panels) show onset behaviour, the bottom cell shows a low level of sustained activity. The difference in the threshold tuning curves of the cells, however, is more significant. In the lower panel it is very reminiscent of octopus cells (compared figure 1.2.1). On the other hand, the cell in the upper panels shows a distinct w-shape. This, most likely, hints to more complex network dynamics, such as inhibition or integration over differently tuned inputs. Figure 1.19 depicts additional examples of VNLL onset cell [62]. The two leftmost columns show the respective PSTHs. Every panel indicates the centre frequency of the cells. Akin to octopus cells, the onset cells in the VNLL also respond to

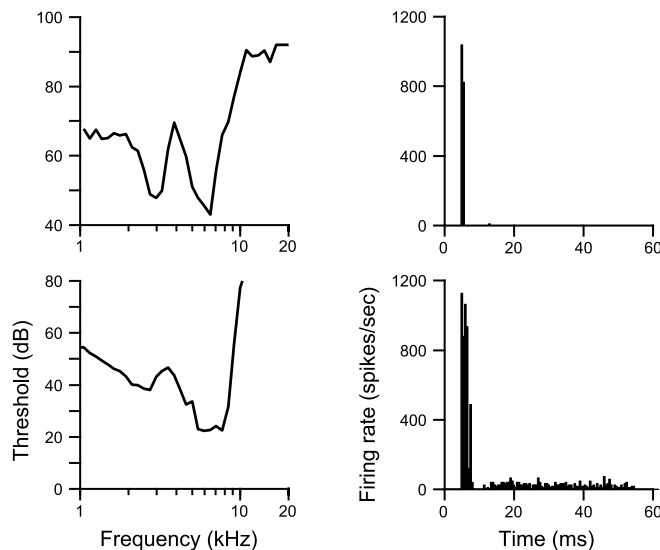


Figure 1.18: Threshold tuning curves and PSTHs of two VNLL onset cells. One cell exhibits an ideal onset response (upper panel) another shows low levels of sustained firing. Taken from [62] (with permission).

amplitude modulated stimuli [34, 87, 62]. Figure 1.19 also includes rate (third and fourth columns) and temporal (rightmost two columns) modulation transfer functions[62] to sinusoidal amplitude modulation of a pure tone carrier with the respective cell's centre frequency. Each set of columns depicts the same neurons.

The cells exhibit a wide range of centre frequencies mostly exceeding 10kHz. The rate transfer functions in the middle set of columns in figure 1.19 show, that not all onset neurons respond to these amplitude modulated stimuli. In the panels that have multiple traces the thickness depicts the stimulus intensity. The responsiveness to these amplitude modulations seems to be independent of centre frequency and, where existent, is consistently confined to a narrow band of modulation frequencies. The temporal modulation transfer function show a high degree of phase locking in most cases. It decreases only slightly with rising modulation frequency.

The VNLL also contains sustained firing and chopper cells, that will not be taken into account here. Analysis of the onset network described above can therefore only reveal part of the functionality of the VNLL. Furthermore, there exists evidence of inhibition in the VNLL originating from the MNTB and internal collaterals [21, 36, 49], about which very little is known. Because of this, the inhibition will not be elaborated in here, although it is implemented in the proposed model.

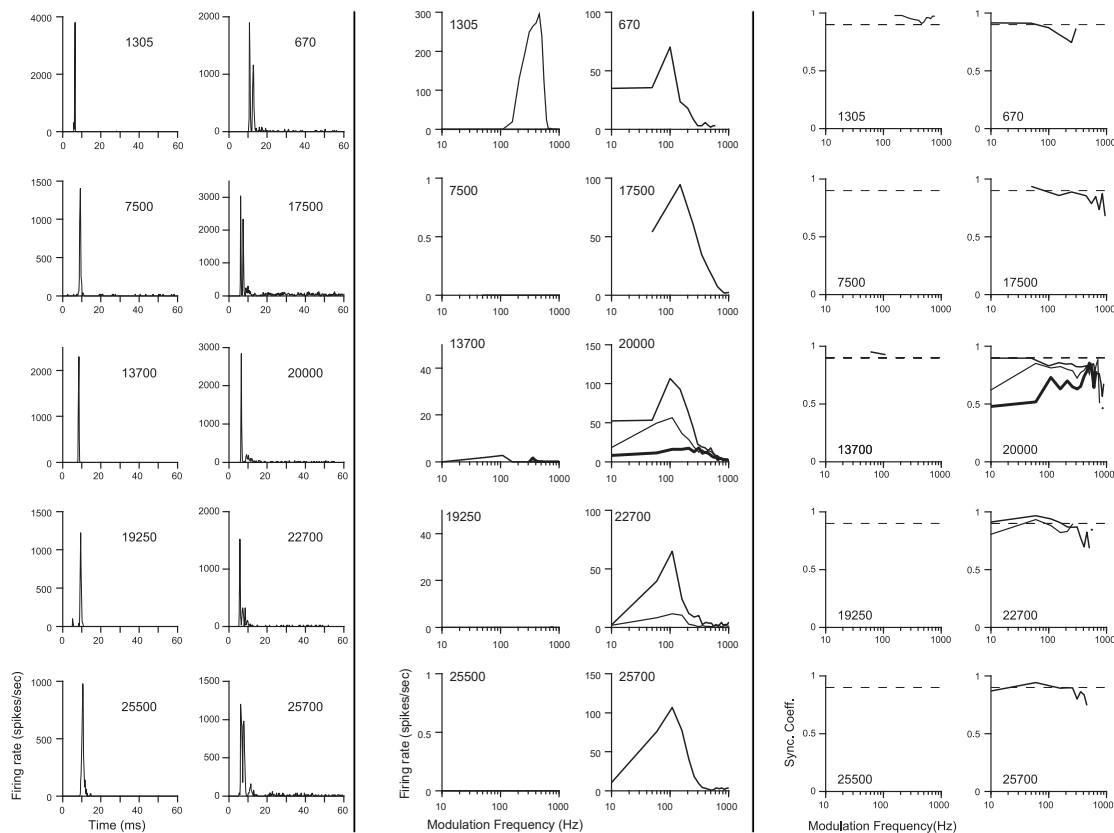


Figure 1.19: Examples of VNLL onset responses. The leftmost to columns shows the responses to pure tone stimuli. The two columns in the middle depict the rate modulation transfer functions for those cells for sinusoidal amplitude modulated stimuli. The temporal modulation transfer functions for the same cells and stimuli are shown in the rightmost columns. Taken from [62] (with permission).

However, understanding the origin and details of the onset cell response, as well as the synaptic effects involved, already gives an idea about the functional purpose of the strong inhibition from the VNLL on the IC. The response properties of this cell population is putatively especially important for complex stimuli and natural sounds such as human speech and other conspecific vocalisation.

1.3 Speech perception

Human speech and how it is processed in central nervous system is a traditional field of study. However, there still remain many unanswered questions. A detailed overview can be found in [8] and [46].

In its essence, speech is a complex code consisting of a sequence of a fixed set of units. The units are in this case drawn from the phonetic alphabet given by the language spoken. Each word, or sequence of (phonetic) letters, and sequence of words encode a specific meaning which has to be retrieved from the long term memory. This leads to a complex spectrotemporal pattern, that has to be analysed and matched with already stored patterns. In order to ensure practical communication, recognising and distinguishing specific letters has to be done reliably and fast.

In general, each word consists of two different kind of letters - vowels and consonants. Vowels can be identified by the relation the resonant frequencies of the vocal tract, the formants, have to each other. The formants can be modified by physically changing the dimensions of the vocal tract's component. Therefore speech signals exhibit energy peaks at the formant frequencies. The identification and discrimination of vowels is strongly dependent on the frequency decomposition taking place in the cochlea and the auditory nerve. In ANFs tuned to higher formants the response to components with lower frequencies are suppressed. Concurrently, formants cannot be resolved in high frequency ANFs as the bandpass filter width becomes very broad. Therefore, these are ill suited for the perception of vowels and strong low frequency hearing becomes essential. This is further supported by the finding, that the human auditory nerve is better suited for vowel discrimination than that of cats, the latter's auditory system is much stronger tuned to high frequencies.

The spectrotemporal pattern of consonants is more complex. Formant transitions in particular and spectral changes in general contribute significantly. Also, amplitude modulations and periods of silence bordered by transient factor into the construction of different consonant sounds. Therefore, temporal aspects carry a major part of the information content and precise timing in the internal representation of the speech signal becomes crucial. The complexity of consonant sounds leads to the challenging task of detecting and processing a variety of temporal features of the envelope, such as gaps, transients and other amplitude modulations.

The words "time" and "space" are used here as illustrations in figure 1.20. The physical waveforms of the corresponding sounds are depicted in the top panels. The lower panels show the constituent frequency components similar to its representation in the human auditory periphery. The vowels in the middle of the words can be discriminated by the clear formant structures of the

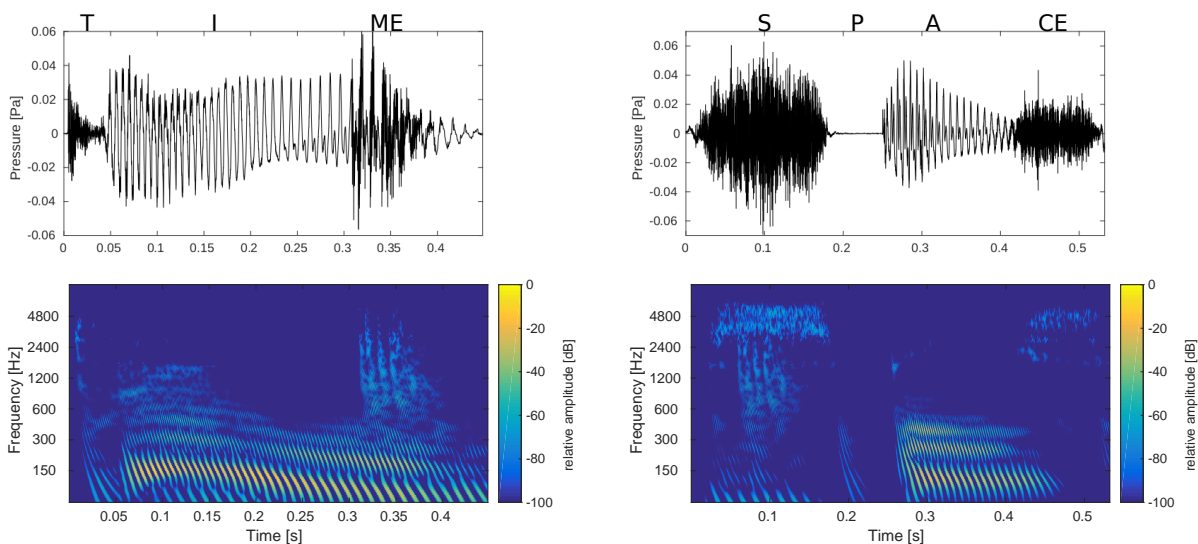


Figure 1.20: Depictions of the word "time" (left panels) and "space" (right panels). The physical waveforms are shown on the top, the spectrotemporal patterns on the bottom.

vowel; in the waveform as well as in frequency space. The preceding and succeeding consonants exhibit distinctly different and more diverse spectra. Visible examples here include the gap in the stop-consonant <p>, which is present but less pronounced in <t> as well, and the last phoneme of the word "time" where the formant structure of adjacent vowels are preserved in certain consonants that incorporate formant transitions. The fundamental frequencies are solely speaker dependant and, therefore, carry no information about the content of the speech.

Consequently, cross-frequency comparison is of vital importance for the processing of speech. Only the ratios between multiple formants allows for the discrimination of vowel sounds. The broad and shifting spectra of consonants likewise require a high resolution in frequency space as well as in time. The envelope of the stimulus carries important information, which, can best be analysed in a broad band regime. So the internal representation of the sound, generated by the ANFs, has to be further processed in higher levels the auditory system where broadly tuned cells integrate over multiple different ANFs. There, information about correlations between frequency bands can be extracted.

The importance of higher level areas in the auditory pathways is further accentuated by the fact that few acoustic stimuli in a natural environment are presented in isolation. This leads to another challenging aspect of the processing of speech. By its very nature, vocalisation is a code sequence. Multiple letters make up a code word which have to be identified individually but

decoded in sequence. So the entire sequence has to be grouped together into a single auditory stream. It appears that the brain uses multiple cues to discriminate which components of the acoustical environment belong to the stream which is currently being followed. Pitch perception plays an important role¹. Psychophysical studies have shown the different tones tend to be grouped into the same stream when they encompass a similar frequency range. Furthermore, it has been suggested that tones with similar timbre are more likely to be assumed to come from the same source². The assessment of sound sources seems to be a major factor when generating auditory streams [46]. As such, the perceived location of different sounds influences their grouping together as well.

Natural sounds tend to not be static concerning their frequency compositions and envelope shapes. Such changes are usually highly correlated over the different frequency components of a single sound and tend to be rather smooth. Precisely detecting the timing and course of these changes can be useful to judge the grouping of different components of the acoustical environment. Asynchronous changes between frequency bands, might point to sounds stemming from different sources while abrupt changes can indicate entirely new elements entering the acoustic environment. Since sensory systems are interconnected, multimodal cues heavily influence the auditory perception, as well. It is also worth mentioning that every single tone can only be attributed to a single auditory stream, an aspect known as disjoint allocation. This hints to at the intrinsic and reasonable assumption that a single tone must have exactly one source [46].

Human speech and other forms of conspecific vocalisation are clearly powerful tools to exchange information and therefore enable cooperation. The complexities in its structure are what enable the incredibly high information density. The question about the evolution of these forms of communication is an interesting but challenging one. It can be studied from two different points of view. A talker oriented approach not only requires the obvious point, that the vocal tract of the animal actually needs to be able to produce the required sounds but also the selection of sounds for communication is thought to include briefness and efficiency of usage. The acquisition of foreign languages show that the latter of which is, at least in humans, a partially learned trait. From a listener oriented point of view, the important characteristic is a maximum distinctiveness of the sounds used in communication. This serves as a potential explanation for the large variety of

¹Pitch means the perceived height of tones which allows them to be ordered on a scale from lower to higher

²Timbre is the attribute of a tone that allows it to be judged as dissimilar to different tones with similar pitch and loudness, presented in a similar manner.

phonetic properties present in human speech. Using many aspects of auditory perception allows for a larger, more internally distinct set of letters and consequently for a more efficient language. Therefore, it stands to reason that human speech, and conspecific vocalisation in general, shares many aspects with other natural sounds, as the mammalian auditory systems would have already been tuned to these when vocalisation emerged.

Chapter 2

Methods

2.1 Auditory periphery model

The characteristics and functionality of the auditory periphery, i.e., the organs and processes involved with the transduction of the physical pressure fluctuation into the neuronal signal of the main auditory nerve, are intricate and complex. Therefore, creating a sufficiently comprehensive periphery model would go beyond of the scope of this study, instead the model of Zilany et al. [92, 91, 28] is deployed here. This model is phenomenological in nature and has been developed for many years [90, 91]. It consists of two components, the first models cochlear processes while the second emulates the auditory nerve fiber as well as the associated synapse. This study is concerned with high sound pressure thresholds and broadband stimuli. As such, it is important that the periphery model is tuned to a wide physiological and dynamic range. The precise response to stimuli of vastly different SPLs is achieved by deploying multiple filter pathways in the cochlear model. A narrowly tuned chirp-filter governs the response to stimuli of low and medium intensities. This filter is further adjusted by a separate non-linear control path and is followed by a sigmoidal transduction function. Stimuli of a high SPL are mostly processed by static linear chirp filter, that is more broadly tuned. Additionally, a non-linear inverted transduction function is implemented in the second path, which is crucial for the transition region between medium and high intensity stimuli. The summed up outputs of the different pathways are then fed into an low pass filter, representing an effect of inner hair cells [90].

To analyse human speech, it might become necessary to use longer samples in order to include the entire stimulus statistics. Also, the envelope amplitude over time, as well as the spectral power,

can vary strongly and gaps of silence within sounds and between words are crucial for intelligibility, adding to the complexity of the stimuli. Therefore the short-term adaptation properties of the AN synapse are of great importance. The model by Zilany et al. ensures this by using a two component model. Faithful short term depression is ensured by a fast exponential adaptation. Effects on a longer timescale, like long term recovery, are implemented via a slow power-law dynamics [92]. It has been shown that the latter significantly improves the response to amplitude modulations and sound level statistics, especially in regard to human speech [93].

After initial publication of the entire periphery model, feedback from the community was implemented, as well. This led to the release of a updated set of parameters that improves the responses, especially for low frequency stimuli, which again, is important for the analyses of human speech [91]. However, the response to low frequency stimuli in high frequency ANFs still seems unusually strong. Finally the model already include different sets of parameters for cats as well as humans. For developmental purposes the cat is the more useful model animal because there is in vivo data available to emulate. However, a setting for humans is desirable for the analysis of speech perception

2.2 Synaptic models

For the next step, a modelled synapse connecting the PVCN with the VNLL has to be included. As shown in 1.2.2, the synapse studied here shows depression as well as facilitation. Therefore, for this study a model has been chosen that incorporates both of these effects without requiring in depth knowledge about the biophysical properties of the synapse. It consists of a system of equations modelling the available reservoir of neurotransmitters R and the probability of release P :

$$P_n = (f(p_{max} - P_{n-1}) + (P_{n-1} - p_{min}))e^{-\frac{\Delta t_n}{\tau_P}} + p_{min}$$

$$R_n = R_0 + ((1 - P_{n-1})R_{n-1} - R_0)e^{-\frac{\Delta t_n}{\tau_R}}.$$

p_{min} and p_{max} are hereby the limits of the probability of release. τ_P and τ_R are the timescales on which the P returns to its resting value and R is restored, respectively. f is the replenishment and controls the facilitation.

From the perspective of computational efficiency, a major advantage of this model is that it

only has to be evaluated at each spiking event n instead of at each sampled timestep. Δt_n is here the inter-spike interval between the n th and the $(n - 1)$ th event. Assuming the system to be at rest at the time of the 1st spike, it can be expressed by $\lim_{\Delta t_1 \rightarrow \infty}$. Consequently the resting state encompasses $P_1 = p_{min}$ and $R_1 = R_0$. This also gives further credence to the significance of f for the facilitation: Assuming $P_1 = p_{min}$ and $f = 0$ leads to $P_n = p_{min} \forall n$.

The relative amplitude of the post synaptic voltage change is determined by the amount of neurotransmitters released in the synaptic cleft. With an additional normalisation to the 1st spike, this leads to a relative amplitude of

$$A_n = \frac{P_n R_n}{p_{min} R_0}.$$

2.3 Leaky-integrate-and-fire model

Since it is the goal of this project to study inherited behaviour, it is sensible to model the VNLL onset cells with as little bias as possible. The leaky-integrate-and-fire model (LIF) is a well known spiking model for neurons. It is used to simulate the membrane voltage of a neuron as response to synaptic inputs. It is deterministic, does not introduce additional noise and derives its results from the basic electrophysiological properties of the neuron. The membrane potential U is derived by solving the differential equation:

$$\frac{d}{dt}U = \frac{1}{C} \left(g_l(U_r - U) + \sum_i g_i(U_i - U) \right).$$

The first term on the right hand side represents the intrinsic properties in of the cell, the resting potential U_r and the leak conductance g_l . $g_l(U_r - U)$ gives the current induced to reset the cells potential to its resting potential. The strength of this current is thereby adjusted by the conductance g_l .

The second half is determined by the the external inputs of the cells. The index i here determines the different receptor types that mediate the change of membrane potential. The corresponding reversal potential U_i reflects the excitatory or inhibitory nature of the synaptic input. $U_i > U_r$ leads to excitation; $U_i < U_r$ to inhibition. For the input conductances it usually holds that

$$g_i = g_i(t) = g_{i,0} I_i(t),$$

where $g_{i,0} = \frac{1}{U_h - U_i}$ includes the properties of the involved receptor type i and the holding potential

U_h for which, the current amplitude was determined. It translates the corresponding input current to a change of the cell conductance. Finally, C is the cell membrane capacitance and therefore acts as an electrodynamical inertia.

Spiking in the LIF-model is realised by explicitly comparing the potential U at each time step with a threshold U_{th} . More complex spiking behaviour can be implemented by using a dynamic threshold or by including a differential threshold with which $\frac{d}{dt}U$ is compared. It is noteworthy that this model does not employ any random processes and is therefore entirely deterministic.

2.4 Information Theory

In order to get an idea of the functionality of the modelled system, its results will be analysed from the point of view of information theory.

Information theory provides powerful tools to quantify information and its communication [13]. Its core concept is the uncertainty of an event X . Due to the similarities between thermodynamics and information theory, this uncertainty is usually referred to as (Shannon's) entropy H . Assume X to be a random variable with a sample space $\{x_i\}$ and a probability mass function P , the entropy is then given by

$$H = - \sum_i p_i \log_b p_i$$

with $p_i = P(x_i)$. The base b of log determines the unit. Most commonly, base 2 is used, which corresponds to the unit bit. 1 bit then corresponds to a single (even) "yes-or-no" (0/1,true/false) question, as $H = -0.5 \frac{\log_b(0.5)}{\log_b 2} - 0.5 \frac{\log_b(0.5)}{\log_b 2} = 1$. In the following, the base b of the logarithm will be omitted, consistently assuming $b = 2$.

Information about an event is then the negation of the entropy and reduces the uncertainty. Sampling a signal with non-zero entropy yields an information content (or self-information) of

$$I(x_i) = -\log(p_i).$$

This can be understood by assuming that an infinite number of samples should always allow for the entire information to be gained. In this case one would get every possible element of the sample space x_i with a probability of p_i . A linear combination of the total information gained would lead to $-\sum_i p_i \log_b p_i = H$. For the expected value it then holds that $E(I) = H$. Furthermore, by observing X it may be possible to obtain information about a separate event Y , as long as X and

Y are not statistically independent. This mutual information is given by

$$I(X, Y) = \sum_{i,j} p(x_i, y_j) \log \left(\frac{p(x_i, y_j)}{p(x_i)p(y_j)} \right).$$

If X and Y are statistically independent it holds that $p(x_i, y_j) = p(x_i)p(y_j)$, which yields $I(X, Y) = 0$.

In neuroscience, the tools of information theory are used to analyse the capacity for information transfer of spike trains [79, 83]. Given a spike train of length L sampled at a rate $\frac{1}{\tau}$, the statistical properties necessary for a statistical treatment can be extracted by dividing it words of length T . Consequently, each word consists of $\frac{T}{\tau}$ letters. The alphabet in this case only consists of two different letters; these are usually denoted as 1, in case a spike occurred in the observed time window, and 0 otherwise (alternative alphabets like Ising spins \uparrow and \downarrow can sometimes be found as well). The entropy of the spike train is then given by

$$H_S = - \sum_i p_i \log p_i,$$

where i indexes the different occurring words and p_i is the normalised occurrence of each word. The information is then given by

$$I = H_S - H_N,$$

where H_N is the noise entropy of the observed system. It can be determined analogue to H_S with the exception that instead of presenting the whole stimulus of length L a shorter stimulus of length T is presented repeatedly. $I = I(\tau, T, L)$ is highly dependent on the specific stimulus presented and therefore derived quantities are often observed. The information per spike $I_s = R/N$, where N is the spike count averaged over all words, or the information rate $I_t = R/T$ are more useful to characterise the capacity for information transmission. However, even these values present difficulties as high precision would require observing the limes $T \rightarrow \infty$. How to deal with this particular problem is outlined in detail in [79].

Apart from calculating the information rate directly as shown above it can be estimated using alternative methods [7]. The advantage of an estimation approach is that significantly less data is required. By approximating the neuronal encoder as a Gaussian channel, one can derive the upper bound on the information rate. Under this assumption, repeated stimulation with the same input would lead to a response of the form $R = \bar{R} + N$, with N being an additive noise

term. Therefore all information about the stimulus that can be extracted lies in \overline{R} . For Gaussian channels, the information rate I_t is given by

$$I_t = \int \log(1 + SNR(f))df.$$

The signal-to-noise power ratio $SNR(f)$ can be determined by the ratio of the variances σ_R^2 and σ_N^2 . The variances correspond to the Fourier transformations of \overline{R} and \overline{N} , respectively.

Complementary, the lower bound on the information rate can be estimated by calculating SNR on an alternative route. Starting from the response R one can estimate S using linear filtering: $S_{\text{est}}(f) = F(f) \cdot R(f)$. For a linear filter it holds that

$$F(f) = \frac{\langle R^*(f) \cdot S(f) \rangle}{\langle R^*(f) \cdot R(f) \rangle},$$

where R^* is the complex conjugate of R and $\langle \rangle$ denotes the average in sample-space. The noise term can then derived by $N = S - S_{\text{est}}$. Consequently, the signal-to-noise ratio

$$SNR(f) = \frac{\langle S_{\text{est}}(f) \cdot S_{\text{est}}(f)^* \rangle}{\langle N(f) \cdot N(f)^* \rangle},$$

which can be used to derive I_t analogues to the upper bound, mentioned above.

Calculating the information rate not only allows for the transmission properties of a system to be studied of stimulus duration but it also makes it far more practical to study the information transmission in multiple distinct frequency bands. This spectral decomposition in turn can hold clues about the kind of information that is extracted and retained, especially if one is concerned with stimuli of a broad frequency spectrum.

Chapter 3

Results

3.1 Octopus Cells

The first step to on the way to the onset network is a functional octopus cell model. The following paragraphs on this model are taken directly from an unpublished manuscript of *A phenomenological spiking model for octopus cells in the posterior-ventral cochlear nucleus* by M. Rebhan and C. Leibold [61].

3.1.1 Model

The general structure of the proposed effective model is outlined in Figure 3.1. In short, the sound stimulus is translated to simulated ANF firing rates $r_i(t)$, where i labels the respective frequency channel. The ANF rates are then translated into the octopus cell input by a weighted sum over frequency channels with weight factors g_i . The cellular membrane potential is derived from these inputs by a combination of differentiation and low-pass filtering. Finally, the output rate $r(t)$ of the octopus cell is obtained by a sigmoidal transformation of the membrane potential. Spike trains can subsequently be obtained by using $r(t)$ as the density of an inhomogenous Poisson process. All individual transformations will be explained in detail in the following paragraphs.[61]

Arborisation

By integrating over multiple ANFs the information about the stimulus' fine structure is removed, whereas envelope information is conserved. Especially the phase locking to low frequency modulations is best preserved in high frequency channels. The model generates the cochlear output of

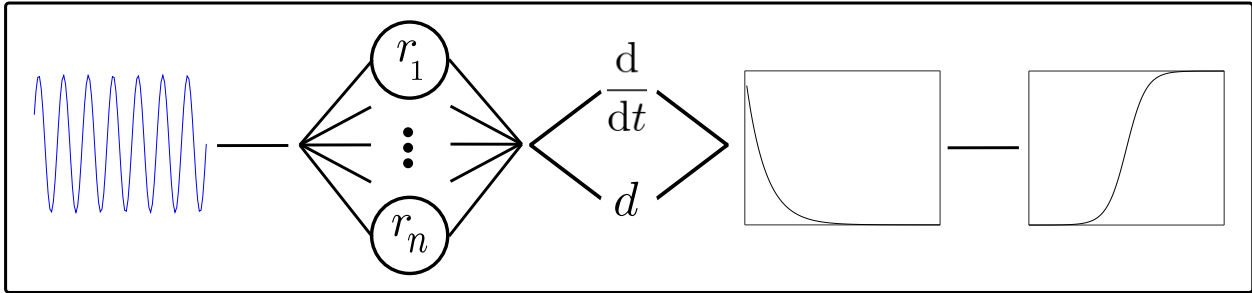


Figure 3.1: schematic representation of the octopus cell model.

an array of ANFs with a wide range of center frequencies, using the model described in [92, 91, 28]. The resulting ANF rates $r_i(t)$ are linearly combined to the octopus cell's input current

$$I(t) = \sum_i g_i r_i . \quad (3.1)$$

The weights are obtained from a log-normal distribution around the centre frequency f_c :

$$g_i = \exp \left(- \frac{\log_2 \left(\frac{f_i}{f_c + f_0} \right)^2}{2\Delta^2} \right) . \quad (3.2)$$

For high frequency cells it is necessary to introduce a shift f_0 to properly control the observed best frequency. This necessity arises from the overlap of the individual peripheral filters.

The parameter Δ describes the width of the arborization and will be the essential fit parameter to model the afferent arborization. For the sake of representation, the distribution above is designed so that Δ is expressed in octaves.

This approach however gives a low frequency response even for high- cf octopus cells that is not present in the tuning curves from literature [75]. We therefore remove these components forcefully by applying an additional high pass filter:

$$k_{bp} = \delta(t) - \frac{1}{t} \exp(-\pi f_{hc} t) .$$

This filter has been hand-tuned to a cutoff frequency of 900Hz. In this frequency range the filter suppresses most of the low-frequency-tail, while still preserving the general response patterns of the modelled cells. We apply this filter before the periphery model as to prevent interferences between

the two.[61]

Membrane potential

The octopus cells respond to rising envelopes of the sound stimuli, which we model via a differentiation following [18]. The integration time scale of the membrane is accounted for by an additional low pass filter $k_{lp} = t \exp(-\pi f_{lp} t)$. The low-pass frequency f_{lp} is the second fit parameter of the model. This leads to the postsynaptic membrane voltage

$$P(t) = k_{lp} * \left(\frac{dI}{dt} + dI \right) . \quad (3.3)$$

The parameter d allows to include an additional non-derivative component [9]. If d is large the cell has a more primary-like response, whereas for small d the response is more onset type. One finds that for values $d_a < 700\text{Hz}$ the overall response patterns is onset. However a higher values within the above limit improves the entrainment to modulated stimuli. As cells with high SPL-thresholds tend to loose sensitivity to modulated stimuli in the proposed paradigm, higher values of d can be used to compensate.[61]

Spike generation

To derive the spike outputs from $P(t)$, we use a sigmoid function

$$R(P) = \frac{R_{max}}{(1 + Q \exp(\beta(P - \rho)))^{\frac{1}{\gamma}}} \quad (3.4)$$

from which we derive spikes according to a Poisson process. The parameter R_{max} is the maximal firing rate of the neuron and $Q = \frac{R_{max}}{R_\rho} - 1$ sets the firing rate R_ρ at the threshold parameter ρ . $R_{max} = 12000$ Hz is set to fit measured firing probability density when taking into account a refractory period of 2 ms [75]. Further on, we set $R_\rho = 1200$ Hz such that 10% of pure tone stimuli generate an onset spike.

There is little data available on the distribution of SPL-thresholds. However the seem to be in a range of 40 – 60dB. As a default we assume a linear The exact values for ρ are calculated on the fly by generating a short pure-tone-pulse with $f = cf$ on threshold level. If desired, the SPL-threshold can be adjusted differently, without affecting the functionality of the model.

The slope parameters β and γ take values of around $4 * 10^4$ and 2, respectively, for cat-tuned ANFs generating relatively steep tuning curves, which ensures suppression of spontaneous and

sustained firing owing to the non-derivative component from equation (3.3). Furthermore, since in low-frequency octopus cells, the membrane potential fluctuates in only a small interval, the steep slope ($\beta = 4 * 10^4$ compared to d in the order of 10^6) ensures that such a limited range in P is translated to the full dynamic range of R .

The parameters of the sigmoid not only ensure that the model responds reliably and temporally precise to pure-tone stimuli above threshold. The specific choice of the parameters β and ρ was also checked to not introduce unphysiological islands in the receptive fields from Figure 3.2.

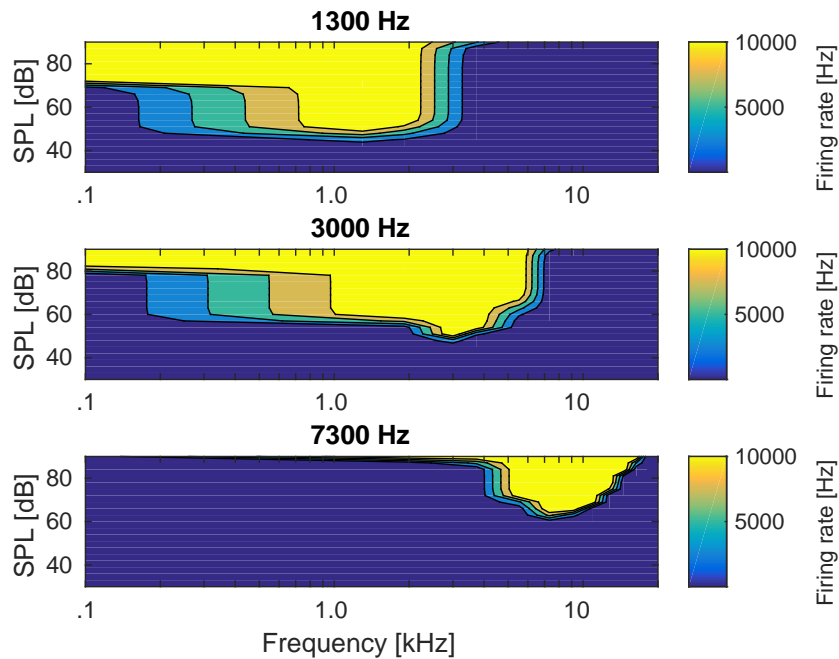


Figure 3.2: Tuning curves for three cells with different best frequencies. Colour-coded are the firing rates for pure tones of different frequencies and sound pressure levels.

Figure 3.3 illustrates the evoked activity of the model for a pure tone stimulus and a sinusoidally amplitude modulated sound stimulus. As by design, the model only fires on the onset of the pure tone, whereas it phase-locks to each cycle of the amplitude modulated sound.[61]

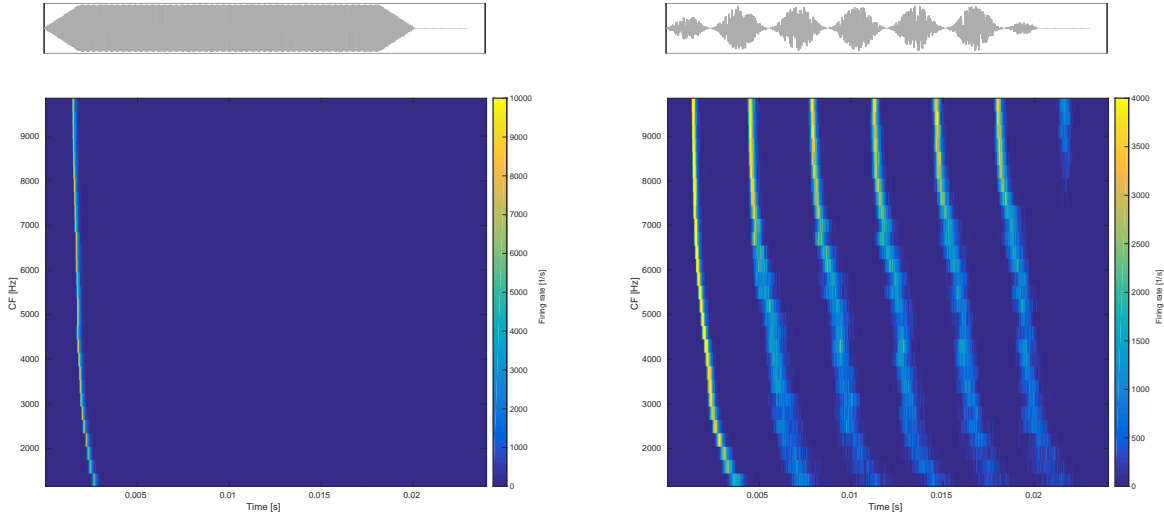


Figure 3.3: Population response. Firing rates (color-coded) of the modeled octopus cells with different characteristic frequencies (on the y-axis) for two representative stimuli (top: grey). Left: Pure tone stimuli of 80 dB SPL with their frequencies matching the characteristic frequency of the octopus cell. Right: Sinusoidal modulated noise stimulus of 20 dB above threshold and a modulation frequency of $f_m = 300$ Hz.

3.1.2 Mathematical analysis

To better understand the model dynamics, we analyse it for an amplitude modulated pure tone stimulus

$$s(t) = \Theta(t - t_0) A(t) \sin(2\pi f_w t) . \quad (3.5)$$

Here, Θ represents the Heaviside function that implements the onset at time $t = t_0$. The stimulus frequency is denoted by f_w . The amplitude $A(t)$ is assumed to vary much more slowly than the sinus term and thus can be taken as constant $A(t) \approx A$ during the period $1/f_w$.

Due to its combination of low pass and band pass filtering the response of a single ANF to a pure tone stimulus (with frequency f) can be approximated as

$$r_i \approx A(t) [a_i(f_i, f) + b_i(f_i, f) \sin(2\pi f_w t)] .$$

with a constant component a_i and the oscillatory component proportional to b_i . With this, equation (3.1) can be rewritten as

$$I = \Theta(t - t_0) A(t) [a_g(f_o, f) + b_g(f_o, f) \sin(2\pi f_w t)] \quad (3.6)$$

with

$$a_g(f_o, f) = \sum_i g_i(f_o, f_i) a_i(f_i, f) \quad (3.7)$$

and

$$b_g(f_o, f) = \sum_i g_i(f_o, f_i) b_i(f_i, f) \quad (3.8)$$

Due to the filtering properties of the periphery model a_i grows with f_i while b_i decays. Since octopus cells receive input mostly from high frequency ANF [76]s, one can neglect the b_g -component of equation (3.6) and simplify it to:

$$I \approx \Theta(t - t_0) A(t) a_g(f_o, f) \quad (3.9)$$

The postsynaptic potential P is mostly governed by the derivative component of equation (3.3) [18]. Thus for simplicilty, in the next paragraph we will assume that $d_a \approx 0$.

Using the input approximation (3.9) for a non-modulated pure tone ($A(t) = A = \text{const.}$), equation (3.3) simplifies to a delta-like postsynaptic response

$$P_{\text{PT}} \approx A k * \delta(t - t_0) a_g(f_o - f). \quad (3.10)$$

Conversely, for an amplitude modulated stimulus, the differentiation of the input approximation (3.9) by equation (3.3) yields an additional additive component extracting the derivative of $A(t)$,

$$P_{\text{SAM}} = P_{\text{PT}} + k * \Theta(t - t_0) a_g \frac{d}{dt} A(t). \quad (3.11)$$

This term $\propto \frac{d}{dt} A(t)$ acts as a modulation detector in our octopus cell model and thus accounts for phase locking to sinusoidally amplitude modulated tones up to a certain modulation frequency (governed by the low-pass kernel k). Therefore, by design, the model can replicate the essential firing characteristics on pure tone and AM stimuli.

What remains open is, how to find the parameters that reliably produce such physiological responses. Since $R_{\text{max}}, Q, \beta, \rho, d_a, \gamma$ are constrained by basic cellular measurements (see above) we next will explore the effect of the two thus far unconstrained parameters k and Δ^2 by simulations.[61]

3.1.3 Simulations

The above considerations leave only two parameters that are not directly constrained by the desired firing pattern.

1. The width of the arborisation Δ (equation 3.1) and
2. the cutoff frequency f_{lp} of the low pass filter in equation 3.3 will be evaluated by simulations shown in Figure 3.4.

Three criteria are monitored in Figure 3.4 to evaluate the quality of a given parameter configuration.

The first criterion (upper panels) is the mean number of spikes for an 80 dB SPL pure tone stimulus at the octopus cell's best frequency (varying along x-axis). A mean spike count of 1 indicates that the cell produces the experimentally reported onset response. A mean spike count of about one is realized for all Δ -values between .4 and 1 and $f_{lp} > 250\text{Hz}$. The exception are cells with very low f_c . These generally show low levels of sustained firing.

As a second criterion we use the vector strength $V = \frac{1}{n} |\sum_{j=1}^n \exp 2\pi i f_m t_j|$ (middle panel), where t_j is the time of the j th spike and n is the total number of spikes. It indicates the cell's ability to phase-lock to sinusoidal amplitude-modulated noise stimuli with a modulation frequency of $f_m = 300$ Hz. High values of V indicate good phase locking and are preferable for choosing parameters. Low values of V are generally only observable for $\Delta < .4$ in the mid-cf range, and for $f_{lp} > 100$ Hz, which would exclude these choices for the two parameters.

A third criterion is the entrainment $E = \frac{n}{(f_m t_{stim})}$ of the response to the stimulus. E can be interpreted as the probability that the neuron fires at a modulation cycle. High values of E are thus desirable. We find generally low values of E at $\Delta > .8$ and at $f_{lp} < 350$ Hz.

As a result of these considerations we suggest the model parameters $f_{lp} = 300$ Hz and $\Delta = .9$, where none of the criteria exhibit extensive regions of low unfavorable values along the f_c axis.[61]

3.1.4 Modulation transfer functions

Figure 3.5 shows the modulation transfer functions of modelled octopus cells with different centre frequencies. With rising modulation frequencies the entrainment goes asymptotically to zero. The vector strength depends more strongly on cf . However, it generally tends to be stable for low modulation frequencies and decrease once the latter grow to large. Overall the model follows modulation up to 500Hz very well and breaks down above that.[61]

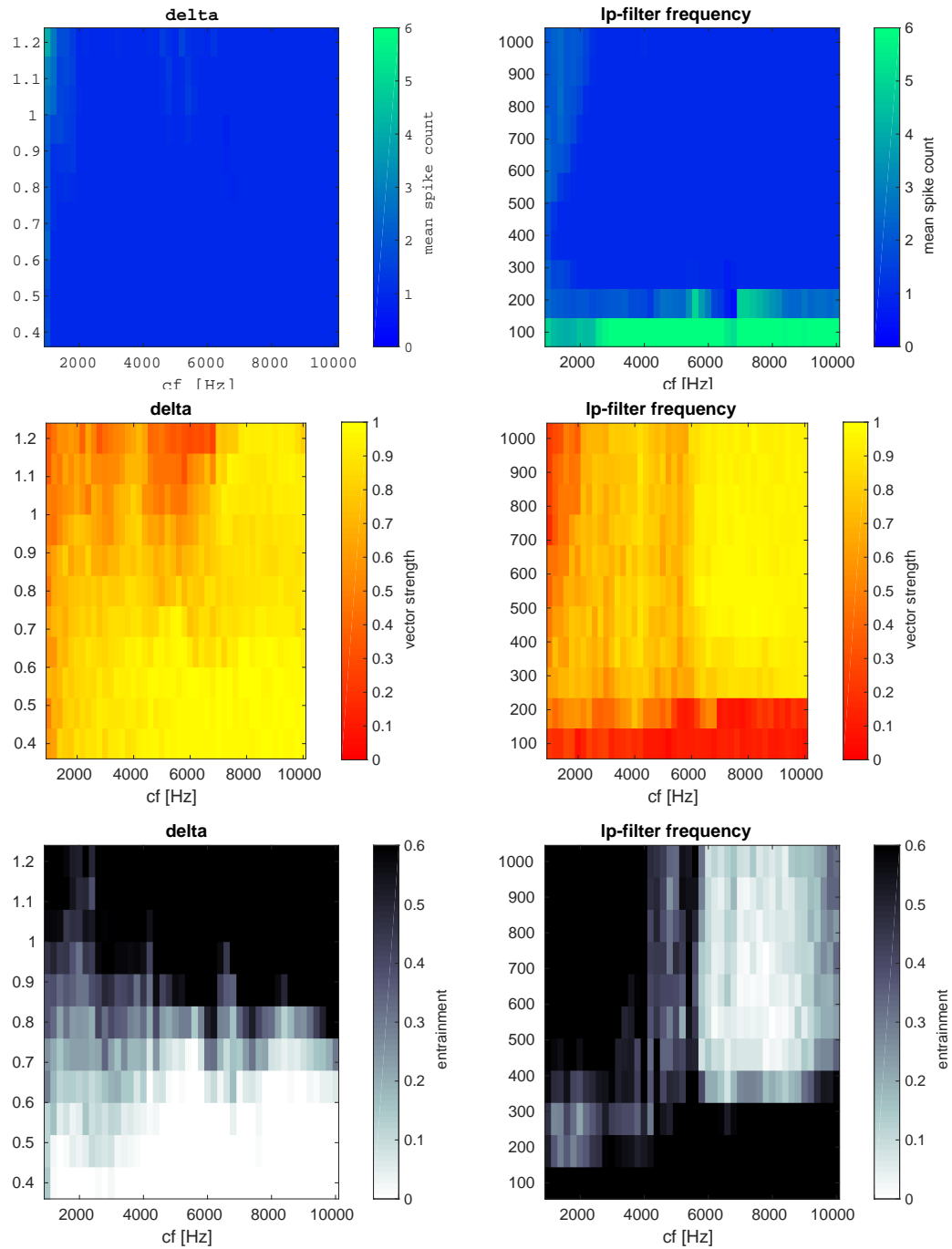


Figure 3.4: Effects of different low pass filter frequencies f_{lp} (left panels) and arborization width Δ (right panels). All x axes refer to the best frequency of the octopus cell. Top: the average number of spikes as response to pure tones (at Best frequency). Middle: Vector strength of the response to sinusoidally amplitude modulated tones (300 Hz modulation frequency). Bottom: Entrainment to the same AM stimulus as in the middle panels.

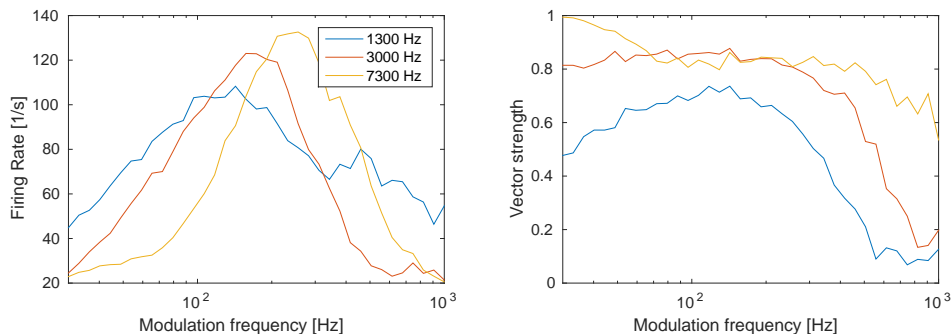


Figure 3.5: Responses of octopus cells with different centre frequencies to sinusoidal modulated noise. The modulation frequency is shown on the x-axis. The left panel depicts the entrainment of the response to the stimulus. The corresponding vector strength is shown in the right one.

3.1.5 Complex Stimuli

To demonstrate the potential of our model for naturalistic sound stimuli, we applied it to two exemplary speech sounds. Figures 3.6 and 3.6 show its results for the speech stimuli “time” and “space” from a male speaker, presented at 50dB and 60dB SPL.

The qualitative observation from these plots is that the octopus cells fire selectively on sharp transients, the strong modulations as well as parts of the stimulus with a locally broad spectrum. Cells with different center frequencies thereby select different parts of the stimuli with an overall trend for lower firing probability at higher center frequency. It is noteworthy that the regime where a sustained firing to phonemes with a broader spectrum ceases coincides with pure tone threshold discussed above rises above the stimulus intensity.[61]

3.1.6 Discussion

Owing to the high technical challenges in both in-vivo and in-vitro physiology preparations, octopus cells, despite their putative crucial role in the processing of natural sounds [64],[52], have not been investigated to a similarly large extent as other cells in the ascending auditory brainstem, like, e.g. bushy cells, or MNTB and SOC principal cells. We therefore still have a very incomplete picture on how the octopus cell pathway processes sound. Here, we present a modelling approach complementing detailed physiological studies and propose a phenomenological computational model for a population of octopus cells. The model is constrained by the well-studied responses of octopus cells

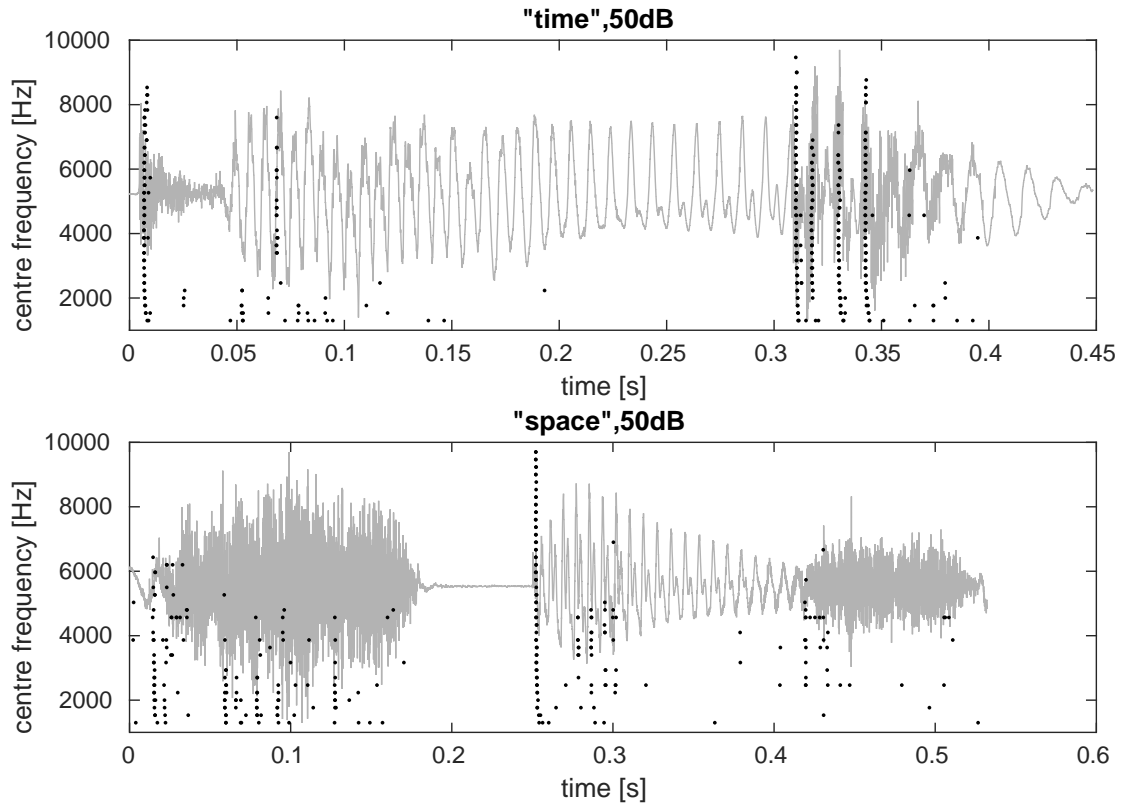


Figure 3.6: Raster-plot of the model's spiking behaviour when applied to speech signals of 50dB SPL. The upper panel depicts the word "time" the lower one the word "space". The y-axis shows the centre frequency of the octopus cell. In the background (grey), the waveform is shown for temporal comparison.

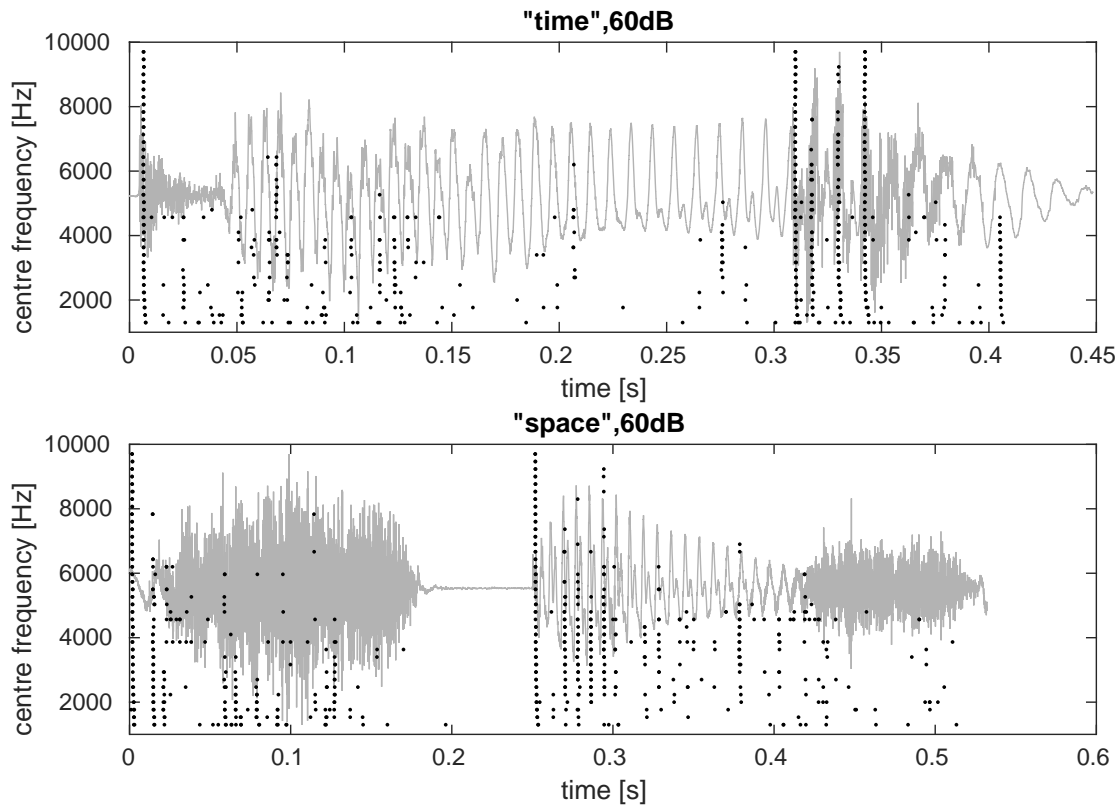


Figure 3.7: Raster-plot of the model's spiking behaviour when applied to speech signals of 60dB SPL. The upper panel depicts the word "time" the lower one the word "space". The y-axis shows the centre frequency of the octopus cell. In the background (grey), the waveform is shown for temporal comparison.

to pure tones and amplitude-modulated noise and implements their basic known physiological operation of a differentiation. Such a phenomenological approach allows to test functional hypothesis on large sets of natural stimuli and thereby generate hypotheses for follow-up experimental studies.

In preliminary test, we have shown that the model responds strongly and selective to naturalistic stimuli (Figures 3.6 and 3.7). Due to an abundance of sharp transient and strong modulations, speech seems to be a suitable test bed. These preliminary results support the long standing believe that octopus cells are involved in the processing of conspecific vocalisation ([10]).

The necessity for the highpass filter arises from the fact that high intensity tones with $f < 1000\text{Hz}$ evoke a strong responses even in modeled auditory nerve fibers of multiple kHz, bypassing adaption in low pass filtering to a large degree. Due to the combination of the differential kernel and low pass filtering in the octopus cell model, a strong signal is elicited there as well. It is unclear if this is because of numerical imperfections. Another possibility might be a oversimplified sampling. Additionally, octopus cells loose modulation sensitivity. Because of the differentiation of the octopus cells and short term depression in the auditory nerve fibers, the onset potential that determines the thresholds grows faster the the potential evoked by the modulated stimuli. Taken together this could also hint towards a non-linearity in the octopus cells' synapse that dampens fast high intensity inputs that has not yet been fully understood [61].

3.1.7 Additional Notes

Given the speed and precision of the studied system, it is tempting to tune the octopus cell model towards high frequencies by including strong high-pass- and weak low-pass-filters. And in fact, this yields similar results to those seen in figure 3.3. However, deeper investigation revealed that driven in these configurations the model actually detects the high frequency fluctuations of the noise carrier, riding the modulations, not the modulations directly. Therefore, the modulation detection breaks down when stimulating with modulated pure tone carriers, as these are lacking said random fluctuations. Potentials evoked by this class of stimuli would be entirely subthreshold. In contrast, the model, presented above and ultimately used, features a low pass filter of a higher order as well lower cutoff frequencies for all filters involved. Figure 3.8 shows its final results when stimulated with a modulated pure tone.

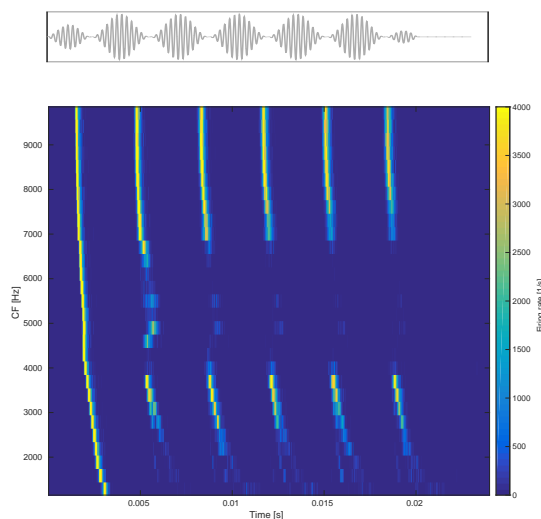


Figure 3.8: Population response to Sinusoidal modulated noise stimulus of 20 dB above threshold and a modulation frequency of $f_m = 300$ Hz. Depicted are firing rates (colour-coded) of the modelled octopus cells with different characteristic frequencies (on the y-axis). An example stimulus is shown in the top panel.

The model as presented here yields the expected results for most of the frequency range. This is achieved by balancing the high- and low-pass aspects of the model against each other. The differential kernel acts as a high pass filter, as well, which is compensated by the second order low-pass-filter and a larger non-differential component. Additionally, it is necessary to carefully adjust the sampling width. It is usually set to 1.3Δ to achieve a good compromise between sampling range

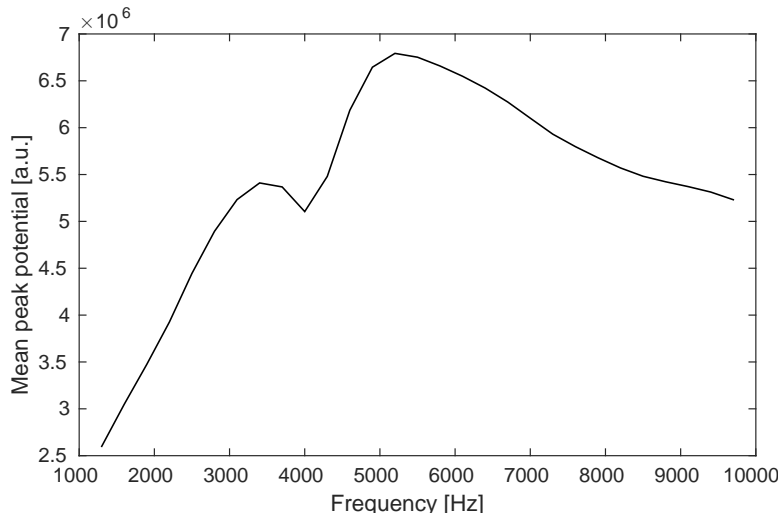


Figure 3.9: Mean response for stimulation with pure tones of different frequencies (on the x-axis). The y-axis shows the mean peak potential for a range of octopus cells equal to the stimulation range.

and density as well as computation efficiency (only nine ANFs have to be computed). The modulation of a pure tone carrier is transmitted in two frequency bands adjacent to the centre frequency, while the noise carrier is detected at the entire frequency range.

The latter aspect is the indirect cause for the lack of responsiveness in the frequency range between 4 and 7 kHz. The immediate cause can be inferred from figure 3.9. The responsiveness of the octopus cells to pure tones varies for different stimulation frequencies and shows a maximum at around 5400 Hz and a minimum at 4200 Hz. Because of this, the equilibrium between onset and phase-locking response is broken. A high onset responsiveness leads to a high threshold and consequently to a suppressed phase locking response and vice versa for a low onset responsiveness. In the model, this is remedied by adjusting the widening or narrowing the sampling range respectively, thereby adjusting the sampling density. Since the frequency bands transmitting sinusoidal modulations of a pure tone carrier are distinct and rather narrow, these are not represented well enough.

Assuming these strong variations in responsiveness are physiological, this problem is tied into another minor inconsistency. Due to the interplay between the dynamics of the ANFs and the differential kernel, the pseudopotential shows nonmonotonous behaviour to variation in sound pressure levels of the stimuli. This effect can mostly be compensated by the proper adjustment of the non-

differential component and the sigmoidal spike generator. Together, both effect could point to an additional synaptic effect not accounted for in this model, such as lateral inhibition, that acts as an equaliser on the synaptic input.

3.2 Synaptic connection

This section is based on the results from a collaboration with Linda Fischer and Felix Felmy from the the University of Veterinary Medicine Hannover, who investigated the properties of the synapses connecting the octopus cell area in the PVCN with the VNLL in great detail [19]. Determining the consequences of these properties on the response patterns of the VNLL onset cells is a major focus here. In particular, this study will investigate the roles of a weaker and slower NMDA current, in contrast to solely AMPA driven cells, as well as the consequences of short term synaptic depression and facilitation.

3.2.1 Currents

Two distinct types of currents have been recorded in the PVCN - VNLL synapse. As outlined in 1.2.2 those currents differ widely in amplitude and speed. Compared to currents mediated by AMPA receptors, NMDA mediated currents have an amplitude being an order of magnitude smaller but working on a much longer time scale. To model the synaptic currents we use a modified but otherwise common double exponential kernel:

$$K_c = A \left(e^{\left(\frac{t-t_0}{\tau_{\text{grow}}}\right)} - e^{\left(\frac{t-t_0}{\tau_{\text{decay}}}\right)} \right),$$

where A are the corresponding amplitudes, t_0 governs the offset while the time scales τ_{grow} and τ_{decay} determine the currents' shapes. Figure 3.10 shows the AMPA and NMDA currents and the fitted model. The model faithfully represents the fast and strong AMPA current as well as the slow and weak NMDA current with the corresponding parameters shown in table 3.1. The vast differences of the current types gives rise to the question of the interplay between the types and their effect on the VNLL response. This will be investigated in detail below.

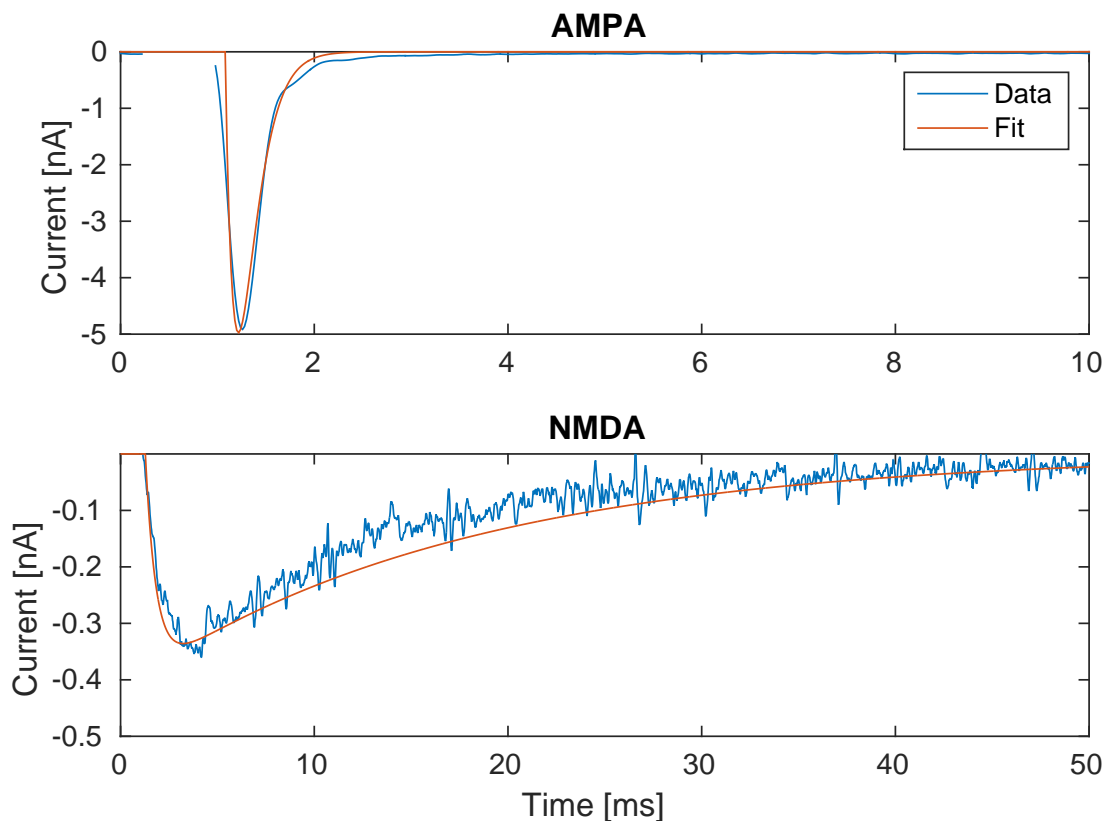


Figure 3.10: Comparison of the measured currents mediated by AMPA and NMDA receptors and the model fits.

3.2.2 Synaptic effects

Aside from the additional NMDA current, this study will investigate the effects of short term depression and facilitation on the response patterns of the VNLL cells. Both properties are modelled together following the paradigm outlined in 2.2. The results, in comparison with experimental data from [19] are depicted in figure 3.11 using the fitted parameters given in table 3.2. In cases where only short term depression, but not facilitation were observed, $f = 0$ is set, which yields $P_n = p_{min} \forall n$. Figure 3.11 shows the spike amplitudes for strictly periodic stimuli of various frequencies. The amplitudes are normalised to the first action potential elicited.

Similar to the depiction in figure 3.11, the model can be normalised by setting $R_0 = 1$. The fit matches the data well. However, the data is more diverse in the area of facilitation and when

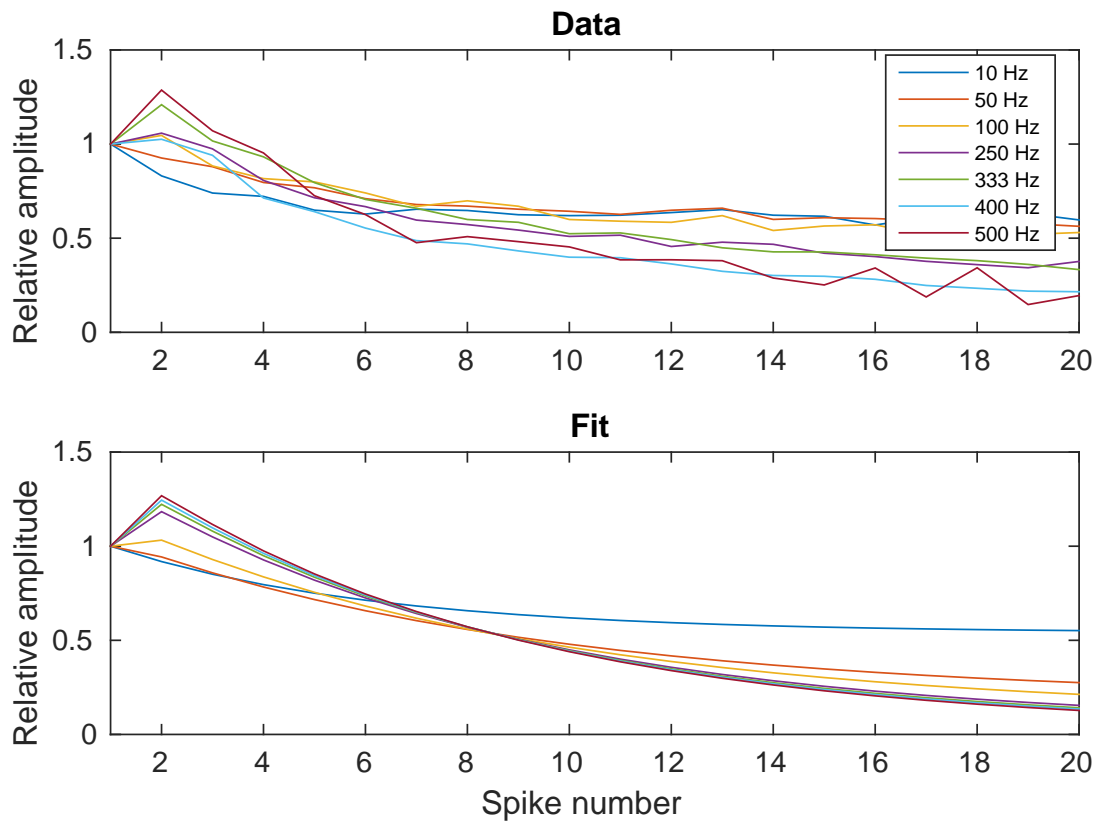


Figure 3.11: Normalised amplitude of action potentials elicited by periodic stimulation with different frequencies (colours). The top panel shows the experimental data, the bottom one the corresponding fits.

	AMPA	NMDA
A	1.166 mA	3.883 nA
t_0	1.121 ms	1.342 ms
τ_{grow}	0.1363 ms	10.92 ms
τ_{decay}	0.1379 ms	1.071 s

Table 3.1: Parameters for the current fits.

f	0.978
p_{max}	0.0807
p_{min}	0.0609
τ_P	10.9 ms
τ_R	1.07 s

Table 3.2: Parameters for the current fits.

approaching the steady state with respect to the stimulation frequency. This could be remedied by the involvement of an additional time scale, which in turn could suggest a missing reservoir in the simple model above.

3.3 VNLL onset cells

At this point, the question presents itself if the firing behaviour of the onset cells within the VNLL can be explained solely by the afferent octopus cells. This study will follow [5] and assume a pair of octopus cells converging on a single onset neuron in the VNLL. That expands the aforementioned question to how octopus cells with different CF interact.

The neurons of the VNLL are modelled using a common leaky-integrate-and-fire approach, as described in 2.3, using physically plausible values. Following the arguments laid out in 1.2.3 the firing threshold is adjusted to not fire reliably in response to a single incoming action potential but to respond perfectly when the amplitude is raised by a factor of 1.2. This ensures that the simulated cell requires a certain level of coincidence, but not perfect synchrony, to function.

To investigate the dynamics of interaction and integration, an array of octopus cells within the interval of 1 and 10 kHz is deployed and every possible doublet permutation thereof is simulated. Consequently, n octopus cells give rise to n^2 putative VNLL onset neurons.

3.3.1 Test stimuli

At first, the basic firing properties will be determined using by probing the model with pure tone stimuli and sinusoidal modulated broadband noise. In accordance with the established characteristics of the cells, in the first case the onset spikes will be observed while in the latter case the responses to the modulation are of interest.

Onset response

To gauge the onset response, the cells are stimulated by a pure tone at 80 dB SPL with a frequency of $f = .5 * (CF_1 + CF_2)$, where CF_1 and CF_2 are the centre frequency of the constituent octopus cells. The high intensity of the stimuli ensures that the octopus cells' receptive fields are close to their maximum width, which in turn results in the upper limit of interactivity between octopus cells.

Figure 3.12 shows the probabilities of a population of simulated VNLL cells to elicit an onset spike, when stimulated with pure tones according to the paradigm outlined above. It depicts the six observed configurations. The left column only include the AMPA currents while the right column takes the additional NMDA current into account. On the top row no further synaptic effects are applied. The middle row allows for short term depression, the bottom row, finally, adds facilitation as well. In the most basic case (top left panel), where only AMPA currents and no synaptic effects are taken into account, the VNLL cells respond on a large portion of the observed frequency space about two octaves around the diagonal. This result is consistent with the widening of the receptive fields towards higher frequencies observed in ANFs as well as octopus cells. However, there is an indenture for very low frequencies, which is due to the delay differences depicted in Figure 3.3. Including NMDA currents removes this gap. Apart from that, the cells close to the fringes of the operational area become more reliable. The operational area itself gets wider only very slightly. Including short term depression and facilitation does not change the results (middle and bottom column). This is consistent as the afferent spike trains are supposed to only consist of a single onset spike which does not trigger either effect. Because of this, table 3.3 only shows the mean values for two configuration. The standard deviation, as a measure of homogeneity, are listed,as well.

VNLL onset cells are distinct by having near constant onset latencies [15, 62]. Figure 3.13 shows the mean time of the onset spike follow the same probing scheme as above. Again, different configurations including the additional NMDA currents (left columns), short term depression (middle row) and facilitation (bottom row, including depression as well) are depicted. However,

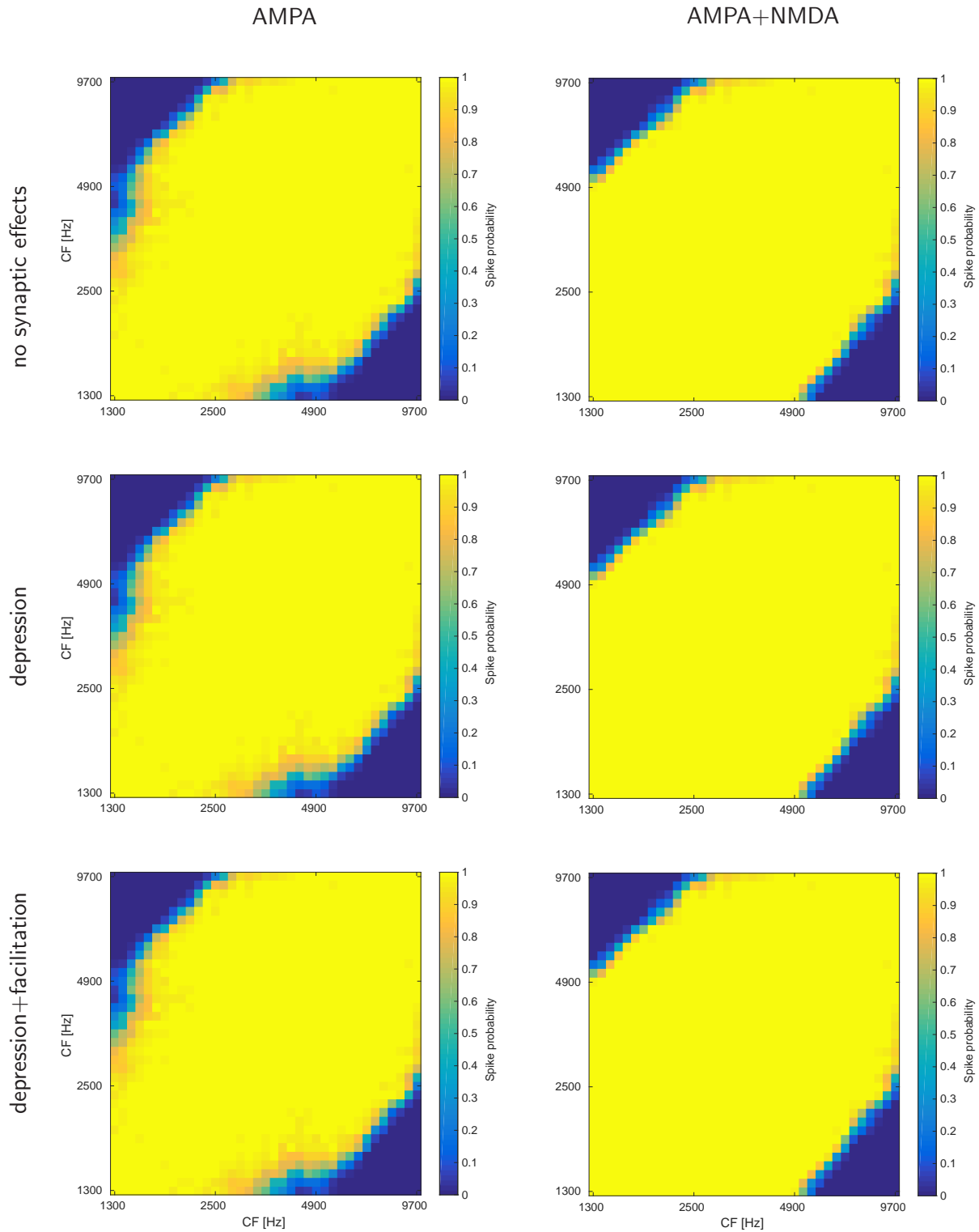


Figure 3.12: Population response of VNIL cells to pure tone stimuli. Depicted are the probabilities to elicit an onset spike (colour coded) in relation to the afferent octopus cells (x- and y-axis, logarithmic scale). Left panels only include AMPA currents, right panels take NMDA currents into account. Top: No synaptic effects. Middle: With short term depression. Bottom: With short term depression and facilitation.

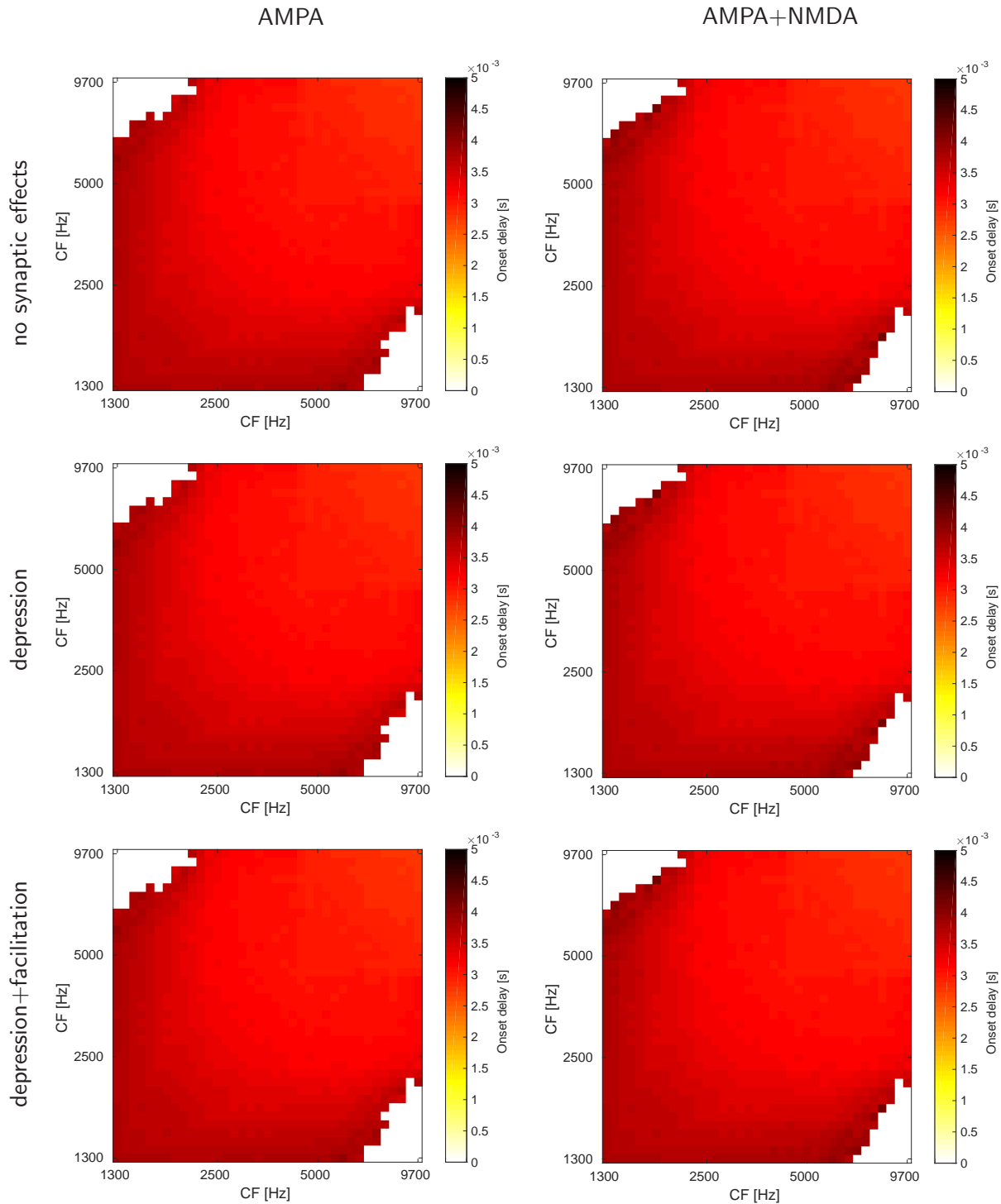


Figure 3.13: Population response of VNLL cells to pure tone stimuli. Depicted are the mean latency of the onset spike (colour coded) in relation to the afferent octopus cells (x- and y-axis, logarithmic scale). Left panels only include AMPA currents, right panels take NMDA currents into account. Top: No synaptic effects. Middle: With short term depression. Bottom: With short term depression and facilitation.

	AMPA only	AMPA+NMDA
firing probability	0.845 ± 0.142	0.878 ± 0.137
onset delay	3.0 ± 0.16 ms	3.1 ± 0.16 ms

Table 3.3: Mean firing probability and spike times, with the respective standard deviations, for the onset response to a pure tone stimulation over the entire population.

none of these show any change in the results. In case of the synaptic effects (middle and bottom row) this is to be expected as those effects are not supposed to be triggered in the case of pure tone stimulation, analogues to the above. The lack of effect of the inclusion of NMDA currents hints towards the fact, that even where the NMDA currents improve the reliability of the onset response, the additional spikes are consistent with those elicited due to AMPA currents only. For all six configurations, the latencies are within 0.6 ms at about 3.1 ms, the mean values are shown in table 3.3. The small elevation, when NMDA mediated currents are taken into account, can be attributed to the slight widening of the responsive area as the responses of the fringes are slower to respond. However, a dependence on the constituent octopus cell *CF*s is obvious. On first glance, this seems to conflict with the near constant delays observed experimentally. This line of argument, however, disregards the non-surjective properties of the mapping from the octopus cell *CF*s on the VNLL cell’s best frequency, i.e. two VNLL cells can have the same best frequency but an entirely different constituent configuration and therefore different latencies. If this is taken into account, the aforementioned dependency would translate to a slight tendency to decrease with rising best frequencies of the VNLL cells. This, in turn, is consistent with the experimental data [15]. The mean value as well as the deviation of the delay is below the experimentally observed values. Since the model as presented here does include neither travel times nor random noise, except from the poison process, this is to be expected.

Phase locking response

The second observed set of test stimuli, analogous to 3.1, will consist of sinusoidal modulated broadband noise carriers with fixed $f_m = 300$ Hz.

Herein it is assumed that the VNLL cell requires more than a single incoming action potential to elicit a new action potential in return. Consequently, it appears counter-intuitive that the VNLL cells would exhibit levels of entrainment, the fraction of modulation cycles that elicit an action potential, similar or even exceeding those of octopus cells (compare for example [63] and [87]). The direct line of thought would yield that the VNLL cells only become active in cycles

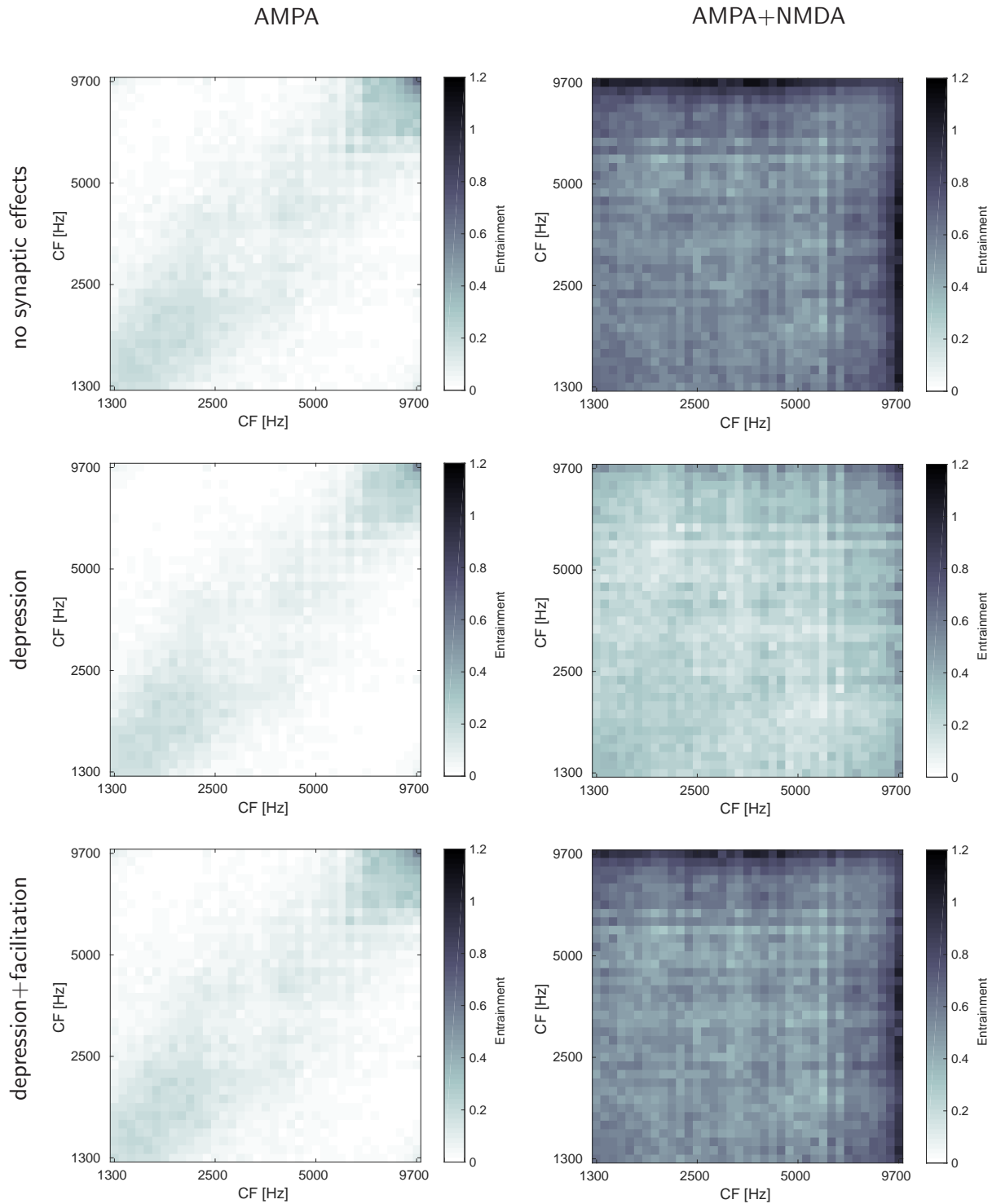


Figure 3.14: Population response of VNLL cells to pure tone stimuli. Depicted is the entrainment to sinusoidal amplitude modulated noise (colour coded) in relation to the afferent octopus cells (x- and y-axis, logarithmic scale). Left panels only include AMPA currents, right panels take NMDA currents into account. Top: No synaptic effects. Middle: With short term depression. Bottom: With short term depression and facilitation.

	AMPA only	AMPA+NMDA
no synaptic effects	0.0704 ± 0.0634	0.597 ± 0.137
short term depression	0.0574 ± 0.0604	0.264 ± 0.0939
depression and facilitation	0.0675 ± 0.0579	0.514 ± 0.127

Table 3.4: Entrainment to sinusoidal amplitude modulate noise averaged over the entire population of VNLL onset cells with standard deviation.

where both incoming octopus cells are, which, in turn, would result in lower entrainment values. Figure 3.14 shows the entrainment in relation to the constituent octopus cells; again for the six configuration as above. And indeed, taking only the AMPA currents into account (left panels) yields only marginal levels of phase locking response. Introducing short term depression (middle left panel) on these levels changes little. The bottom left panel shows the effects of facilitation. It causes a slight raise in entrainment. Here, the NMDA mediated currents have a significant impact (right panels). Without synaptic effects (top panels) it is obvious that the additional currents improve the phase locking response significantly. Consistent with the experimental data, it even exceeds the octopus cell's response in parts. Instead of coincidental firing of both afferent cells, the accumulated NMDA currents cause every spike from either octopus to elicit an VNLL action potential in return. This however creates a limit for the dynamic range. Due to shorter delay for high frequency cells (compare figure 3.3), cells with too different CF (greater than 1.5 octaves) produce entrainment of > 1 . Cycles that excite both octopus cells are, in part at least, registered twice in the VNLL cells. At this point it is unclear if this boundary condition is physiological or if the natural cell corrects for this, using an effect not accounted for in this model. The mean values and standard deviations for all six configurations, averaged over the entire population, are shown in table 3.4. The synaptic effects illustrate the somewhat fragile balance of the VNLL cells. As discussed above, without the NMDA current the phase locking response is marginal. Including the short term depression in the model (middle panel) again disrupts that balance and reduces the entrainment again. However, this effect is weaker than the rise induced by the NMDA current, resulting in still elevated entrainment levels. Finally, the facilitation (bottom right panel) seems to completely counteract the short term depression on average. Therefore, the NMDA mediated currents are required for the VNLL cells to respond as expected to amplitude modulated stimuli, the facilitation in turn stops the short term depression from affecting the entrainment significantly.

The entrainment to sinusoidal amplitude modulated noise has to be investigated in conjunction with the synchronicity of the response to evaluate the firing patterns of the VNLL cells. Figure 3.15

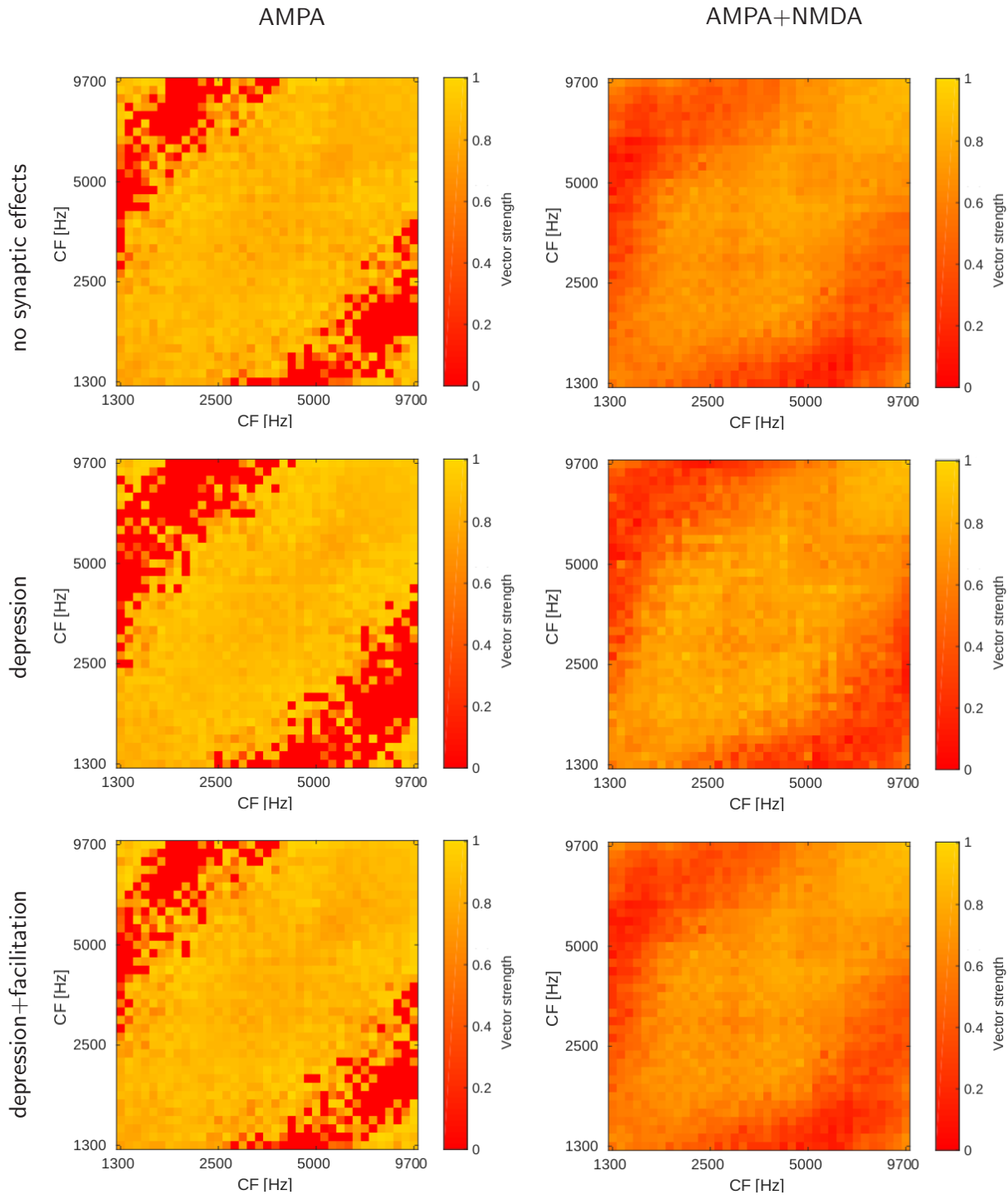


Figure 3.15: Population response of VNLL cells to pure tone stimuli. Depicted is the vector strength of the response to sinusoidal amplitude modulated noise (colour coded) in relation to the afferent octopus cells (x- and y-axis, logarithmic scale). Left panels only include AMPA currents, right panels take NMDA currents into account. Top: No synaptic effects. Middle: With short term depression. Bottom: With short term depression and facilitation.

	AMPA only	AMPA+NMDA
no synaptic effects	0.624 ± 0.320	0.588 ± 0.287
short term depression	0.5897 ± 0.357	0.603 ± 0.301
depression and facilitation	0.639 ± 0.327	0.578 ± 0.289

Table 3.5: Vector strength of the response to sinusoidal amplitude modulate noise averaged over the entire population of VNLL onset cells with standard deviation.

shows the mean vector strength over 130 runs for all six configurations and an array of possible afferent octopus cells. The vector strength as a criterion for synchronicity is defined as $V = \frac{1}{n} |\sum_{j=1}^n \exp 2\pi i f_m t_j|$, where j is the spike index, n is the total number of spikes in the spike train and finally t_j are the individual spike times. The calculation is adjusted to yield a result of 0 for if no phase locking response is registered; these are not factored in the mean calculation either. Onset spikes are removed beforehand. If only AMPA mediated currents are taken into accounts (left panels), the area of effect is less than an octave wide. The achieved values are very close to one. This is due to the fact, that most spike trains consist at most of a single spike past the onset. These cases result in a contribution of $V = 1$. This results in a trade off between entrainment and synchronicity. Consequently, the vector strength is diminished closer to the diagonal, compared to those values farther on the edge of the field of effect. With only the AMPA currents in effect, coincidental firing is required for the VNLL cell to become active. Taken all this together means that the vector strength values have little explanatory power. They do, however, illustrate again the area of possible coincidences between the incoming octopus cells. The top left and bottom right corners show a weak but existing signal. In this area the delays are large enough for the responses to different cycles of the stimulus to interact. Introducing short term depression (middle left panel) and additionally facilitation (bottom left panel) does not change the results. Given the the entrainment results discussed above, this is not surprising. It is equally unsurprising that adding NMDA mediated current does result in significant change, as depicted in the right panels of figure 3.15. The values lower when compared to the left panels but that can be explained by the trade off elaborated upon above; this effect is more obvious for the mean vector strengths shown in table 3.5. Still, the VNLL responses show high values of synchronicity. It again shows the same area of effect of around 1.5 octaves around the diagonal. The values slightly rise due to the short term depression (middle right panel). However, analogous of the above, this is undone again by introducing facilitation (bottom right panel).

The results shown in figures 3.14 and 3.15 show that integrating over octopus cells alone enable

VNLL cells that show firing behaviour closely emulating the experimentally determined data. Apart from that, they allow for two conclusions already. On one hand, it became obvious that the NMDA mediated currents are essential for the faithful representation of amplitude modulated currents. On the other hand, a boundary of the area of effect could be established. Octopus cells can interact well within a range of 1.5 octaves, slightly varied by the frequency range of the afferent octopus cells. A wider area of effect would be advantageous from a efficiency driven point of view, allowing for a stronger and more diverse population response with a lower number of necessary octopus cells. This area of effect is limited by the difference in delay of the octopus cell responses depending on their CF . For the short stimuli used to probe the modelled VNLL cells the short term depression and facilitation cancel each other out on average. Apart from that, no functional relationship between the synaptic effects and the firing behaviour could be established, at this point.

3.3.2 Complex stimuli

While probing with simple test stimuli, such as the above, is useful in classifying the neurons or neuronal systems by their basic firing behaviour it can only convey limited understanding about the system's role in the analysis of complex acoustic environments. One great advantage of the modelling approach is that the selection and the number of stimuli used is not limited by experimental practicability and laboratory conditions. As an example for complex natural sounds, human speech is used here to study the modelled system and its response properties. Testing with stimuli such as these might provide a deeper insight into the function of the system as a whole and the additional effects already discussed above.

Figure 3.16 shows the mean response of an array of VNLL onset neurons to the sample sentence "*All the world's a stage.*" by a female speaker, presented at 50dB. To get the mean population response octopus cells are simulated in a frequency range from 1 to 10kHz, spaced logarithmically. Averaging is done over all VNLL onset neurons generated from every possible combination of two afferent octopus cells. Following the same pattern as was used above, the left panels show the responses if only AMPA mediated currents are taken into account while the right panels include NMDA currents, as well. The synaptic effects are applied consecutively. The top panels show the responses without additional synaptic effects. The middle panels take into account short term depression, while for the bottom panels facilitation is applied as well. For each case the firing rates are of orders of magnitude between $1\frac{1}{5}$ and $10\frac{1}{5}$. These low firing rates hint towards the high selectivity of the cells. This is directly inherited from the octopus cells and, therefore, not

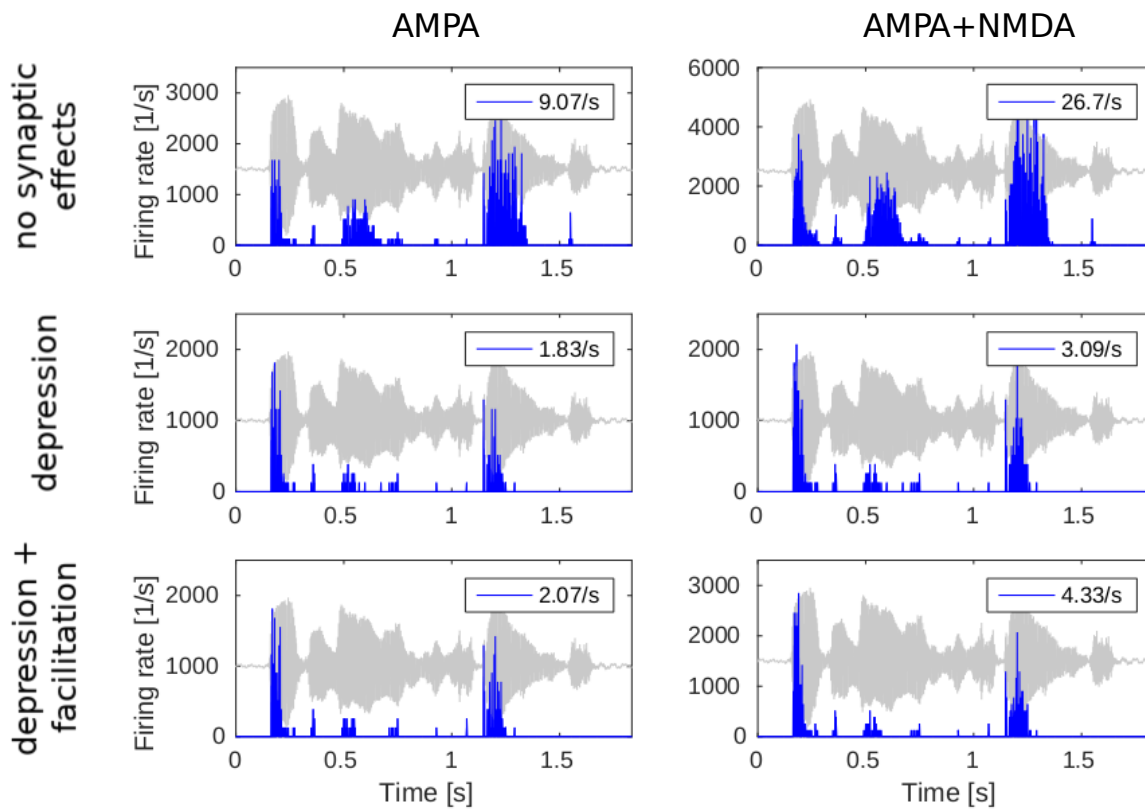


Figure 3.16: Mean response of an array of VNLL onset neurons to a human speech sample. In the left panels cells receive only AMPA currents as input while the right panels take NMDA currents into account as well. Top: No synaptic effects are applied. Middle: Short term depression is taken into account. Bottom: Short term depression as well as facilitation are considered. The waveform of the stimulus is included in grey for comparison. The inlay gives the mean firing rate over the entire stimulus.

unexpected. Starting at the top left panel, VNLL onset neurons show a preference to fire at phoneme onset. While the responses to different segments of the stimulus are more or less pronounced on a population level. For some phonemes (e.g. around 1.2s to 1.4s), this effect is strong enough for the population to show almost primary-like behaviour, i.e. following the waveform more or less faithfully. At these points, the simulated responses seemingly conflict with the assumption that the observed system generates precise temporal markers of sorts. This type of behaviour is suppressed almost entirely by including short term depression, as shown in the middle left panel of Figure 3.16. Some smaller islands of activity disappear entirely while the remaining ones are far more narrow with respect to the time-axis. This gain in precision, however, comes at a cost. The mean firing rate drops severely. It is likely that every single VNLL cell only responds to a fraction of the stimulus. This hints towards a trade-off between precision and reliability, which is reminiscent of a similar trade-off, shown above, between entrainment and vector strength in case of stimulation with sinusoidal amplitude modulated stimuli. Contrary to these (as shown in Figures 3.15 and 3.14) facilitation does not cancel the effects of short term depression (bottom left panel). The qualitative changes induced are preserved and the overall response and therefore the reliability is enhanced. Including NMDA mediated currents more than doubles the mean firing rate if no synaptic effects are included. The trade-off mentioned above still seems to be in effect and the responses show very long islands of activity up to 0.3s. This, again, equates to a severe reduction in precision. The changes induced by short term depression are analogue to the "AMPA-only" configurations shown in the left panels. Consistently, the only major difference due to the added NMDA currents is an improved mean firing rate. The same can be said if one further includes facilitation. The narrowing of the firing windows is maintained while the overall strength of the response is enhanced.

The responses to speech stimuli show that the observed effects, short term depression, facilitation as well as NMDA mediated currents, do not interfere with or cancel each other, as it appeared in the results above. Rather, they complement each other. Only when stimulated with the more complex stimuli used here, the potential of the interplay between these effects becomes apparent. The expectation of precise and reliable spiking can only be fulfilled due to the qualitative changes induced by the short term depression and the quantitative recovery due to facilitation and the added power of the NMDA mediated currents.

Studying the responses to more complex stimuli has already conveyed deeper insight into the interplay of the synaptic effects and the different types of current. Analysing the responses on another level, using information theoretical tools, could provide an even deeper understanding of the function of the system and its individual components. To improve the reliability of the following

analyses a longer stimulus is advantageous. This will also make sure that most properties of human speech are captured. Therefore, from here on, the stimulus used will be the first act of "The Importance of Being Earnest, A Trivial Comedy for Serious People", written by Oscar Wilde. It is around half an hour long and features two male and two female speakers (a third male speaker contributes only very little). Again, it will be presented at 50 dB SPL.

Figure 3.17 shows the distribution of the information transmission over frequency bands for all six configurations; analogue to the preceding figures. Inlaid are the total information transmission rates for each panel, calculated as $R_I = \int Idf$ ([7]). Following the methods outlined above, in 2.4, upper and lower bounds of the information transmission are determined using the Gaussian channel and the linear filtering approach, respectively. However, both are almost indistinguishable. This is due to the low levels of randomness intrinsic to the Poisson point process and the lack of additional noise. Therefore, only the average is presented to improve the clarity of the depiction. The general shape of the frequency distribution of the information transmission, without synaptic effects, combines low pass and band pass characteristics (top panels). The cut-off frequency of the low pass filter is of the order of magnitude of 10^0 Hz while the band pass component has its maximum between 10^2 Hz and 10^3 Hz. The inclusion of NMDA currents (right panels) does not change the shape information transmission function only the absolute values are raised. This is due to the increased firing induced by the additional current component (compare figure 3.16). Including short-term depression, however, reveals a bimodal distribution with maxima of the orders of magnitude of 10^0 Hz and 10^2 Hz, respectively. Again, facilitation only raises the absolute values because of the additional spikes (lower panels).

Comparing the information transmission function of figure 3.17 with the response pattern to human speech in figure 3.16 might offer further insights into the former. The latter shows unevenly spaced islands of activity with a mean $\Delta t \approx 0.25$ s. The exact times of and differences between these islands of activity are stimulus dependent. However, given the structure of human speech, the order of magnitude can be expected to remain the same. The islands appear to mark certain phonemes, which have an average duration between 0.1 and 0.2 s. However, the model does not respond to every phoneme. This, in turn, would correspond to a frequency of the order of magnitude of 10^0 Hz. Therefore, it stands to reason, that the first peaks in figure 3.17 represents the time differences between those islands of activity. Conversely, the second peaks contain information about the internal structures of the islands and the stimulus components represented by it. Given the spectral properties of human speech, these are most likely founded of the residues of the formant structures contained in the stimulus.

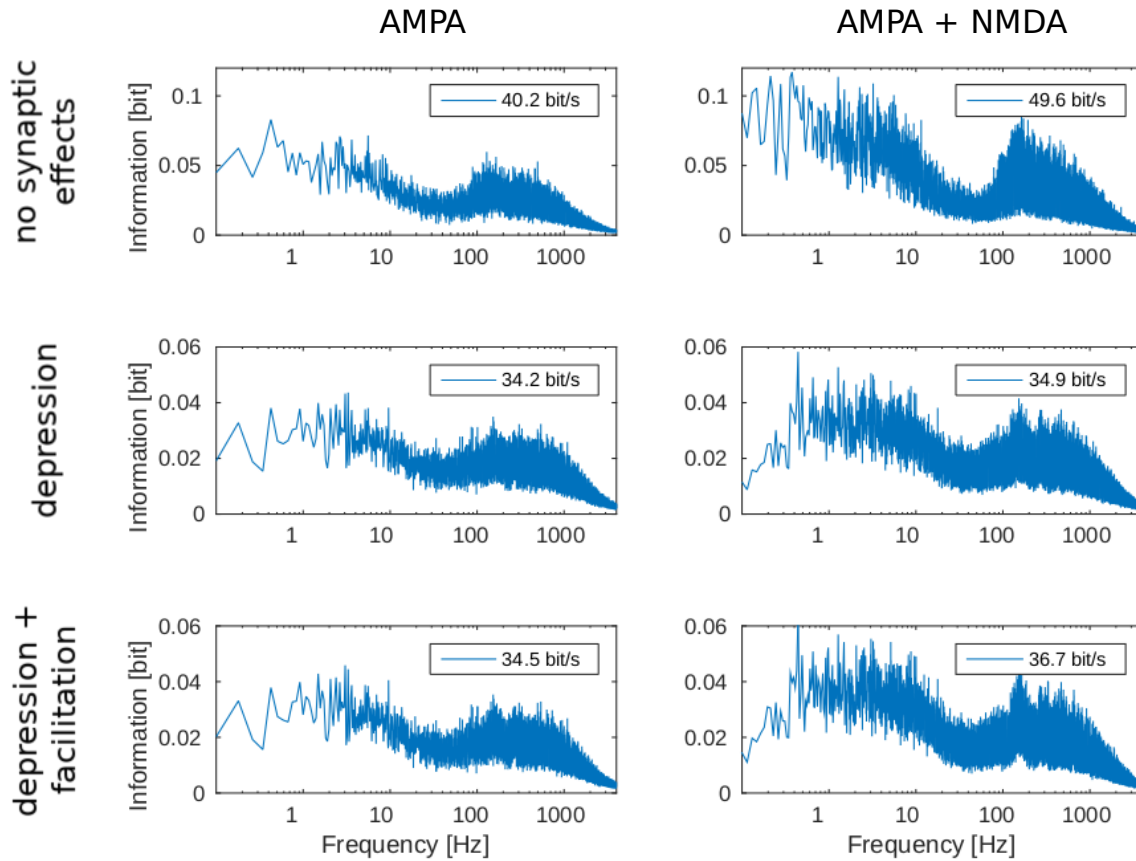


Figure 3.17: Mean information transmission of a VNLL onset cell population per frequency band. Inlaid are the rates of information transmission. In the left panels cells receive only AMPA currents as input while the right panels take NMDA currents into account as well. Top: No synaptic effects are applied. Middle: Short term depression is taken into account. Bottom: Short term depression as well as facilitation are considered. The waveform of the stimulus is included in grey for comparison. The inlay gives the mean firing rate over the entire stimulus.

Comparing figures 3.16 with figure 3.17 reveals another effect the synaptic properties have on the information transmission. While the average strength of the response is sharply curtailed by short-term depression and enhanced by NMDA currents, these effects are reflected in the information transmission to a much smaller degree. While the individual peaks follow the responses more faithfully the local mean values change less, leading to an improved efficiency in information transmission.

Up to this point, The studies of the responses to human speech have revealed, that the system, due to its special properties, strikes a balance between temporal precision and reliability as well as has a very efficient information transmission on a single cell level. The latter aspect works in sync with enhanced population response shown before, as high efficiency on a single cell level allows for a larger population without an additional demand of resources. This immediately raises two further questions. One about the encoding of the information and one about the individual responses of the population as well as the effects of the synaptic properties. In order to answer the first question, figure 3.18 shows the rate information. This contrasts with figure 3.17, which includes the entire information content. The rate information is assessed by dividing the spike train into discrete time windows (in this case $\tau = 0.4\text{s}$) and calculating the mean firing rate in each window as $r_i = \frac{n_i}{\tau}$, where n_i is the number of spikes in the i th window. The information is then calculated on the basis of the probability for an interval τ to have a specific rate r_i , as $I_r = -\sum_r p_r \log(p_r)$, where r is the set of all possible values of r_i . The relatively long τ is offset by the low mean firing rates involved (compare figure 3.16) and the long stimulus used. To investigate the effects of the synaptic properties on the population level, figure 3.18 follows the pattern established for figures 3.12-3.15, that is, the left panels show only AMPA current, the right panels take AMPA as well as NMDA currents into account. Synaptic effects are not included in the top panels, while the middle panels allow for short term depression and the bottom panels depict the results for short-term depression and facilitation.

As higher firing rates usually add to the information content of a spike train, figure 3.18 shows the rate information normalised by the number of spikes. The top left panel immediately raises suspicion that the correlation between rate information and spike count is not linear in this system. This is consistent with the results obtained before. Therefore, the rate information per spike is large for neurons excited by octopus cells with high or widely different CF s, the fringes of the responsive area. Taking short term depression into account (middle left panel) confirms a qualitative difference between VNLL cells with very low frequency inputs and those with afferent $CF \in [2.5, 5.5]$ kHz. Short term depression reduces the coincidental firing necessary for an VNLL cell action potential,

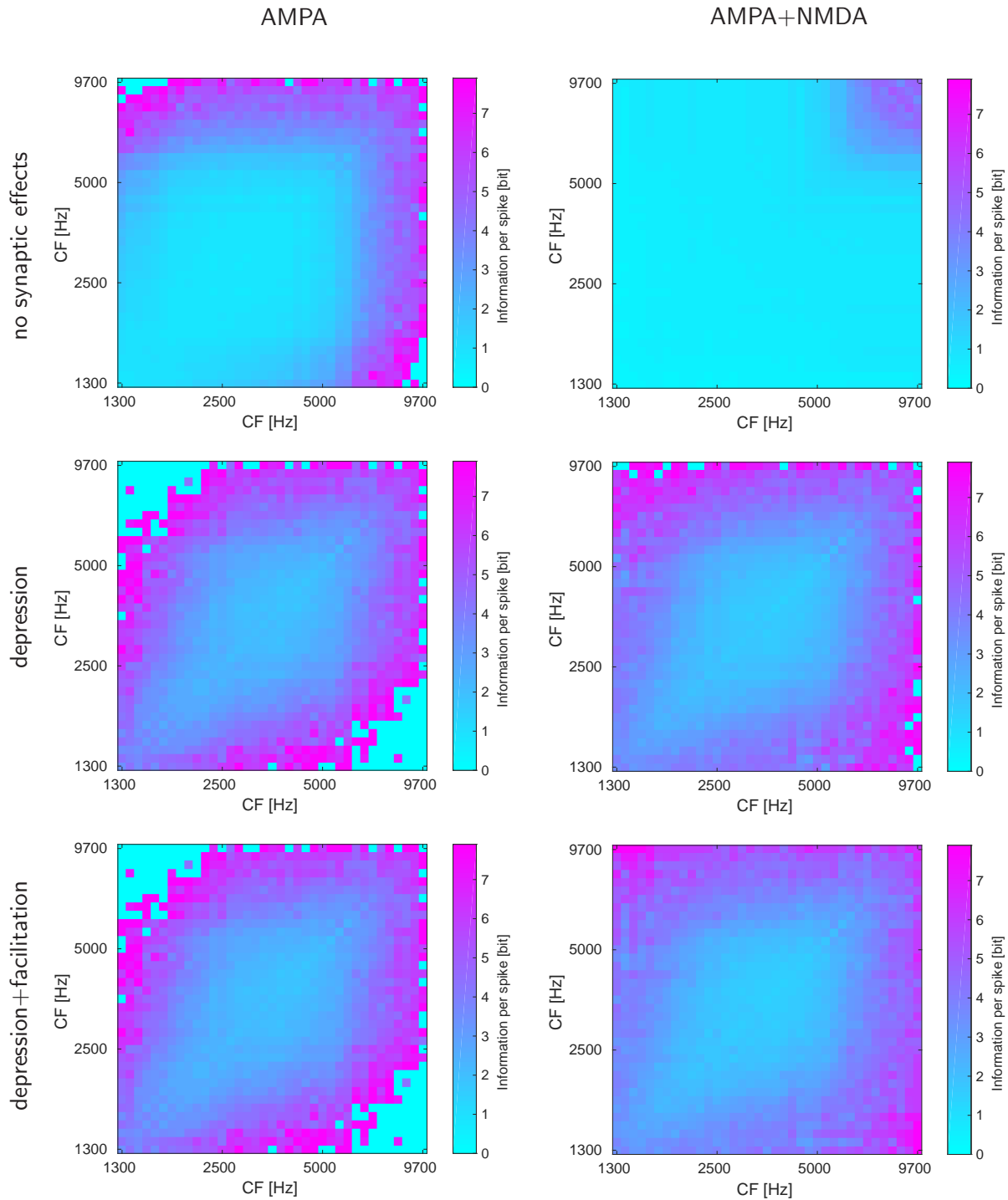


Figure 3.18: Rate information per spike (colour coded) of the response of VNLL onset cells, stimulated by human speech, in relation to the afferent octopus cells (x- and y-axis, logarithmic scale). Left panels only include AMPA currents, right panels take NMDA currents into account. Top: No synaptic effects. Middle: With short term depression. Bottom: With short term depression and facilitation.

	AMPA only	AMPA+NMDA
no synaptic effects	2.66 ± 1.67 bit/spike	0.868 ± 0.472 bit/spike
short term depression	3.81 ± 1.61 bit/spike	3.75 ± 1.24 bit/spike
depression and facilitation	3.72 ± 1.59 bit/spike	3.53 ± 1.07 bit/spike

Table 3.6: Rate information per spike of the response to human speech averaged over the entire population of VNLL onset cells with standard deviation.

which hints towards the fact, that these coincidences are not only based of synchronised firing but also in high levels of sustained firing. This leads to an area with a minimum of rate information per spike in the middle of the observed distribution. Overall, this leads to a stronger equalisation within the distribution. Introducing facilitation (bottom left panel) does not show any significant changes in the information content of VNLL responses.

The right panels of figure 3.18 take AMPA as well as NMDA mediated currents into account. The top right panel, where synaptic effects are not included, shows a qualitatively change pattern. The constituent with the lowest CF becomes completely dominant and solely determines the information content of the VNLL's response. Consequently, the mean firing rate increases faster than the information content, which, in turn, leads to a severely reduced rate information per spike. As mentioned above, high frequency cells respond to speech stimuli with growing selectivity, therefore, the above is mitigated were both constituent neurons have a $CF > 6500$ Hz. Including short term depression, as depicted in the middle right panel, restores counteracts this and restores the additional pattern. This further confirms the suspicion that NMDA currents and short term depression counteract and balance each other. Similar to the results obtained above, the pattern modulated by these two effects is wider (in reference to its diagonal) than without NMDA currents. Facilitation, again, appears to play a supporting role, stabilising and enhancing the changes induced by the NMDA mediated currents (bottom right panel). Under the assumption, that the primary function of the VNLL onset cells is the delivery of temporal precise and reliable markers, a low rate information content seems preferable as to have the spike train contain primarily temporal information. Therefore, broadening the central region around the diagonal, again, enlarges the subset of potential combinations that yield favourable results and, thereby, enhances the population response.

Table 3.6 shows the mean values, averaged over the entire population, of figure 3.18. It has already been discussed that, while the low number for the configuration, that includes NMDA currents but no synaptic effects, seems favourable, the comparison with figure 3.16 reveals that

	AMPA only	AMPA+NMDA
no synaptic effects	5.97 ± 2.53 bit/s	11.97 ± 1.86 bit/s
short term depression	2.31 ± 1.04 bit/s	2.87 ± 1.13 bit/s
depression and facilitation	2.42 ± 1.08 bit/s	3.10 ± 1.13 bit/s

Table 3.7: Rate information transmission of the response to human speech averaged over the entire population of VNLL onset cells with standard deviation.

this is due to a high number of additional spikes with a low information content. Apart from that, however, the explicit mean values show that the rate information per spike actually increases between the configuration with all synaptic properties accounted for (bottom right) and the one with none (top left), which seems to contradict the assumption that VNLL onset cells are tuned for a high content of temporal information. Figure 3.18 shows that this is due to the equalisation within the population. Cells with low CF constituents respond exhibit similar spike counts with or without NMDA currents. Following the same argument outlined above, the average information per spike decreases. One can take this into account and estimate the transmission of rate information as $R_{I,r} = I_r \bar{r}$, where \bar{r} is the mean firing rate over the entire stimulus duration. These values are shown in table 3.7. It shows that for the simplest case, only AMPA currents and no synaptic effects taken into account, rate information already only makes up a minority of the information content. So, again, the focus lies on temporal information. The qualitative change seen in figure 3.18 when including NMDA currents reflects here as well. Without short term depression the fraction of rate information in the entire information content rises to over 0.24. This is reversed by short term depression. Taking all synaptic properties into account shows, that the fraction of rate information is reduced from 0.15 to 0.08 .

The synaptic properties influencing the VNLL onset cells are remarkably well balanced, complementing and counteracting each other to greatly enhance already prevalent response properties of the neurons, generated by integrating over a small number of octopus cells. This becomes most apparent by combining the result of all three analyses on human speech performed in this study, presented in figures 3.16 to 3.18. The mean firing rates drop severely while maintaining most of the information content, rising the efficiency by over 70%. The loss of information is mainly rate information while the temporal information content is mostly preserved. This provides a strong hint towards the hypothesis that VNLL onset cells provide very precise temporal information about specific characteristics of the sound stimulus. Furthermore, the results obtained with the test stimuli are supported - the number of possible octopus cell combination, that yield the expected results

are increased with reduced dependency on afferent *CFs*. Together with the improved efficiency on a single neuron level, this points towards a strong focus on the population response. This fits well with the fact, that the VNLL inhibits and gates the inferior colliculus, where reintegration of information about the sound stimulus begins.

Chapter 4

Discussion

Modelling approaches - on a strong foundation of experimental data - have been an integral part of auditory neuroscience for decades ([45]). The advances in computation only enhanced that trend, as it allowed for more and more sophisticated models, which can provide powerful tools to further the understanding of the processing of sounds in the central nervous system. They allow for an arbitrarily large set of stimuli to be used to gauge the behaviour of types of neurons under a wide variety of circumstances. Any aspect of a model can readily be changed, added and removed, which can convey a deeper understanding of the processes underlying neuronal functions. Also, studying the behaviour of circuits on a population level becomes more feasible with a numerical approach because any number of cells can be modelled, the only limiting factor being the computational cost. Even differences between modelled behaviour and experimental results can be useful as these point towards aspects that are not yet understood. However, numerical approaches rely on a pre-existing understanding of input-output relationships and, therefore, must rely heavily on experimental data. As such, the more experimentally challenging the study of a brain area is the less it is accessible to a numerical approach. While there is a certain number of cochlea models available (see, for example, [71]), models for areas further downstream become more scarce ([45]). Although, the octopus cells and the VNLL onset circuit have been modelled before ([27, 77]), these models do not include all the known properties of the system with such computational efficiency. Therefore they do not offer themselves to study responses to complex, naturalistic stimuli on a population level.

The octopus cell model proposed in this work emulates the experimentally determined response patterns to pure tones and amplitude modulated stimuli. It takes into account sensitivity to voltage change of as well as the broadband input received by octopus cells. The latter, especially, is repre-

sented in the realistic tuning curves, the model generates. Without additional assumptions, except what has been determined experimentally, the model faithfully emulates its natural counterparts. Therefore, it allows for reliable prediction and can also be readily employed to generate inputs for the experimental study of areas further downstream the auditory pathway.

It has been shown, that integrating over two afferent octopus cells is sufficient to emulate the onset cells of the VNLL faithfully. It allowed to study, the interplay of AMPA and NMDA mediated currents and the effects of short term depression and facilitation, as well, which, as it turned out, where crucial for the VNLL cell's well known capacity to phase lock to amplitude modulations. Using human speech as test bed and information theoretical tools revealed that the system is ideally suited to detect slow amplitude modulations precisely. The balance of the additional synaptic effects, taken into account, not only enhances these capabilities but also establishes a balance between precision and reliability, increases the efficiency of the system significantly as well as increasing the the functional fraction of possible configurations on a population level.

It stands to reason to divide the final reflection on this study into two parts. First, a critical deliberation from a mechanistic point of view seems to be in order, which will discuss the models capabilities, limitations and potential. Finally, with the insights gained from the information theoretical analyses of human speech, it is possible to venture hypotheses on the studied system's functional role in the analysis of natural sound environments.

4.1 Mechanistic aspects

The model presented here does fulfil its twofold goal. On the one hand, it shows that only a few well known aspects of and little assumptions about the system are required to generate the expected response patterns in their entirety. The amount of fine tuning necessary suggests an unknown modulatory factor not accounted for in the model paradigm. On the other hand it provides a computational efficient tool to generate neuronal responses even for long and complex stimuli. Theses can be employed to further study the system's role in the analysis of acoustic environments and upstream areas of the brain. For example, the octopus cell model can be used to generate realistic templates for electrophysiological studies of the VNLL cells.

Reliably simulating cells further improves the computational efficiency, as less cells are required to get a faithful representation of the population response. To this end, no additional noise influences the model. Due to the high firing rates and short firing windows involved, the noise accompanying the Poisson point process is minimal. Especially the simulated octopus cells show

little variance in their response patterns. The behaviour is only influenced by CF and the stimulus, which is further enhanced by the small functional area of the parameter space. Natural cells show a larger variability (e.g. [63, 75, 52]). In contrast, the model aims at generating the "ideal" octopus cell and, as such, is designed to show little variations. Studying the interdependence between Δ and f_{lp} in greater depth could widen the functional area of the parameter space and, therefore, reintroduce said variability.

Simplicity and reliability are also the reasons for keeping as many parameters as possible independent of CF and SPL-threshold. Homeostatic effects could explain a deviation from this paradigm. Keeping the parameters involved constant also has the side effect that the simulated cells rise faster from threshold to maximum firing rates than observed in their natural counterparts ([22]). To maintain a pure onset behaviour for pure tone stimulation over the entire range of SPL-thresholds requires a steep slope of the sigmoidal spike generator. A lower slope could reduce this effect. However, this would also result in more cells exhibiting low levels of sustained firing for pure tone stimuli (in some publications these are called O_L neurons, in contrast to the desired O_I neurons, i.e. those exhibiting a pure onset response), especially for low SPL-thresholds. It has been shown that some octopus cells exhibit said low levels of sustained firing [75, 65].

The relevance of voltage activated K^+ channels has been stressed before (e.g. [24, 53]), which is mostly represented by the differentiation in the model. Especially simulated neurons with a high SPL-threshold, however, require a balance between the differential and non-differential components to properly lock to amplitude modulated stimuli. The differential component is, even after applying the low-pass filter, still dominant. It is uncertain if this has a real basis or compensates for shortcomings of the model at other points. The phase locking behaviour is also diminished in a frequency range of around 2.5 kHz when stimulated with amplitude modulated pure tone. Experiments that included modulated noise as well as pure tone carriers showed similar response levels in both cases ([63]). It is very unlikely that this gap affects the response to complex, natural stimuli and particular to modulated pure tones, as its causes are well understood. Both of these effects, together with the small functional area in the parameter space, could hint towards an unknown synaptic effect, such as a negative feedback loop, that acts in a modulatory capacity on the summed ANF outputs.

The strict correlation between CF and SPL-threshold assumed above is not necessarily present in natural octopus cells ([22, 75]). This assumption was made from a coarse estimate of the available data and a sensible choice for descriptive and testing purposes. For low SPL-thresholds and low CF the simulated octopus cells tend towards a more primary like behaviour, in this case: higher

levels of sustained and spontaneous firing. Generating (and consequently showing) onset behaviour in this regime ensures its reliability. Likewise, on the opposite end of the parameter space, i.e. high SPL-thresholds and *CFs*, the response to human speech diminishes, as its maximum spectral power is in lower frequency bands. Likewise, the human auditory system is tuned best towards that range. In natural environments, speech is usually presented between 40 dB and 60 dB. Hence, presenting these stimuli in that regime yields the entire range of responses.

Different sound pressure levels are a challenge for multiple parts of the auditory system. In the auditory nerve this is mediated by different types of ANFs. The fiber thresholds decrease with the spontaneous firing rates, therefore, stimuli of low intensities are best encoded by highly sensitive fibers with a high spontaneous firing rates, while fibers with very low spontaneous firing rates only respond to stimuli of high intensity. These groups are complemented by a third intermediate group bridging both response types. It has been suggested, that octopus cells receive inputs of all three types of ANFs. And indeed, the model can only work for high sound pressure if fibers with low and intermediate spontaneous firing rates are included. The model uses the distribution determined in [40]. Moreover, it has been shown that the different types of ANFs are synchronized in the dendritic tree of octopus cells [25, 24]. Due to their reduced sensitivity, fibers with lower spontaneous firing rates lag behind; this is compensated for by exciting the dendrites closer to the soma. This synchronization is not included in the paradigm presented here. The consistent results produced by the model suggest that this effect is not crucial to the function of octopus cells. Neglecting to synchronize the afferent ANFs, however, comes at a cost. The pseudopotential at sound onset is prolonged. Therefore the modelled cells require a longer refractory period to elicit a single onset spike. In some cases, natural octopus cells fire secondary spikes as well. The higher refractory time scale leads to a reduced capacity to follow fast inputs. Natural octopus cells fire at a rate of up to $800\frac{1}{s}$ while the simulated cells have an upper limit of $500\frac{1}{s}$ and therefore might skip additional cycles at higher rates. This results in a slightly steeper flank of the modulation transfer function at the high frequency end. The band pass characteristic is still common to the simulated as well as natural cells. Superficial testing has hinted to the idea that varying the ratios of ANF types might be a superior way of implementing different SPL-thresholds. High threshold cells would receive a stronger contribution of ANFs with low spontaneous firing rate. The increased capacity of those fibers to transmit modulation could counteract these cells' decreased sensitivity to stimulus modulations beyond the onset.

What has been said about octopus cells applies to the VNLL onset cells as well, since the basic response patterns are directly inherited. It has been shown above that in the model paradigm, the

different current shapes and synaptic effects focus and enhance those on a population level. The short-term depression helps enforcing the onset characteristic and suppresses unwanted sustained firing; the facilitation and addition of NMDA mediated currents enhance the modulation response. However, in other aspects the studied cell types show differences. While the modulation transmission and tuning curves are more or less homogeneous, those of the VNLL onset cells show a greater variability (compare, for example, [22, 67, 75] with [15, 87, 62]). The tuning curves of octopus cells usually show a unimodal V-shape while those of VNLL onset neurons range from unimodal V- to U- to bimodal W-shapes. Similarly, temporal modulation transfer functions of octopus cells have band-pass characteristics (sometimes with an all-pass component) while there are few bimodal cases in the VNLL. The model paradigm assumed here offers an explanation. Owing to the synaptic effects and different currents, modelled octopus cells with CF -differences of multiple kHz can constitute to a functional VNLL cell. The overlay of two V-shaped tuning curves would indeed yield a V-shape for similar CF s and a W-shape for CF s far apart. An analogous argument can be made for the modulation transfer functions. Given that the best modulation frequencies show a far lower range the CF s it is not surprising that the bimodal cases of the latter are rare.

The tuning curves of the octopus cells in particular were important for the confidence in the response patterns to complex stimuli as well as a useful control for the model as such. While the combination of the differentiation kernel, low-pass filter and properly adjusted sigmoidal spike generation is sufficient to generate the onset behaviour in most cases, the response to modulated stimuli necessarily requires broad band inputs. The corresponding information is best transmitted by frequency channels adjacent to the CF -band. For reasons of computational efficiency only a limited number of samples in the ANF frequency space can be taken into account. This adds to the technical difficulties as there is a potential of resonances and gaps between the samples. Therefore the model needs to reach a balance between a stable CF with a realistic tuning curve and a strong, supra-threshold modulation response. Only if this balance is achieved, one can confidently assume that the modelled octopus cell faithfully emulate their natural counterpart.

One additional conclusion can be drawn from the tuning curves of the octopus cells and the VNLL cells. The presented model paradigm assumes exactly two constituent octopus cells and a requirement for coincidental firing [5]. However onset cells in the VNLL show a similar range of SPL-thresholds than octopus cells [15, 62]. Given the assumptions above, this would only be possible for very similar constituent CF s. There are two likely solutions for this apparent contradiction. Integration might not be strictly required and constitute more of a fail safe mechanism or an enhancement of the octopus cells already broad tuning. Alternatively there could be larger (but,

compared to octopus cells, still small) number of afferents with coincidental firing being required only for a subset of those. Given the range of animal models found in the data, it stands to reason that this might be a species dependent property.

While a few potential improvements for the model have been outlined above, those are not strictly necessary to generate a realistic emulation of the octopus cells and their response patterns. The small number parameters and assumptions about the system in the model, as it is presented here, are sufficient. In addition, it is an efficient and useful tool, to generate octopus cell responses to a large number of even complex and long stimuli, which would be difficult to study in vivo. The latter aspect has already been used here to gain a deeper understanding of the onset cells within the VNLL on a population level and to explain the different current shapes and synaptic effects involved.

4.2 Functional aspects

Due to its selective firing behaviour and the high precision the VNLL onset circuit is ideally suited for the analysis of temporal properties of sounds. This is of even greater importance when dealing with stimuli apart from the simpler probing sound (such as pure tones or sinusoidal amplitude modulations). In the presented study, human speech has been used to represent the complex sound involved in natural acoustic environments. It is the best understood and most intuitively accessible form of conspecific vocalisation. Decoding vocal calls is not only of prime importance for most species, the observed onset system is thought to play a role in this process [15, 64, 51, 77]. Apart from that, speech is a good test bed for analysing complex sounds in general. The mammalian auditory system has obviously evolved before human speech. So, the latter adapted to the former instead of vice versa. Following the arguments of talker and speaker orientations, outlined in 1.3, it stands to reason that speech encompasses the entire range of acoustic properties the auditory system can analyse. Having a multitude of phonemes is advantageous from a talker oriented perspective as information can be encoded more efficiently if the possible number of short codewords is greater. From a speaker oriented point of view, however, phonemes are ideally structurally as different from each other as possible. This improves differentiability and, consequently, the efficiency of communication. Therefore, one can assume, that speech evolved to utilize the human auditory system to much of its capacity, which, in turn, allows to draw conclusions about the capabilities of a given system by observing its response to human speech.

Figure 4.1 reproduces figures 1.20 and 3.6 for a direct comparison. The octopus cells respond

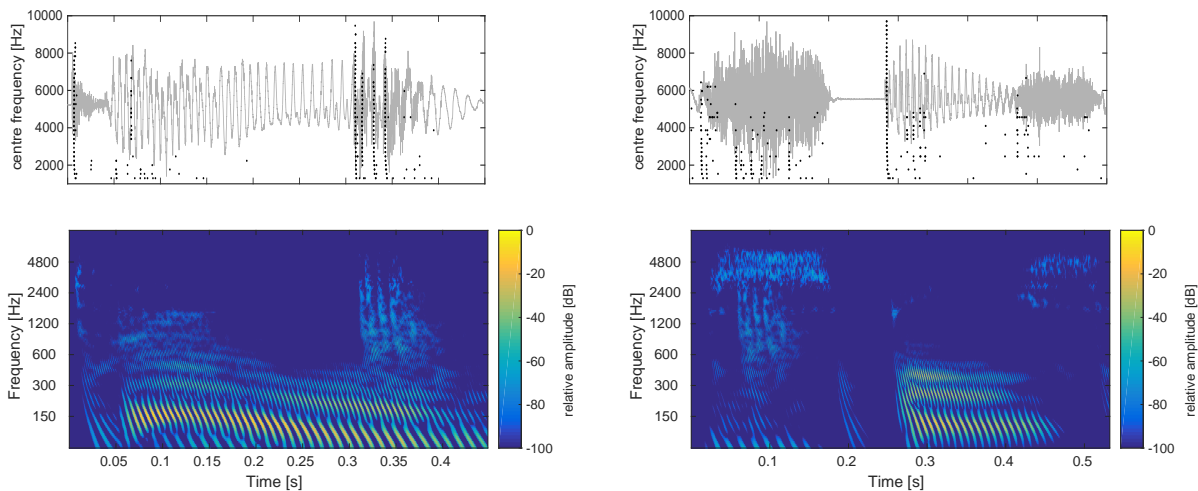


Figure 4.1: Depictions of the word "time" (left panels) and "space" (right panels). Top panels show scatter plots of the octopus cell responses underlain with the waveform (in grey). Bottom panels show the corresponding spectrotemporal patterns.

strongest - on a population level - to where an underlying formant structure is supplemented with high frequency components. This is supported by similar, yet more abstract, experimental findings ([64, 76]). This high frequency component can be due to a sharp onset or intrinsic to the phoneme in question. Cells with low CF s show additional firing during phonemes with strong component of frequencies higher than the typical formant structures. For the population of VNLL onset cells, this aspect is suppressed on one hand by the nature of the the input distribution. It would only evoke a potential response if all constituent cells would show sustained firing for the same phonemes. On the other hand it is suppressed by the short term depression of the afferent synapse. While facilitation and NMDA mediated currents can recover the mean firing rates to a significant portion, the temporal structure of the overall response remains dominated by the short term depression. Hence, the system in its entirety is tuned to precisely respond to the onset of broadband structures with strong phoneme and high frequency components. Taken into account that the VNLL inhibits the inferior colliculus, the question remains what functions these strong and precise markers fulfil.

It has already been mentioned that the VNLL inhibits the IC, the first brain areas where reintegration of the different types of information, extracted from the acoustic stimuli, is thought to occur. In this context, precise temporal information about sharp onsets of formant-like structures might be useful for attention control. Such a transient signal might indicate an imminent new element entering the the acoustic environment that is of paramount importance, e.g. the call of a

predator. The synaptic effects appeared to put focus on the population level, which means the onset response to this kind of stimuli would inhibit the IC on a very wide frequency band and, therefore, silence almost the entire acoustic environment for a brief period of time in which attention could be shifted exclusively to the new stimulus. The high precision of the system would, in this scenario, serve mostly to achieve high levels of synchronicity of the population. The short and near constant delay times of these cell could support this hypothesis.

It has already been suggested that onset cells in the VNLL can reduce spectral splatter [77]. Since for complex auditory environments frequency analyses are of particular importance, this effect would be especially advantageous. It is thought that higher brain areas rely on frequency as well as timing information for sorting sound components into auditory streams, i.e. the attempt to group components of the auditory environment together that are related and/or stem from the same source [46]. Strong transients would appear in frequency bands other than the corresponding formants. This would disrupt the forming of reliable auditory streams not only by disrupting the frequency analyses, but also by introducing temporal cues into uncorrelated frequency bands. Mitigating these disruptions would require for the effects to be broadly tuned, precise, fast as well as synchronous; all of which are properties the system has been shown to have. In this scenario, the system would not provide the auditory pathway with an additional functionality but correct for unwanted side effects that might occur.

A non-exclusive, third possibility would be, that the system plays more of a supporting role. The inhibition at sound onset and strong transients could provide less immediate benefits. Due to the short delays the VNLL onset cells could hyperpolarise higher level neurons at or before the onset of their respective responses, therefore, delaying it. This would improve gap detection, which has been shown to provide an important temporal cue for sound processing. Diminished gap detection has, for example, been linked to auditory neuropathy, the inability to process speech with otherwise unimpaired hearing [51]. The model's strong and selective response to speech would seem to support that assumption. Additionally, strong transients in the stimuli can evoke powerful responses in the auditory pathways. Depending on the synaptic properties involved, these can lead to the neuron desensitising, due to short term depression. Such an effect can contribute towards forward masking, i.e. one tone negatively impacting the perception of another, immediately following tone. Inhibition at stimulus onset can mitigate this and, thereby, improve and accelerate tone discrimination.

The computational approach employed for this study revealed in more depth the response properties of the VNLL onset cells and, by demonstrating the effects of the system's specific synaptic

properties, provided hints as to what the to what stimuli and firing behaviour it is most attuned. With this numerical model it was possible to faithfully analyse the responses to long an complex sounds and, thereby, asses the potential and capabilities of the system.

Bibliography

- [1] Joe C Adams. Ascending projections to the inferior colliculus. *J Comp Neurol*, 183(3):519–538, 1979.
- [2] Joe C. Adams. Projections from octopus cells of the posteroventral cochlear nucleus to the ventral nucleus of the lateral lemniscus in cat and human. *Aud. Neurosci.*, 3(4):335–350, 1997.
- [3] Julian J Ammer, Benedikt Grothe, and Felix Felmy. Late postnatal development of intrinsic and synaptic properties promotes fast and precise signalling in the dorsal nucleus of the lateral lemniscus. *J. Neurophysiol.*, 107(4):1172–1185, 2012.
- [4] Ranjan Batra and Douglas C Fitzpatrick. Monaural and binaural processing in the ventral nucleus of the lateral lemniscus: a major source of inhibition to the inferior colliculus. *Hear. Res.*, 168(1-2):90–97, 2002.
- [5] Christina Berger, Elisabeth MM Meyer, Julian J Ammer, and Felix Felmy. Large somatic synapses on neurons in the ventral lateral lemniscus work in pairs. *J. Neurosci.*, 34(9):3237–3246, 2014.
- [6] Maryline Beurg, Robert Fettiplace, Jong-Hoon Nam, and Anthony J Ricci. Localization of inner hair cell mechanotransducer channels using high-speed calcium imaging. *Nat. Neurosci.*, 12(5):553, 2009.
- [7] Theunissen F. Borst, A. Information theory and neural coding. *Nat Neurosci.*, 2:947–957, Nov 1999.
- [8] Lorraine K. Tyler Brian C.J. Moore and William Marslen-Wilson, editors. *The perception of speech - from sound to meaning*. Oxford University Press, Oxford, 2009.

-
- [9] Xiao-Jie Cao and Donata Oertel. Temperature affects voltage-sensitive conductances differentially in octopus cells of the mammalian cochlear nucleus. *J Neurophysiol*, 94(1):821–832, 2005.
- [10] Xiao-Jie Cao and Donata Oertel. Auditory nerve fibers excite targets through synapses that vary in convergence, strength, and short-term plasticity. *J. Neurophysiol.*, 104(5):2308–2320, 2010.
- [11] Franziska Caspari, Veronika J Baumann, Elisabet Garcia-Pino, and Ursula Koch. Heterogeneity of intrinsic and synaptic properties of neurons in the ventral and dorsal parts of the ventral nucleus of the lateral lemniscus. *Front. Neural Circuits*, 9:74, 2015.
- [12] JH Casseday, D Ehrlich, and E Covey. Neural tuning for sound duration: role of inhibitory mechanisms in the inferior colliculus. *Science*, 264(5160):847–850, 1994.
- [13] Thomas M Cover and Joy A Thomas. *Elements of information theory*. Wiley-Interscience, 2nd edition, 2006.
- [14] E Covey and JH Casseday. Connectional basis for frequency representation in the nuclei of the lateral lemniscus of the bat *epptesicus fuscus*. *J. Neurosci.*, 6(10):2926–2940, 1986.
- [15] E Covey and JH Casseday. The monaural nuclei of the lateral lemniscus in an echolocating bat: Parallel pathways for analyzing temporal features of sound. *J. Neurosci.*, 11(11):3456–3470, 1991. Copyright 1991 Society for Neuroscience.
- [16] Carl L Faingold, Cathy A Boersma Anderson, and Marcus E Randall. Stimulation or blockade of the dorsal nucleus of the lateral lemniscus alters binaural and tonic inhibition in contralateral inferior colliculus neurons. *Hear. Res.*, 69(1-2):98–106, 1993.
- [17] Felix Felmy. The nuclei of the lateral lemniscus. In *The Oxford Handbook of the Auditory Brainstem*, page 445. Oxford University Press, 2019.
- [18] Michael J Ferragamo and Donata Oertel. Octopus cells of the mammalian ventral cochlear nucleus sense the rate of depolarization. *J Neurophysiol*, 87(5):2262–2270, 2002.
- [19] Linda Fischer. *Synaptic Mechanisms Underlying Temporally Precise Information Processing in the VNLL*. PhD thesis, University of Veterinary Medicine Hannover, Hannover, 2020. supervised by Prof. Dr. Felix Felmy.

- [20] E Friauf and J Ostwald. Divergent projections of physiologically characterized rat ventral cochlear nucleus neurons as shown by intra-axonal injection of horseradish peroxidase. *Experimental brain research.*, 73(2):263–284, 1988.
- [21] KK Glendenning, JK Brusno-Bechtold, GC Thompson, and RB Masterton. Ascending auditory afferents to the nuclei of the lateral lemniscus. *J Comp Neurol*, 197(4):673–703, 1981.
- [22] Donald A Godfrey, Nelson YS Kiang, and Barbara E Norris. Single unit activity in the posteroventral cochlear nucleus of the cat. *J Comp Neurol*, 162(2):247–268, 1975.
- [23] Nace L Golding, Michael J Ferragamo, and Donata Oertel. Role of intrinsic conductances underlying responses to transients in octopus cells of the cochlear nucleus. *J Neurosci*, 19(8):2897–2905, 1999.
- [24] Nace L Golding and Donata Oertel. Synaptic integration in dendrites: exceptional need for speed. *J. Physiol.*, 590(22):5563–5569, 2012.
- [25] Nate L Golding, Donald Robertson, and Donata Oertel. Recordings from slices indicate that octopus cells of the cochlear nucleus detect coincident firing of auditory nerve fibers with temporal precision. *J Neurosci*, 15(4):3138–3153, 1995.
- [26] Benedikt Grothe, Michael Pecka, and David McAlpine. Mechanisms of sound localisation in mammals. *Physiol. Rev.*, 90(3):983–1012, 2012.
- [27] Werner Hemmert, Marcus Holmberg, and Ulrich Ramacher. Temporal sound processing by cochlear nucleus octopus neurons. In *International Conference on Artificial Neural Networks*, pages 583–588. Springer, 2005.
- [28] Rasha A Ibrahim and Ian C Bruce. *Effects of peripheral tuning on the auditory nerve’s representation of speech envelope and temporal fine structure cues*, pages 429–438. Springer, 2010.
- [29] Irvine. The auditory brainstem. In Perl ER Schmidt RF Shimazu H Willis WD Autrum H, Ottoson D, editor, *Progress in sensory physiology*. 1986.
- [30] Stephen K Itaya and Gary W Van Hoesen. Retinal innervation of the inferior colliculus in rat and monkey. *Brain Res.*, 233(1):45–52, 1982.

- [31] Bishop D.C. Ito, T. and D.L. Oliver. Functional organization of the local circuit in the inferior colliculus. *Anat. Sci. Int.*, 91:22–34, 2016.
- [32] Roshini Jain and Susan Shore. External inferior colliculus integrates trigeminal and acoustic information: unit responses to trigeminal nucleus and acoustic stimulation in the guinea pig. *Neurosci. Lett.*, 395(1):71–75, 2006.
- [33] PX Joris and Trussel LO. The calyx of held: a hypothesis on the need for reliable timing in an intensity-difference encoder. *Neuron*, 100(3):534–549, 2018.
- [34] PX Joris, CE Schreiner, and A Rees. Neural processing of amplitude-modulated sounds. *Physiol Rev*, 84(2):541–577, 2004.
- [35] Eileen Cohen Kane. Octopus cells in the cochlear nucleus of the cat: Heterotypic synapses upon homeotypic neurons. *Int. J. Neurosci*, 5(6):251–279, 1973.
- [36] Jack B Kelly, Brian A Van Adel, and Makoto Ito. Anatomical projections of the nuclei of the lateral lemniscus in the albino rat (*rattus norvegicus*). *J Comp Neurol*, 512(4):573–593, 2009.
- [37] Nelson Yuansheng Kiang. *Discharge patterns of single fibers in the cat’s auditory nerve*. Number 13 in Special technical report (Massachusetts Institute of Technology. Research Laboratory of Electronics). the M.I.T Press, 1965.
- [38] Cornelia Kopp-Scheinpflug, Susanne Dehmel, Gerd J Dörrscheidt, and Rudolf Rübsamen. Interaction of excitation and inhibition in anteroventral cochlear nucleus neurons that receive large enbuldb synaptic endings. *J. Neurosci.*, 22(24):11004–11018, 2002.
- [39] Richard I Kuo and Guangying K Wu. The generation of direction selectivity in the auditory system. *Neuron*, 73(5):1016–1027, 2012.
- [40] M Charles Liberman. Auditory-nerve response from cats raised in a low-noise chamber. *J. Acoust. Soc. Am.*, 63(2):442–455, 1978.
- [41] M Charles Liberman. Central projections of auditory-nerve fibers of differing spontaneous rate: I. anteroventral cochlear nucleus. *J Comp Neurol*, 313(2):240–258, 1991.
- [42] William C Loftus, Deborah C Bishop, Richard L Saint Marie, and Douglas L Oliver. Organization of binaural excitatory and inhibitory inputs to the inferior colliculus from the superior olive. *J. Comp. Neurol.*, 472(3):330–344, 2004.

- [43] Ariana Lumani and Huiming Zhang. Responses of neurons in the rat's dorsal cortex of the inferior colliculus to monaural tone bursts. *Brain Res.*, 1351:115–129, 2010.
- [44] Matthew J McGinley, M Charles Liberman, Ramazan Bal, and Donata Oertel. Generating synchrony from the asynchronous: compensation for cochlear traveling wave delays by the dendrites of individual brainstem neurons. *J Neurosci*, 32(27):9301–9311, 2012.
- [45] Ray Meddis, Enrique A Lopez-Poveda, Richard R Fay, and Arthur N Popper. *Computational models of the auditory system*, volume 35. Springer, 2010.
- [46] Brian C.J. Moore. *An Introduction to the Psychology of Hearing*. Brill, 6th edition, Leiden, Boston, 2013.
- [47] Lucille A Moore and Laurence O Trussell. Corelease of inhibitory neurotransmitters in the mouse auditory midbrain. *J. Neurosci.*, 37(39):9453–9464, 2017.
- [48] Judith Mylius, Michael Brosch, Henning Scheich, and Eike Budinger. Subcortical auditory structures in the mongolian gerbil: I. golgi architecture. *J Comp Neurol*, 521(6):1289–1321, 2013.
- [49] David AX Nayagam, Janine C Clarey, and Antonio G Paolini. Powerful, onset inhibition in the ventral nucleus of the lateral lemniscus. *J. Neurophysiol.*, 94(2):1651–1654, 2005.
- [50] Donata Oertel. The role of intrinsic neuronal properties in the encoding of auditory information in the cochlear nuclei. *Curr. Opin. Neurobio.*, 1(2):221–228, 1991.
- [51] Donata Oertel. Importance of timing for understanding speech. focus on “perceptual consequences of disrupted auditory nerve activity”. *J Neurophysiol*, 93(6):3044–3045, 2005.
- [52] Donata Oertel, Ramazan Bal, Stephanie M Gardner, Philip H Smith, and Philip X Joris. Detection of synchrony in the activity of auditory nerve fibers by octopus cells of the mammalian cochlear nucleus. *PNAS*, 97(22):11773–11779, 2000. Copyright 2000 National Academy of Sciences.
- [53] Donata Oertel, Xiao-Jie Cao, James R Ison, and Paul D Allen. Cellular computations underlying detection of gaps in sounds and lateralizing sound sources. *Trends in Neuroscience*, 40(10):613–624, 2017.

- [54] Donata Oertel, Samantha Wright, Xiao-Jie Cao, Michael Ferragamo, and Ramazan Bal. The multiple functions of t stellate/multipolar/chopper cells in the ventral cochlear nucleus. *Hear. Res.*, 276(1-2):61–69, 2011.
- [55] Donata Oertel and Eric D Young. What’s a cerebellar circuit doing in the auditory system? *Trends Neurosci.*, 27(2):104–110, 2004.
- [56] Douglas L Oliver. Neuronal organization in the inferior colliculus. In *The inferior Colliculus*, pages 69–114. New York: Springer, 2005.
- [57] James O. Pickles. *An Introduction to the Physiology of Hearing*. Brill, 4th edition., 2012.
- [58] James O. Pickles. Auditory pathways: Anatomy and physiology. In *Handbook of clinical neurology*, number 1, pages 3–25. Elsevier, 2015.
- [59] JO Pickles, SD Comis, and MP Osborne. Cross-links between stereocilia in the guinea pig organ of corti, and their possible relation to sensory transduction. *Hear. Res.*, 15(2):103–112, 1984.
- [60] Christian P Porres, Elisabeth MM Meyer, Benedikt Grothe, and Felix Felmy. Nmda currents modulate the synaptic input-output functions of neurons in the dorsal nucleus of the lateral lemniscus in mongolian gerbils. *J Neurosci*, 31(12):4511–4523, 2011.
- [61] M.J. Rebhan and C. Leibold. A phenomenological spiking model for octopus cells in the posterior-ventral cochlear nucleus. unpublished, preliminary version, 2020.
- [62] Alberto Recio-Spinoso and Philip X Joris. Temporal properties of responses to sounds in the ventral nucleus of the lateral lemniscus. *J Neurophysiol*, 111(4):817–835, 2014.
- [63] WS Rhode. Temporal coding of 200 percent amplitude modulated signals in the ventral cochlear nucleus of cat. *Hear Res*, 77(1-2):43–68, 1994.
- [64] WS Rhode. Neural encoding of single-formant stimuli in the ventral cochlear nucleus of the chinchilla. *Hear Res*, 117(1-2):39–56, 1998.
- [65] WS Rhode and S Greenberg. Encoding of amplitude modulation in the cochlear nucleus of the cat. *J Neurophysiol*, 71(5):1797–1825, 1994.

- [66] WS Rhode, D Oertel, and PH Smith. Physiological response properties of cells labeled intracellularly with horseradish peroxidase in cat dorsal cochlear nucleus. *J Comp Neurol*, 213(4):448–463, 1983.
- [67] WS Rhode and PH Smith. Encoding timing and intensity in the ventral cochlear nucleus of the cat. *J Neurophysiol*, 56(2):261–286, 1986.
- [68] Raquel Riquelme, Enrique Saldaña, Kirsten K Osen, Ole P Ottersen, and Miguel A Merchán. Colocalization of gaba and glycine in the ventral nucleus of the lateral lemniscus in rat: An in situ hybridization and semiquantitative immunocytochemical study. *J. Comp. Neurol.*, 432(4):409–424, 2001.
- [69] Luis Robles and Mario A Ruggero. Mechanics of the mammalian cochlea. *Physiol. Rev.*, 81(3):1305–1352, 2001.
- [70] Jason S Rothman and Paul B Manis. Differential expression of three distinct potassium currents in the ventral cochlear nucleus. *J Neurophysiol*, 89(6):3070–3082, 2003.
- [71] Marek Rudnicki, Oliver Schoppe, Michael Isik, Florian Völk, and Werner Hemmert. Modeling auditory coding: from sound to spikes. *Cell and tissue research*, 361(1):159–175, 2015.
- [72] Brett R Schofield and Nell B Cant. Ventral nucleus of the lateral lemniscus in guinea pigs: cytoarchitecture and inputs from the cochlear nucleus. *J. Comp. Neurosci.*, 379(3):363–385, 1997.
- [73] Ida Siveke, Julian J Ammer, Sarah A Gleiss, Benedikt Grothe, Christian Leibold, and Felix Felmy. Electrogenic n-methyl-d-aspartate receptor signaling enhances binaural responses in the adult brainstem. *Eur J Neurosci*, 47(7):858–865, 2018.
- [74] Philip H Smith, Philip X Joris, Laurel H Carney, and Tom CT Yin. Projections of physiologically characterized globular bushy cell axons from the cochlear nucleus of the cat. *J Comp Neurol*, 304(3):387–407, 1991.
- [75] Philip H Smith, Ann Massie, and Philip X Joris. Acoustic stria: Anatomy of physiologically characterized cells and their axonal projection patterns. *J Comp Neurol*, 482(4):349–371, 2005.
- [76] Martin J Spencer, David B Grayden, Ian C Bruce, Hamish Meffin, and Anthony N Burkitt. An investigation of dendritic delay in octopus cells of the mammalian cochlear nucleus. *Front Comput Neurosci*, 6:83, 2012.

- [77] Martin J Spencer, David AX Nayagam, Janine C Clarey, Antonio G Paolini, Hamish Meffin, Anthony N Burkitt, and David B Grayden. Broadband onset inhibition can suppress spectral splatter in the auditory brainstem. *2015*, 10(5):e0126500, Plos one.
- [78] GA Spirou, J Rager, and PB Manis. Convergence of auditory-nerve fiber projections onto globular bushy cells. *Neuroscience*, 136(3):843–863, 2005.
- [79] S. P. Strong, Roland Koberle, Rob R. de Ruyter van Steveninck, and William Bialek. Entropy and information in neural spike trains. *Phys. Rev. Lett.*, 80(1):197–200, Jan 1998.
- [80] Joshua Sturm, Tuan Nguyen, and Karl Kandler. Development of intrinsic connectivity in the central nucleus of the mouse inferior colliculus. *J. Neurosci.*, 34(45):15032–15046, 2014.
- [81] DP Sutherland, RB Masterton, and KK Glendenning. Role of acoustic striae in hearing: reflexive responses to elevated sound-sources. *Behav. Brain Res.*, 97(1-2):1–12, 1998.
- [82] Laurence O Trussell. Synaptic mechanisms for coding timing in auditory neurons. *Annu. Rev. Physiol.*, 61(1):477–496, 1999.
- [83] J.D. Victor. Approaches to information-theoretic analysis of neural activity. *Biol. Theory*, 1(3):302–316, Sep 2006.
- [84] Henrique Von Gersdorff and J Gerard G Borst. Short-term plasticity at the calyx of held. *Nat. Rev. Neurosci.*, 3(1):53–64, 2002.
- [85] SH Wu and JACK B Kelly. In vitro brain slice studies of the rat’s dorsal nucleus of the lateral lemniscus. iii. synaptic pharmacology. *J. Neurophysiol.*, 75(3):1271–1282, 1996.
- [86] Eric D Young and Donata Oertel. Cochlear nucleus. In *The synaptic organization of the brain*, volume 5. Oxford University Press, 2004.
- [87] Huiming Zhang and Jack B Kelly. Responses of neurons in the rat’s ventral nucleus of the lateral lemniscus to amplitude-modulated tones. *J. Neurophysiol.*, 96(6):2905–2914, 2006.
- [88] Huiming Zhang and Jack B Kelly. Responses of neurons in the rat’s ventral nucleus of the lateral lemniscus to monaural and binaural tone bursts. *J. Neurophysiol.*, 95(4):2501–2512, 2006.

-
- [89] Min Zhao and Shu Hui Wu. Morphology and physiology of neurons in the ventral nucleus of the lateral lemniscus in rat brain slices. *J Comp Neurol*, 433(2):255–271, 2001.
- [90] Muhammad SA Zilany and Ian C Bruce. Representation of the vowel ε in normal and impaired auditory nerve fibers: Model predictions of responses in cats. *J Acoust Soc Am*, 122(1):402–417, 2007.
- [91] Muhammad SA Zilany, Ian C Bruce, and Laurel H Carney. Updated parameters and expanded simulation options for a model of the auditory periphery. *J Acoust Soc Am*, 135(1):283–286, 2014.
- [92] Muhammad SA Zilany, Ian C Bruce, Paul C Nelson, and Laurel H Carney. A phenomenological model of the synapse between the inner hair cell and auditory nerve: Long-term adaptation with power-law dynamics. *J Acoust Soc Am*, 126(5):2390–2412, 2009.
- [93] Muhammad SA Zilany and Laurel H Carney. Power-law dynamics in an auditory-nerve model can account for neural adaptation to sound-level statistics. *J Neurosci*, 30(31):10380–10390, 2010.

Acknowledgements

This work was mostly funded by the Priority Program 1608 "Ultrafast and temporally precise information processing: Normal and dysfunctional hearing" of the Deutsche Forschungsgemeinschaft.

Beyond the funding, however, there are a number of people whose personal contribution were essential to me during my doctoral work. First and foremost I would like to thank Prof. Dr. Christian Leibold who has been a great supervisor and teacher. It was a pleasure working with him. This work relies heavily upon experimental data provided courteously and kindly by Prof. Dr. Felix Felmy and Dr. Linda Fischer, who were always welcoming hosts.

My friends, family and colleagues were always amazing sources of valuable input, much needed support and welcome distraction. The core and extended team organising the monthly social event made even the not-coming-up-with-theme a lot of fun. The end of my work was enriched by many interesting and pleasurable walks, as well. Especially, I would like to thank my sister with my brother-in-more-or-less-law, who listened to me rambling on so often she might be able to recite every single obstacle I had to overcome, Ernesto von Lübcke-Schüttenbreit for valuable input, usually on entirely different topics and Florian Arends together with his moms for him being born as well as all the play dates and home-cooked meals. Doctoral work is not only a scientific endeavour but a journey; because of people like these.

List of Figures

1.1	Firing patterns of different simulated ANFs as a response to pure tones with the cell's centre frequency, generated with the models proposed in [92, 28, 91].	3
1.2	Threshold tuning curves of ANFs with different centre frequencies, generated with the models proposed in [92, 28, 91].	3
1.3	Main excitatory auditory pathway through the brainstem. Redrawn from [58]. . . .	4
1.4	Octopus cell responses to pure tones. The top left panel shows the receptive field of neurons with different <i>cfs</i> . Additionally, the firing patterns of the indicated cells are shown in the other panels. The cell marked with a triangle is at the edge of the detection range and therefore not reliable. Taken from [75] (with permission).	9
1.5	Camera lucida representation of an octopus cell. Taken from [75] (with permission).	10
1.6	Rate and temporal modulation functions (upper and lower panels) of two onset (centre frequencies 6.7 kHz and 7 kHz, left and right panels) units in the PVCN. Taken from [63] (with permission).	10
1.7	Temporal modulation function of an onset unit in the PVCN, stimulated by an amplitude modulated broadband noise. Taken from [63] (with permission).	11
1.8	Octopus cell response to click stimulation with a click frequency of 500Hz. Depicted in the right panels are the timing of the stimulation (top), the post-stimulus time histograms (middle) and the dot raster diagram for 10 trials(bottom). The right panels show the collapsed result onto a 2ms period: the single click stimulus in this time window (top), the period histogram with a bin-width of $8\mu s$ (middle) and the ordered dot rasters (bottom). Taken from [52] (with permission, copyright 2000 National Academy of Science, U.S.A).	12
1.9	Effects of short-plasticity on the projection to the VNLL arising in the octopus cell area of the PVCN. From [19] (with permission).	13

1.10	Schematic representation of a synapse to illustrate its basic function. See text for explanation.	14
1.11	Glutamatergic postsynaptic currents at different holding potentials. Taken from [19] (with permission)	15
1.12	Currents for 1.11 with NMDA blocker (top panel) and additionally AMPA blocker (bottom panel) applied. Taken from [19] (with permission).	15
1.13	Amplitude of both current components with and without CPP for different holding potentials. Taken from [19] (with permission).	16
1.14	Components of the glutamatergic postsynaptic potential change. AMPA currents are shown on the top, NMDA currents on the bottom. Taken from [19] (with permission).	16
1.15	Constant-latency onset Neuron in the VNLLc. Shown are single trials above a PTSH of 100 trials as response to a 5 ms stimulation (black bar). Taken from [15] (with permission, copyright 1991 Society for Neuroscience).	17
1.16	Receptive fields of VNLLc cells (top) compared to those of cells in another part of the VNLL. Taken from [15] (with permission, copyright 1991 Society for Neuroscience).	17
1.17	Reliability of VNLL cells for different input intensities and stimulus frequencies. In the left panel NMDA currents are taken into account while it is absent in the right panel. Taken from [19] (with permission).	18
1.18	Threshold tuning curves and PSTHs of two VNLL onset cells. One cell exhibits an ideal onset response (upper panel) another shows low levels of sustained firing. Taken from [62] (with permission).	19
1.19	Examples of VNLL onset responses. The leftmost to columns shows the responses to pure tone stimuli. The two columns in the middle depict the rate modulation transfer functions for those cells for sinusoidal amplitude modulated stimuli. The temporal modulation transfer functions for the same cells and stimuli are shown in the rightmost columns. Taken from [62] (with permission).	20
1.20	Depictions of the word "time" (left panels) and "space" (right panels). The physical waveforms are shown on the top, the spectrotemporal patterns on the bottom.	22
3.1	schematic representation of the octopus cell model.	32
3.2	Tuning curves for three cells with different best frequencies. Colour-coded are the firing rates for pure tones of different frequencies and sound pressure levels.	34

3.3	Population response. Firing rates (color-coded) of the modeled octopus cells with different characteristic frequencies (on the y-axis) for two representative stimuli (top: grey). Left: Pure tone stimuli of 80 dB SPL with their frequencies matching the characteristic frequency of the octopus cell. Right: Sinusoidal modulated noise stimulus of 20 dB above threshold and a modulation frequency of $f_m = 300$ Hz.	35
3.4	Effects of different low pass filter frequencies f_{lp} (left panels) and arborization width Δ (right panels). All x axes refer to the best frequency of the octopus cell. Top: the average number of spikes as response to pure tones (at Best frequency). Middle: Vector strength of the response to sinusoidally amplitude modulated tones (300 Hz modulation frequency). Bottom: Entrainment to the same AM stimulus as in the middle panels.	38
3.5	Responses of octopus cells with different centre frequencies to sinusoidal modulated noise. The modulation frequency is shown on the x-axis. The left panel depicts the entrainment of the response to the stimulus. The corresponding vector strength is shown in the right one.	39
3.6	Raster-plot of the model's spiking behaviour when applied to speech signals of 50dB SPL. The upper panel depicts the word "time" the lower one the word "space". The y-axis shows the centre frequency of the octopus cell. In the background (grey), the waveform is shown for temporal comparison.	40
3.7	Raster-plot of the model's spiking behaviour when applied to speech signals of 60dB SPL. The upper panel depicts the word "time" the lower one the word "space". The y-axis shows the centre frequency of the octopus cell. In the background (grey), the waveform is shown for temporal comparison.	41
3.8	Population response to Sinusoidal modulated noise stimulus of 20 dB above threshold and a modulation frequency of $f_m = 300$ Hz. Depicted are firing rates (colour-coded) of the modelled octopus cells with different characteristic frequencies (on the y-axis). An example stimulus is shown in the top panel.	43
3.9	Mean response for stimulation with pure tones of different frequencies (on the x-axis). The y-axis shows the mean peak potential for a range of octopus cells equal to the stimulation range.	44
3.10	Comparison of the measured currents mediated by AMPA and NMDA receptors and the model fits.	46

- 3.11 Normalised amplitude of action potentials elicited by periodic stimulation with different frequencies (colours). The top panel shows the experimental data, the bottom one the corresponding fits. 47
- 3.12 Population response of VNLL cells to pure tone stimuli. Depicted are the probabilities to elicit an onset spike (colour coded) in relation to the afferent octopus cells (x- and y-axis, logarithmic scale). Left panels only include AMPA currents, right panels take NMDA currents into account. Top: No synaptic effects. Middle: With short term depression. Bottom: With short term depression and facilitation. 50
- 3.13 Population response of VNLL cells to pure tone stimuli. Depicted are the mean latency of the onset spike (colour coded) in relation to the afferent octopus cells (x- and y-axis, logarithmic scale). Left panels only include AMPA currents, right panels take NMDA currents into account. Top: No synaptic effects. Middle: With short term depression. Bottom: With short term depression and facilitation. 51
- 3.14 Population response of VNLL cells to pure tone stimuli. Depicted is the entrainment to sinusoidal amplitude modulated noise (colour coded) in relation to the afferent octopus cells (x- and y-axis, logarithmic scale). Left panels only include AMPA currents, right panels take NMDA currents into account. Top: No synaptic effects. Middle: With short term depression. Bottom: With short term depression and facilitation. 53
- 3.15 Population response of VNLL cells to pure tone stimuli. Depicted is the vector strength of the response to sinusoidal amplitude modulated noise (colour coded) in relation to the afferent octopus cells (x- and y-axis, logarithmic scale). Left panels only include AMPA currents, right panels take NMDA currents into account. Top: No synaptic effects. Middle: With short term depression. Bottom: With short term depression and facilitation. 55
- 3.16 Mean response of an array of VNLL onset neurons to a human speech sample. In the left panels cells receive only AMPA currents as input while the right panels take NMDA currents into account as well. Top: No synaptic effects are applied. Middle: Short term depression is taken into account. Bottom: Short term depression as well as facilitation are considered. The waveform of the stimulus is included in grey for comparison. The inlay gives the mean firing rate over the entire stimulus. 58

-
- 3.17 Mean information transmission of a VNLL onset cell population per frequency band. Inlaid are the rates of information transmission. In the left panels cells receive only AMPA currents as input while the right panels take NMDA currents into account as well. Top: No synaptic effects are applied. Middle: Short term depression is taken into account. Bottom: Short term depression as well as facilitation are considered. The waveform of the stimulus is included in grey for comparison. The inlay gives the mean firing rate over the entire stimulus. 61
- 3.18 Rate information per spike (colour coded) of the response of VNLL onset cells, stimulated by human speech, in relation to the afferent octopus cells (x- and y-axis, logarithmic scale). Left panels only include AMPA currents, right panels take NMDA currents into account. Top: No synaptic effects. Middle: With short term depression. Bottom: With short term depression and facilitation. 63
- 4.1 Depictions of the word "time" (left panels) and "space" (right panels). Top panels show scatter plots of the octopus cell responses underlain with the waveform (in grey). Bottom panels show the corresponding spectrotemporal patterns. 73

Glossary

- AMPA** *α -amino-3-hydroxy-5-methyl-4-isoxazolepropionic acid receptors*, in the synapse, studied in this work, mediate a fast and powerful current
- ANF** *Auditory Nerve Fiber*, enervated by electromechanical transduction in the cochlea, first neuronal representation of acoustic stimuli, tonotopically arranged.
- CF** *centre frequency or best frequency*, most receptive point of a (mostly monomodal) tuning curve.
- IC** *Inferior Colliculus*, auditory nucleus in the midbrain, putatively the site where reintegration of acoustic information (differentiated in the brainstem) begins.
- NMDA** *N-methyl-D-aspartate acid receptors*. in the synapse, studied in this work, mediate an additional current with large time scales and small amplitudes.
- PVCN** *Posteroventral Cochlear Nucleus*, first step on the dorsal auditory pathway, contains the octopus cell area.
- VNLL** *Ventral Nucleus of the Lateral Lemniscus*, downstream area of the auditory pathway with diverse cell populations, inhibits the Inferior Colliculus.

Curriculum Vitae

Michael Johannes Rebhan

October 2015 - present

Doctorate in Neuroscience
Ludwig-Maximilians-University Munich
Thesis: *The Onset Circuit of the Ventral Nucleus of the Lateral Lemniscus*

Juni 2013 - August 2015

Advisor for academic affairs and public relations
Faculty of Physics
Ludwig-Maximilians-University Munich

September 2010 - August 2012

Master of Science in Physics
Ludwig-Maximilians-University Munich
Thesis: *Magnetic Fields in Young Elliptical Galaxies*

September 2006 - August 2010

Bachelor of Science in Physics
Ludwig-Maximilians-University Munich
Thesis: *Sternentstehung im Multiversum*